Příloha 1

ROUSAROVA, J., SIMA, M., KOZLIK, P., KRIZEK, T. & SLANAR, O. 2021a. Changes in Rosuvastatin Pharmacokinetics During Postnatal Ontogenesis in Rats. J Pharm Pharm Sci, 25, 1-8.

Changes in Rosuvastatin Pharmacokinetics During Postnatal Ontogenesis in Rats

Jaroslava Roušarová[1], Martin Šíma[1], Petr Kozlík[2], Tomáš Křížek[2], Ondřej Slanař[1]

[1]Department of Pharmacology, First Faculty of Medicine, Charles University and General University Hospital, Prague, Czech Republic; [2]Department of Analytical Chemistry, Faculty of Science, Charles University, Prague, Czech Republic

Corresponding author: Martin Šíma, Department of Pharmacology, First Faculty of Medicine, Charles University and General University Hospital in Prague, Albertov 4, Prague 2, 128 00 Czech Republic; TEL: (+420) 224 968 161; email: martin.sima@lf1.cuni.cz; ORCID identifier: 0000-0002-6541-738X

Received, October 15, 2021; Revised, November 2, 2021; Accepted, December 14, 2021; Published, December 23, 2021

ABSTRACT -- Purpose: Statin therapy should be considered in children with familial hypercholesterolemia and sustained high LDL-C levels. There are no data on rosuvastatin exposure in patients <6 years and efficacy/safety can only be derived from case reports. Our aim was to examine developmental changes in pharmacokinetics of rosuvastatin in rats *in vivo* as a basis for clinical development of formulations for patients < 6 years. **Methods:** Rosuvastatin pharmacokinetics was examined in rats aged 1, 4, 7, 10, 14, 21, 28, 35 and 42 days (from birth to sexual maturity). After intraperitoneal dose of 5 mg/kg, blood samples to determine serum rosuvastatin levels were taken at 0.5, 3 and 5 hours. Pharmacokinetic parameters (Vd, CL, AUC_{last}, $AUC_{0-\infty}$) were calculated using pharmacokinecic simulations. **Results:** Both rosuvastatin CL and Vd started to increase systematically between 2 - 3 weeks of age, which was reflected by decreased total drug exposure. The AUC was up to 13 times higher in the age groups ≤14 days compared with the value at 42 days. **Conclusions:** Based on interspecies scaling, a dose reduction could be a feasible way, how to develop appropriate dosing schedule and formulations for children aged 2 - 6 years. However, confirmation in clinical development studies will be needed.

INTRODUCTION

Familial hypercholesterolemia (FH) represents a frequent genetic disorder phenotypically characterized by increased serum cholesterol and low-density lipoprotein (LDL) levels (1). The prevalence of FH is estimated to range between 1/200 – 1:300 in western societies, while the prevalence of homozygous FH is approximately 1:160,000 – 300,000 (2).

FH is, in most cases, caused by mutations in the LDL-receptor gene. Genetic variants of other genes encoding apolipoprotein B, protein convertase subtilisin/kexin type 9 or other targets affecting cholesterol fate in the organism lead to the disease in up to 10% of affected patients. All these variants result in deficient LDL uptake and clearance and predispose patients to premature atherosclerotic cardiovascular diseases. An early diagnosis, adjustment of lifestyle and pharmacotherapy should be utilized as soon as possible to mitigate the risk of clinical complications of early atherosclerosis development (1).

Statins, i.e., 3-hydroxy-3-methyl-glutaryl-CoA reductase inhibitors, are considered the drugs of choice in the therapeutic armamentarium for FH. Especially the highly effective analogs such as rosuvastatin or atorvastatin are recommended for this patient population (3). Most statins have been approved for the use in patients aged 10 years or more by the major drug regulation authorities worldwide, while rosuvastatin may be used in children older than 6 years in the USA and the EU (4-6). The therapeutic guidelines recommend that off label drug therapy should be considered in younger children with sustained LDL-C levels of ≥ 200 mg/dL (7).

However, there are only a few case reports describing beneficial efficacy and safety of statin off-label treatment in younger children. Constantin et al. described the case of a 5-year-old boy, in whom rosuvastatin treatment for 2.5 years has led to the reduction of LDL and total cholesterol levels by 42.4 and 36.4%, respectively. No concurrent adverse effects were observed in this patient (2). Miyagi et al. came with similar findings in 4-year-old twins treated with pitavastatin combined with ezetimibe. In both patients, the reduction by 50 to 60% of LDL levels was achieved, and no adverse effects appeared (8).

Rosuvastatin is a long-acting hydrophilic statin possessing mean steady-state volume of distribution of 134 L in adults, which indicates considerable tissue distribution. Its binding to plasmatic proteins (especially albumin) is about

90%. Metabolism of rosuvastatin is minimal and majority of the drug is excreted unchanged. Approximately 28% of the dose is eliminated via kidneys, while major part (about 72%) is eliminated by hepatic and biliary excretion. Multiple active transporters are involved in the hepatic uptake of rosuvastatin (9, 10).

The drug pharmacokinetics in young children and infants is likely to be altered during postnatal maturation due to the extensive ontogeny of body composition, water content changes and increments of activity of drug related transporters (11). It can be expected that rosuvastatin doses commonly used in adults and older children may lead to overexposure (with potential occurrence of adverse effects) in younger pediatric populations.

FH represents a serious disorder, which early treatment should be initiated to minimize the risk of atherosclerotic cardiovascular disease. However, no clinical data allowing reliable estimate of rosuvastatin exposure, dosing or efficacy and safety are available for patients under 6 years of age. Therefore, our study aims to examine developmental changes of pharmacokinetics (PK) of rosuvastatin in rats *in vivo* as a basis for future clinical development of rosuvastatin formulations for FH patients under 6 years.

MATERIAL AND METHODS

Chemicals

Rosuvastatin calcium, acetonitrile (LC-MS grade), water (LC-MS grade), formic acid (LC-MS grade), and methanol (LC-MS grade) were purchased from Sigma-Aldrich (Saint Louis, USA). Rosuvastatin-d3 Sodium salt (purity ≥ 95%) was supplied by Toronto Research Chemicals (Toronto, Canada). Stock solution was prepared by dissolving rosuvastatin calcium in DMSO to achieve rosuvastatin concentration of 10 mg/mL. This solution was further diluted with water for injection to achieve dosing solution with concentration of 1 mg/mL. Isoflurane was used as IsoFlo 250 mL (Zoetis, Parsippany, USA).

Animals

Pregnant Wistar rats were purchased from Velaz (Prague, Czech Republic) for the purpose of this study. They were maintained under standard conditions (12-h light-dark cycle, 22±2 °C temperature and 50±10% relative humidity) and fed on water and standard granulated diet ad libitum. After delivery, the rat pups were kept with their dam until inclusion into experiment.

All experiments were performed in accordance with the "Guide to the Care and Use of Experimental Animal Care," and every effort was made to minimize animal suffering. The experimental animal project was approved by the animal care review committee of First Faculty of Medicine, Charles University and by the Ministry of Education, Youth and Sports of the Czech Republic under the number MSMT-9445/2018-8.

Experimental procedure

Rat pups 1, 4, 7, 10, 14, 21, 28, 35, and 42 days of postnatal age (PNA) were intraperitoneally dosed with 5 mg/kg of rosuvastatin (5 µL of dosing formulation per 1 g of body weight). After dosing, pups were returned to their dam until sampling. Sparse sampling had to be chosen due to low total volume of blood in rat pups. Systemic blood was drawn at 0.5, 3, and 5 hours after dosing, six rats per each dosing time were used. Blood sample was taken via cardiac puncture in terminal anesthesia (inhalation of 3% isoflurane). Immediately following the sampling, rats were sacrificed by cervical dislocation and death was confirmed by lack of a heartbeat. Blood samples were centrifuged for 10 minutes at 2500×g (4 °C) and serum was extracted. Serum samples were then stored at -80 °C before further processing.

Sample preparation

Serum samples were processed as follows. In 20 µL of serum, proteins were precipitated by the addition of 60 µL of acetonitrile (containing 40 ng/mL rosuvastatin-d_3 as an internal standard). The mixture was vortexed and centrifuged at 9800×g for 6 min. 40 µL of supernatant was transferred into a chromatographic vial. Samples whose concentration exceeded upper limit of quantitation were appropriately diluted with blank serum to reach the concentration within the linear range of the method.

Bioanalytical assay

Determination of rosuvastatin in serum samples was carried out on the Nexera X3 UHPLC coupled with a Triple Quad 8045 tandem mass spectrometer (Shimadzu, Kyoto, Japan). Poroshell 120 SB AQ column (100 × 2.1 mm; 2.6 µm particle size) from Agilent Technologies (Waldbronn, Germany), thermostatted at 40 °C, was used for the analysis. Mobile phase (A: 0.1% formic acid in deionized water, B: 0.1% formic acid in methanol) was pumped in a flow rate of 0.35 mL/min and the following optimized gradient program was applied (min/%B) 0/30, 2.5/90, 3.0/90, 3.5/30, 5.5/30. The

injection volume was 1 µL, and samples were kept at 10 °C. Effluent from the column was directed to the MS ion source between 2.0 and 4.0 min only. For the rest of the time, the effluent was directed to the waste. The tandem mass spectrometry operated in multiple reaction-monitoring mode (MRM) using positive electrospray ionization. MRM transitions of 482.2 > 258.1 (Q1 pre-bias -14 V, Q3 pre-bias -23 V and collision energy -35 V) and 485.2 > 261.1 (Q1 pre-bias -14 V, Q3 pre-bias -25 V and collision energy -35 V) were monitored for rosuvastatin and rosuvastatin-d_3 (internal standard), respectively. The ion source was set as follows: nebulizing gas flow: 3 L/min, heating gas flow: 8 L/min, interface temperature: 320 °C, desolvation line temperature: 300 °C, heat block temperature: 350 °C, and drying gas flow: 10 L/min. Calibration was performed every day before measuring samples and quality control samples were injected after each 6th sample.

Assay validation

The method was fully validated with respect to linearity, LOD, LLOQ, ULOQ, accuracy, precision, selectivity, recovery, matrix effects, dilution integrity, and stability. An eight-point calibration curve was constructed using the analyte-to-internal standard peak area ratio. Weighted least-squares linear regression ($1/x^2$ weighting factor) was used. The linearity was evaluated through the calibrations by coefficients of determination (R^2) and back-calculated concentrations of calibration points. For a succesful verification of the linear range, the back-calculated concentration values should not deviate from the nominal values by more than 15% for the whole calibration range and by 20% for the LLOQ level. LLOQ was the lowest calibration point, and ULOQ was the highest calibration point. LOD value was determined as a concentration providing a signal corresponding to 3.3 times blank matrix baseline noise. Accuracy and precision were determined via analysis of the fortified blank samples (QC samples) at three concentration levels (1, 50, and 500 ng/mL) at six replicates ($n = 6$). QC concentrations were chosen based on the expected concentration range of the majority of the rat samples. The accuracy was expressed as the relative error (RE, %; calculated as ((measured concentration – expected concentration)/expected concentration)*100), and the precision expressed by repeatability as the relative standard deviation (RSD). Recovery of the method was assessed by comparison of rosuvastatin concentration found in a serum sample spiked with the standard before precipitation of proteins and concentration found in a serum sample spiked after precipitation of proteins at three concentration levels (1, 50, and 500 ng/mL). Matrix effect was evaluated at the same concentration levels of six serum samples. It was determined by comparing the area of the rosuvastatin standard peak of the post-protein-precipitation spiked plasma sample with that of the 80% acetonitrile (without matrix effect). Method selectivity was checked by injecting six blank serum samples. Dilution integrity was investigated at six replicates of spiked serum samples with the 15 µg/mL rosuvastatin concentration. Samples were diluted 20-fold using blank serum and assayed. Serum concentrations were measured and recalculated to original concentrations. The stock solutions stability of rosuvastatin and its IS was tested at room temperature for 12 h and refrigerated (-80 °C) for 1 month. Rosuvastatin stability tests on freeze-thaw (three cycles), long-term (-80 °C for 1 month), bench-top (room temperature for 4 h), whole blood (after collection), and autosampler (processed samples in the autosampler for 24 h at 10 °C) were performed using three replicates at three concentration levels (1, 500, 15000 ng/mL).

Pharmacokinetic analysis and statistics

Median and interquartile range (IQR) serum concentration values in each sampling time and each PNA group was calculated using GraphPad Prism 8.2.1 (GraphPad Software, Inc., La Jolla, USA).

Potential differences in $C_{0.5}$, C_3 and C_5 between PNA groups were examined by the Kruscal-Wallis test using GraphPad Prism 8.2.1 (GraphPad Software, Inc., La Jolla, USA). Statistical significance was considered at $P \leq 0.05$.

Rosuvastatin pharmacokinetic parameters – area under the concentration-time curve from 0 to 5 h (AUC_{0-5}), area under the concentration-time curve from 0 to infinity ($AUC_{0-\infty}$), apparent volume of distribution (Vd) and apparent clearance (CL) were calculated in a one-compartmental pharmacokinetic model with first-order absorption and elimination kinetics based on body weight, administered rosuvastatin dose and measured rosuvastatin serum levels using MWPharm^{++} software (MediWare, Prague, Czech Republic). In this simplified model, the bioavailability was set to 100% and the absorption rate constant to 8.5 h^{-1} (corresponds to a t_{max} within half an hour) (12).The simulated rosuvastatin pharmacokinetic profile curve was individualized to maximize fitting with median rosuvastatin measured concentration points in each PNA group. The fitting was performed using Marquardt nonlinear least-square method. The goodness of fit was expressed using weighted sum of squares and root mean square values.

RESULTS

Bioanalytical assay validation

The developed method was linear in the range of 0.2-1000 ng/mL (R^2 > 0.9996). LLOQ was 0.2 ng/mL with precision and accuracy up to 14% (back-calculated). ULOQ was 1000 ng/mL with precision and accuracy up to 6% (back-calculated). The accuracy and precision of back-calculated concentrations of other calibration points were within 7% of the nominal concentration. The detection limit was 0.05 ng/mL, which was sufficient for the determination of rosuvastatin in serum samples. The accuracy of QC samples was within ±8.2 %, and interday and intraday precision were between 1.5 and 6.2 % (Table S1 in Supporting information). Recovery ranged from 97.6 to 102.1 % (Table S2 in Supporting information). The matrix effect ranged from 83 to 105%. The use of an isotope-labeled standard eliminated the matrix effect since the analyte/IS response ratio remained unaffected, even when the absolute responses of the analyte and IS were affected. The developed method was selective since no interfering peaks from endogenous serum components appeared at the retention time of rosuvastatin. The accuracy and precision of dilution integrity samples were within ±8%. No significant rosuvastatin degradation occured under the tested stability conditions. The accuracy of stability samples was within ±8 % with precision <6%. Stock solutions of rosuvastatin and its IS were stable under tested conditions. Representative MRM chromatograms of a serum blank sample, a blank serum sample spiked with rosuvastatin at the LLOQ concentration of 0.2 ng/mL, and a studied sample at the concentration of 23 ng/mL are depicted in Figure S1 (Supporting information). All validation parameters meet the criteria for bioanalytical methods and thus proved the reliability of this novel method developed for the determination of resuvastatin in serum samples.

In vivo pharmacokinetic study

Totally, 162 rat pups were enrolled into this study – six rats per sampling time (0.5, 3, and 5 hour after dosing) in each of nine PNA groups (1, 4, 7, 10, 14, 21, 28, 35, and 42 days). Among them, there were 85 males and 77 females as determined based on anogenital distance. We tried to keep the number of males and females in the PNA groups and sampling time subgroups balanced. Median body weights were 5.5, 9, 12, 17, 23, 39, 75, 125, and 174 g in 1, 4, 7, 10, 14, 21, 28, 35, and 42 PNA groups, respectively. Rosuvastain PK parameters in each PNA group are summarized in Table 1. The $C_{0.5}$, C_3, and C_5 were significantly different between PNA groups (P < 0.0001 at all sampling times). The concentration-time data as a dot plot and fitted pharmacokinetic profiles for each PNA group are presented in supplementary Figure 2 and supplementary Figure 3, respectively. Graphical illustration of rosuvastatin PK parameters against PNA is shown in Figure 1. Median (IQR) weighted sum of squares and root mean square values were 11.49 (5.53-23.90) and 0.95 (0.94-0.98), respectively.

DISCUSSION

The decision on hypolipidemic treatment onsent in patients with FH is currently mainly made based on LDL-C serum levels as this parameeter is thought to be a valid surrogate for clinical atherosclerotic cardiovascular disease and outcomes. Statin should be initiated as early as possible accordining to the current treatment guidelines for pediatric FH and the dose should be uptitrated to the maximum tolerated one (7).

The indication of rosuvastatin has been extended to children from 6 years based on the results of an open-label single arm CHARON study and a dedicated pharmacokinetic study that investigated pharmacokinetics and exposure to the drug as well as its efficacy and safety in this age group (13). Drug exposure in paediatric patients appeared to be dose proportional with only slightly increased drug accumulation observed in the pediatric population (1.8 fold) compared to the adult population (1.1-1.4 fold). This suggested that the t½ in children was only a little longer in comparison with that seen in adults (13).

The key active transporters involved in rosuvastatin hepatobiliary excretion (that is the major rosuvastatin elimination pathway) are multidrug resistance associated protein 2 (Mrp 2), bile salt export pump (Bsep), and multiple organic anion transporting polypeptides (OATP) family (14, 15). Approximate adult rat activities of these transporters may be expected after day 12 of PNA for Bsep and Mrp2 and on day 29 for OATP family based on expression levels relative to adult values achieved in the liver (16). These *in vitro* results well corresponded with the rise of rosuvastatin CL observed in our *in vivo* study. In this study, we observed that both rosuvastatin CL and Vd started to increase systematically between 2 and 3 weeks of rat PNA, which is reflected by the decreased total drug exposure.

Table 1. Pharmacokinetic parameters of rosuvastin according to PNA groups

PNA (days)	$C_{0.5}$ (mg/L)	C_3 (mg/L)	C_5 (mg/L)	AUC_{0-5} (mg.h/L)	$AUC_{0-\infty}$ (mg.h/L)	CL (L/h/kg)	Vd (L/kg)
1	4.150 (2.729-4.915)	0.417 (0.208-0.549	0.199 (0.160-0.503)	6.41	6.64	0.75	1.09
4	2.794 (2.246-3.334)	0.314 (0.240-0.530)	0.271 (0.173-0.350)	4.65	5.02	1.00	1.85
7	5.795 (5.452-8.925)	0.474 (0.322-0.788)	0.403 (0.324-0.566)	8.50	8.95	0.56	0.91
10	9.153 (5.574-11.175)	0.541 (0.212-0.906)	0.217 (0.119-0.510)	11.94	12.13	0.41	0.49
14	7.858 (6.498-9.128)	0.625 (0.526-0.800)	0.249 (0.176-0.351)	11.17	11.42	0.44	0.56
21	2.597 (0.334-2.958)	0.106 (0.867-0.130)	0.044 (0.033-0.064)	3.02	3.05	1.64	1.77
28	0.740 (0.609-0.874)	0.852 (0.387-0.105)	0.014 (0.008-0.018)	1.19	1.21	4.13	4.70
35	0.575 (0.279-0.629)	0.836 (0.380-0.867)	0.015 (0.011-0.023)	0.99	1.01	4.97	6.13
42	0.570 (0.414-0.814)	0.624 (0.332-0.776)	0.023 (0.016-0.031)	0.90	0.93	5.40	7.42

Data are presented as medians (interquartile range) or medians (PK parameters except $C_{0.5}$, C_3 and C_5 were estimated from concentration-time profiles that were simulated from levels obtained from all group probands, and therefore individual PK parameters, and thus variability cannot be calculated). PNA: postnatal age; $C_{0.5}$, C_3 and C_5: observed serum concentrations at 0.5, 3 and 5 hour after rosuvastatin administration; $AUC_{0-\infty}$: area under the curve from zero to infinity; AUC_{0-5}: area under the curve from 0 to 5 hours; CL: apparent clearance; Vd: apparent volume of distribution.

Although it is based only on an indirect comparison of the results from two studies, the ontogenic maturation of rosuvastin transport capacity is likely to explain our PK results. However, the extrapolation of our results to humans needs to be done cautiously as the knowledge about human ontogeny of drug transporter activity, which is essential for application of personalised tretment in pediatric population, is still limited. Mrp2 protein levels were significantly lower in liver specimens from children younger than 8 months in comparison with older children, while no significant age dependence of Mrp2 protein expression was observed in subjects from 7 to 63 years. For OATPs, the mRNA expression was 500 to 600-fold lower in neonates, and 90 to 100-fold lower in infants compared to adults. Similarly, mRNA expression of Bsep increased from neonates to older children and adults (17). Nevertheless, these sparse data correspond to the approximate similarity of rosuvastatin pharmacokinetics in children >6 years to that of adults seen in clinical drug development (13).

Equivalent human ages to the rat PNA ontogeny have been addopted from the study by Picut et al (18), who studied equivalent endocrinne maturational stages between rat and man. This interspecies scaling has been chosen as it has been documented that that hormonal signaling is an important factor for regulation of drug transporter activity (19). Table 2 shows approximate age comparison for developmental stages between rat and man as well as relative rosuvastatine exposure in each age group compared to the exposure in adults.

The C_{max} and AUC values at 35 and 42 days of PNA in our study were almost identical. This stage corresponds to equivalent human age of > 12 years, when the human drug pharmacokinetics is similar to that observed in adults (13, 20). Therefore, no further ontogeny of drug pharmacokinetics likely corresponds to the achievement of adult activities of the key pathways involved.

Table 2. Rosuvastatin exposure in equivalent age ranges for rat and human ontogeny

Age stage	Rat PNA	Human PNA	$AUC_{0-\infty}$ relative to adults
Newborn	0-7 days	0-28 days	540-962%
Infant	8-20 days	1-23 months	1228-1304%
Juvenile/child	21-32 days	2-12 years	109-328%
Puberty/adolescent	> 32 days	> 12 years	100%

Equivalent age ranges between rat and human was adopted from Picut *et al* (18).

At the rat age of 21 days (equivalent to human age of 2 years), the total exposure was approximately 3-times higher than in adults, while in rat pups younger than 21 days (equivalent to human neonates and infants) the drug exposure was extremely increased (from 5- to 13-fold higher) in comparison to the adult values. On the other hand, the drug exposure in rats aged 28 and 32 days have been only slightly increased in comparison to the expected adult exposures.

We acknowledge that there are some limitations of our study. Whereas this is the first exploratory study, several simplifications of the

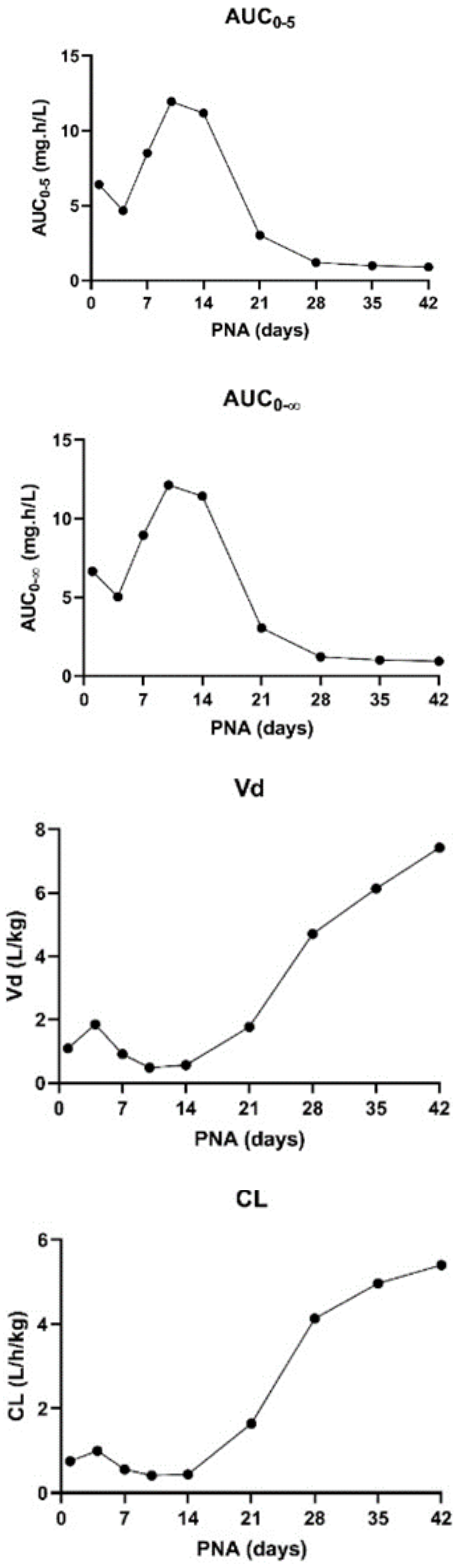

Figure 1. Development of pharmacokinetic parameters of rosuvastatin during postnatal ontogenesis. PNA: postnatal age; $AUC_{0-\infty}$: area under the curve from zero to infinity; AUC_{0-5}: area under the curve from 0 to 5 hours; CL: apparent clearance; Vd: apparent volume of distribution. Data are expressed as medians (PK parameters were estimated from concentration-time profiles that were simulated from levels obtained from all group probands, and therefore individual PK parameters, and thus variability cannot be calculated).

design have been incorporated. Although rosuvastain is intended for chronic treatment, we explored its pharmacokinetics after a single dose administration. Since both rosuvastatin plasma concentrations and AUC were described to be linear (9), this simplification shall not impact on the results and their interpretation. Rosuvastatin was administered intraperitoneally in our study, although oral application is typical in humans. Intraperitoneal administration represents a common technique in exploratory experiments with rodents as it enables reliable administration of relatively large volume of liquid medication and reduces the high variability in pharmacokinetics caused by the absorption phase. Moreover, we aimed to examine developmental changes caused especially by ontogenesis in hepatic transporters, and thus in elimination phase.

As the blood volume of such young pups is very limited, we have chosen sparse sampling approach. Limited number of measured concentrations was compensated by PK simulations to estimate the PK parameters. Since the absence of PK data for rosuvastatin in juveniles, we opted for the Marquardt nonlinear least-square method of fitting. This method fits a parameterized model to the set of data points by minimizing an objective expressed as the sum of the squares of the errors between the model function and a set of data points and thus limits the need for an initial model.

Rat as an experimental animal was chosen as traditionally the species of first choice for juvenile animal studies. Moreover, we aimed to describe mainly rosuvastatin elimination which is provided by the same transporters involved in both humans and rats (15). Both male and female rats were included in our study to mimick the real use of the drug in population. Exploration of the PK ontogeny in the age corresponding to children up to 6 years was the main aim of our study and sexual dimorphism is minor in this age group.

The typical reason for exclusion of female rats from experiments is the variability due to cyclical reproductive hormones (21). As the onset of puberty occurs in rats at PNA of 32 to 34 days, only the 2 highest age groups of rats used in our study (PNA 35 and 42) included females potentially impacted by the hormonal cycle.

CONCLUSIONS

Our study helps to understand exposure differences across age ranges from birth to sexual maturity in rats and the results may serve as a pre-clinical basis for future clinical development of rosuvastatin

containing formulations for FH treatment in pediatric patients up to 6 years of age.

Based on our data, it can be estimated, that rosuvastatin exposure may be substantially increased untill the age of 2 years. For children aged 2 - 6 years a dose reduction could be a feasible way, how to develop appropriate dosing schedule and formulations. However, since the interspecies scaling of PK data may not be fully accurate, the confirmation in clinical development studies will be needed.

ACKNOWLEDGMENTS. JR wishes to acknowledge the support provided by Pharmaceutical Applied Research Centre (The Parc) for her scientific work.

FUNDING. This research was funded by the Charles University Project Progres Q25 and a grant No. SVV 260523.

CONFLICTS OF INTEREST. The authors declare there are no competing interests.

REFERENCES

1. Wiegman A, Gidding SS, Watts GF, Chapman MJ, Ginsberg HN, Cuchel M, et al. Familial hypercholesterolaemia in children and adolescents: gaining decades of life by optimizing detection and treatment. Eur Heart J. 2015;36(36):2425-37.
2. Constantin AT, Covacescu SM, Kozma A, Gherghina I, Lazarescu H. Statins Treatment and Oro-Dental Aspects in a Case of Hereditary Hypercholesterolemia in a Child under 6 Years. Acta Endocrinol (Buchar). 2019;15(3):378-83.
3. Luirink IK, Hutten BA, Wiegman A. Optimizing Treatment of Familial Hypercholesterolemia in Children and Adolescents. Curr Cardiol Rep. 2015;17(9):629.
4. Pang J, Chan DC, Watts GF. The Knowns and Unknowns of Contemporary Statin Therapy for Familial Hypercholesterolemia. Curr Atheroscler Rep. 2020;22(11):64.
5. Braamskamp M, Langslet G, McCrindle BW, Cassiman D, Francis GA, Gagne C, et al. Efficacy and safety of rosuvastatin therapy in children and adolescents with familial hypercholesterolemia: Results from the CHARON study. J Clin Lipidol. 2015;9(6):741-50.
6. Stein EA, Dann EJ, Wiegman A, Skovby F, Gaudet D, Sokal E, et al. Efficacy of Rosuvastatin in Children With Homozygous Familial Hypercholesterolemia and Association With Underlying Genetic Mutations. J Am Coll Cardiol. 2017;70(9):1162-70.
7. Harada-Shiba M, Ohta T, Ohtake A, Ogura M, Dobashi K, Nohara A, et al. Guidance for Pediatric Familial Hypercholesterolemia 2017. J Atheroscler Thromb. 2018;25(6):539-53.
8. Miyagi Y, Harada-Shiba M, Ohta T. Effect of Statin Therapy in 4-Year-Old Dichorionic Diamniotic Twins with Familial Hypercholesterolemia Showing Multiple Xanthomas. J Atheroscler Thromb. 2016;23(1):112-7.
9. Luvai A, Mbagaya W, Hall AS, Barth JH. Rosuvastatin: a review of the pharmacology and clinical effectiveness in cardiovascular disease. Clin Med Insights Cardiol. 2012;6:17-33.
10. Crouse JR, 3rd. An evaluation of rosuvastatin: pharmacokinetics, clinical efficacy and tolerability. Expert Opin Drug Metab Toxicol. 2008;4(3):287-304.
11. Lu H, Rosenbaum S. Developmental pharmacokinetics in pediatric populations. The journal of pediatric pharmacology and therapeutics : JPPT : the official journal of PPAG. 2014;19(4):262-76.
12. Al Shoyaib A, Archie SR, Karamyan VT. Intraperitoneal Route of Drug Administration: Should it Be Used in Experimental Animal Studies? Pharmaceutical research. 2019;37(1):12.
13. European Medicines Agency. Assessment report: EMA/301931/2014. Available online: https://www.ema.europa.eu/en/documents/referral/crestor-article-29-paediatrics-referral-assessment-report_en.pdf (accessed on 02 May 2021).
14. Jemnitz K, Veres Z, Tugyi R, Vereczkey L. Biliary efflux transporters involved in the clearance of rosuvastatin in sandwich culture of primary rat hepatocytes. Toxicology in vitro : an international journal published in association with BIBRA. 2010;24(2):605-10.
15. Ho RH, Tirona RG, Leake BF, Glaeser H, Lee W, Lemke CJ, et al. Drug and bile acid transporters in rosuvastatin hepatic uptake: function, expression, and pharmacogenetics. Gastroenterology. 2006;130(6):1793-806.
16. Gao B, St Pierre MV, Stieger B, Meier PJ. Differential expression of bile salt and organic anion transporters in developing rat liver. Journal of hepatology. 2004;41(2):201-8.

17. Brouwer KL, Aleksunes LM, Brandys B, Giacoia GP, Knipp G, Lukacova V, et al. Human Ontogeny of Drug Transporters: Review and Recommendations of the Pediatric Transporter Working Group. Clinical pharmacology and therapeutics. 2015;98(3):266-87.
18. Picut CA, Dixon D, Simons ML, Stump DG, Parker GA, Remick AK. Postnatal ovary development in the rat: morphologic study and correlation of morphology to neuroendocrine parameters. Toxicologic pathology. 2015;43(3):343-53.
19. Yacovino LL, Aleksunes LM. Endocrine and metabolic regulation of renal drug transporters. Journal of biochemical and molecular toxicology. 2012;26(10):407-21.
20. Macpherson M, Hamren B, Braamskamp MJ, Kastelein JJ, Lundstrom T, Martin PD. Population pharmacokinetics of rosuvastatin in pediatric patients with heterozygous familial hypercholesterolemia. European journal of clinical pharmacology. 2016;72(1):19-27.
21. Zucker I, Beery AK. Males still dominate animal studies. Nature. 2010;465(7299):690.

Supplementary

Table S1. Accuracy and precision of the LC-MS/MS method (n=6 replicates; for 2 days)

Rosuvastatin concentration (ng/mL)	**Intra-day (*n=6*)**			**Inter-day (*n=6*)**		
	Measured concentrations (ng/mL) (mean±SD)	RSD (%)	RE (%)	Measured concentrations (ng/mL) (mean±SD)	RSD (%)	RE (%)
1	0.980 ± 0.031	3.2	-2.0	1.082 ± 0.067	6.2	8.2
50	51.900 ± 1.505	2.9	3.8	52.100 ± 1.771	3.4	4.2
500	494.500 ± 7.417	1.5	-1.1	515.500 ± 14.949	2.9	3.1

SD, standard deviation; RSD, relative standard deviation; RE, relative error

Table S2. Recovery of the LC-MS/MS method (n=6 replicates)

Recovery (%) (mean)	**Recovery (%) (mean)**	**SD (%)**	**RSD (%)**
1	97.6	1.46	1.50
50	99.1	1.90	1.92
500	102.1	1.99	1.86

SD, standard deviation; RSD, relative standard deviation

Příloha 2

HRINOVA, E., SKOREPOVA, E., CERNA, I., KRALOVICOVA, J., KOZLIK, P., KRIZEK, T., ROUSAROVA, J., RYSANEK, P., SIMA, M., SLANAR, O. & SOOS, M. 2022. Explaining dissolution properties of rivaroxaban cocrystals. Int J Pharm, 622, 121854.

International Journal of Pharmaceutics 622 (2022) 121854

Contents lists available at ScienceDirect

International Journal of Pharmaceutics

journal homepage: www.elsevier.com/locate/ijpharm

Explaining dissolution properties of rivaroxaban cocrystals

Erika Hriňová [a,*], Eliška Skořepová [a,c], Igor Čerňa [b], Jana Královičová [d], Petr Kozlík [e], Tomáš Křížek [e], Jaroslava Roušarová [d], Pavel Ryšánek [d], Martin Šíma [d], Ondřej Slanař [d], Miroslav Šoóš [a,*]

[a] Department of Chemical Engineering, University of Chemistry and Technology, Technická 3, 166 28 Prague 6 – Dejvice, Czech Republic
[b] Zentiva, k.s., U Kabelovny 130, 10237 Prague 10, Czech Republic
[c] Department of Structure Analysis, Institute of Physics of the Czech Academy of Sciences, Na Slovance 1999/2, 182 00 Praha 8, Czech Republic
[d] Institute of Pharmacology, First Faculty of Medicine, Charles University and General University Hospital in Prague, Prague, Czech Republic
[e] Department of Analytical Chemistry, Faculty of Science, Charles University, Prague, Czech Republic

ARTICLE INFO

Keywords:
Rivaroxaban
Cocrystal
Dissolution
Solid form transformation
Solubilization
In-vivo studies

ABSTRACT

The aim of this study was to improve rivaroxaban water-solubility by cocrystal preparation and to understand this process. The screening with water-soluble coformers was performed via both mechanochemical and solution-mediated techniques. Two cocrystals of rivaroxaban with malonic acid and oxalic acid were prepared, and the structure of the cocrystal with oxalic acid was solved. Both cocrystals exhibit improved dissolution properties. The mechanism of the supersaturation maintenance was studied by in-situ Raman spectroscopy. The transformation into rivaroxaban dihydrate was identified as the critical step in the improved dissolution properties of both cocrystals. Moreover, the transformation kinetics and solubilization effects of the coformers were identified as responsible for the differences in the dissolution behavior of the cocrystals. In-vivo experiments proved that the use of cocrystal instead of form I of free API helped to increase the bioavailability of rivaroxaban.

1. Introduction

Pharmaceutical cocrystals are multicomponent solid forms that consist of an active pharmaceutical ingredient (API) and coformer (Desiraju, 2003). The creation of cocrystals is used in the pharmaceutical industry to modulate physico-chemical properties of the API, for example melting point, rheological properties or dissolution rate and solubility (Elder et al., 2013; Skořepová et al., 2014; Jirát et al., 2020; Khandavilli et al., 2018; Sládková et al., 2017). In the field of crystal engineering, the selection of the right coformer is essential. It is because any new form's solubility is directly connected with the solubility of its components (Good and Rodríguez-Hornedo, 2009). On the other hand, cocrystals formed with coformers with water solubility over 10 mg/ml often exhibit lower physical stability and incongruent dissolution (Bhardwaj et al., 2017).

With the increasing number of poorly water-soluble APIs (Al-Kassas et al., 2017), supersaturating systems, such as amorphous solid dispersions (Kapourani et al., 2019; Lee et al., 2021; Metre et al., 2018), lipidic formulations (Ganesh et al., 2016; Xue et al., 2018), complexes with cyclodextrines (Sherje and Jadhav, 2018), nanoformulations (Demir et al., 2020; Anwer et al., 2020) and cocrystals (Ober et al., 2013) are gaining popularity. It is generally known that the supersaturating ability of the cocrystal can be caused by factors including higher energy state of the solid form, solubilization effect of the coformer, changes in the pH (Cao et al., 2016) and improved wettability (Machado et al., 2020).

It was previously reported in the literature that supersaturation effect can be erased by the precipitation of the stable API form from the solution (Shiraki et al., 2008). Supersaturation is a non-equilibrium state, and the system tends to stabilize itself by crystallization of the stable API form. The precipitation during the dissolution can be observed especially on the surface of the cocrystal particles (Omori et al., 2020). This can influence further dissolution of the cocrystal particles by covering their surface by a poorly soluble form and thus creating a barrier between the dissolution medium and the cocrystal particle surface. Re-crystallization lowers the positive effect of the cocrystal in the formulation, resulting in the API solubility equal to the more stable, free form's solubility. On the other hand, even if the free form is stable in the used system, the transformation kinetics plays an important role in achieving supersaturation (Bhardwaj et al., 2017). There also exist strategies to inhibit crystallization, i.e., by addition of

* Corresponding authors.
E-mail address: hrinovae@vscht.cz (E. Hriňová).

https://doi.org/10.1016/j.ijpharm.2022.121854
Received 23 February 2022; Received in revised form 5 May 2022; Accepted 20 May 2022
Available online 25 May 2022

the surfactant into the formulation. Surfactant affects the solubility of the API and cocrystal in different way decreasing the gap between cocrystal and API solubility. As a result, API crystallization is minimized (Cao et al., 2016).

In our study, active pharmaceutical ingredient rivaroxaban was used as a model API. Rivaroxaban belongs to the BCS II category because of its low water solubility and high permeability. Low solubility was suggested to be the cause of the food effect on the absorption (Takács-Novák et al., 2013). Cocrystal formation was selected as a promising method to increase solubility because salt formation is not feasible due to the absence of ionizable functional groups. The screening and characterization of the obtained new forms was performed with the emphasis on the dissolution behavior. This includes the measurement of the intrinsic dissolution rate and 12-hour dissolution experiments to obtain information about dissolved amount of rivaroxaban from cocrystals during biologically relevant time interval. The obtained results indicated an increase of solubility during long-term experiments, suggesting a transformation into new form with even higher solubility. A study of solid-phase transformations under the same conditions revealed that this new form is a dihydrate. The effect on the bioavailability was tested in vivo. For the removal of the food effect, fasted state bioavailability of rivaroxaban needs to be increased (Kushwah et al., 2021). In vivo study revealed that the use of cocrystal with increased water solubility leads to significantly increased bioavailability in rats indicating the successful removal of the food effect.

2. Materials and methods

2.1. Materials

Rivaroxaban form I was kindly provided by Zentiva, k.s. Solvents and coformers were obtained by various commercial suppliers and used as received.

2.2. Cocrystals preparation and characterization

2.2.1. Screening

Water soluble dicarboxylic acids were selected as coformers, namely oxalic acid, malonic acid, succinic acid, glutaric acid, fumaric acid, malic acid and tartaric acid. 30 mg of rivaroxaban was dissolved in 1 ml 2,2,2-trifluoroethanol at 50 °C. Two molar equivalents of the coformer were added to the solution and stirred for 1 h. After cooling down, solvent was let to evaporate until solid phase was obtained and analyzed by Raman spectroscopy.

The same coformers were used also for the screening through ball-milling using vibratory ball mill Retsch MM 200 (Retsch, Germany). 40 mg of API and 1 M equivalent of coformer were weighed into the Eppendorf tubes. 10 μl of methanol, tetrahydrofurane or 2,2,2-trifluoroethanol was added to the mixture. Mixtures were milled at 25 Hz for 15 min with one 3 mm metal milling ball. Each experiment was repeated three times to evaluate process reproducibility.

2.2.2. Single crystal preparation

Rivaroxaban and oxalic acid were dissolved in 1:1 M ratio in 2,2,2-trifluoroethanol. One drop of ethanol was added to the solution as an antisolvent. The solution was placed into the vial covered with the needle perforated lid followed by slow evaporation of the solvent. After three weeks, single-crystals were obtained.

2.2.3. Single crystal x-ray diffraction

The analysis was performed at 95 K using a SuperNova diffractometer with a micro-focus sealed tube, mirrors-collimated Cu-Kα radiation (λ = 1.54184 Å), and CCD detector Atlas S2. The data reduction and absorption correction were done with CrysAlisPro software (CrysAlisPro; Oxford Diffraction, 2002). The structures were solved by charge flipping methods using Superflip software (Palatinus and Chapuis, 2007) and refined by full matrix least squares on F squared value using Crystals and Jana2006 (Betteridge, 2003; Petricek et al., 2006) software.

The hydrogen atoms were located in a Fourier difference map, but those attached to carbon atoms were repositioned geometrically. The hydrogen atoms were initially refined with soft restraints on the bond lengths and angles to regularize their geometry (C—H in the range 0.93–0.98 Å, N—H to value of 0.86 Å, O—H to value of 0.82 Å) and Uiso (H) (in the range 1.2–1.5 times Ueq of the parent atom). Then, the hydrogen positions were refined as riding. Molecular graphics were prepared in Mercury (Mercury; CCDC, 2007). The structure was deposited into the Cambridge Structural Database under number 2127012.

2.2.4. Preparation of cocrystals in larger quantities

1 g of rivaroxaban was dissolved in 5 ml of 2,2,2-trifluoroethanol at 80 °C under reflux. 286 mg of oxalic acid dihydrate was added and stirred for 5 min. The solution was then cooled slowly within 4 h to the laboratory temperature. Approximately at 40 °C, the solid form started to crystallize, and dense suspension was obtained and filtered.

In the case of rivaroxaban cocrystal with malonic acid 1 g of rivaroxaban was dissolved in 5 ml of 2,2,2-trifluoroethanol at 80 °C under reflux followed by dissolution of 239 mg of malonic acid. The solution was let to cool down and stirred at laboratory temperature overnight. A suspension was obtained and filtered.

2.2.5. Intrinsic dissolution rate

Intrinsic dissolution rate (IDR) was determined using a Sirius inForm (Pion inc., USA) device. IDR discs with a 6 mm diameter were prepared by the compression of approximately 100 mg of the cocrystals. The material was compressed at a constant load of 100 kg, relaxed for 1 min, and compressed again at a constant load of 100 kg for a second minute. IDR measurements were performed in 60 ml of phosphate buffer solution at pH 6.8 with the addition of 0.2% of sodium dodecyl sulfate (SDS) at the stirring speed of 100 rpm. UV spectra were recorded every 30 s using probe with the optical path length equal to 5 mm. Absorbance between wavelengths of 220–320 nm was used to evaluate the amount of the released API at each time point. IDR was obtained from the linear fit of the first 10 min of the measurement. The first two points were excluded as they usually represent the dissolution of the free powder captured on the disc during the preparation.

2.2.6. Powder dissolutions

Powder dissolution measurements were performed using Sirius T3 (Pion inc. USA) device. The measurements were performed in 3 ml of deionized water at stirring speed 100 rpm. 2 mg of the cocrystal, rivaroxaban, or physical mixtures were suspended in the dissolution medium. The amount of the solid form introduced into dissolution medium was higher than expected solubility to ensure non-sink conditions resulting in the presence of the solid phase during the whole experiment.

UV spectra were recorded every 60 s with the total duration of 720 min. The concentrations were calculated using absorbance measured at 246.9 nm. The physical mixtures were prepared by mixing rivaroxaban and the acid in the same molar ratio as in the cocrystal (1:1 for oxalic acid and 2:1 for malonic acid) and homogenized for 1 min in the table mixer Philips 2860 (Philips, NL).

For the calibration curve measurement, 10.01 mg of rivaroxaban were dissolved in 5 ml of dimethylsulfoxide. 10, 20, 30, 40 and 50 μl of the stock solution was diluted into 5 ml of water and absorbance at 246.9 nm was collected.

2.2.7. Rivaroxaban dihydrate preparation

400 mg of the oxalic acid cocrystal was suspended in 10 ml of water and stirred at 100 rpm overnight. The solid form was filtered, washed with 20 ml of purified water and spread over the glass funnel and let dry for approximately 30 min.

2.2.8. Rivaroxaban dihydrate solubility measurement

To prepare the dihydrate of rivaroxaban and measure its solubility, 30 mg of the rivaroxaban cocrystal with oxalic acid was suspended in 1 ml of water and stirred at 100 rpm overnight. The suspension was centrifuged, the solution was aspirated, and the solid form was washed with 1 ml of 1 M solution of sodium hydroxide to ensure the removal of the oxalic acid from the sample followed by washing with 1 ml of deionized water. After washing, 1 ml of deionized water was added, and the resulting suspension was stirred for 12 h. After this time, the sample was centrifuged, the solution was aspirated and filtered through 0,45 μm filter. 3 ml of the collected solution was used for absorbance measurement at 246.9 nm using Sirius T3 instrument.

2.2.9. Phase transformation measurements

To measure solid state transformations while cocrystal is suspended in the water, EasyMax 402 Workstation (METTLER TOLEDO) with 100 ml reactor was used. To obtain solid form information, Raman spectrometry measured in situ with online probe was used. Sampling interval was set to 3200–100 cm^{-1} and laser power was set to 300 mW. For oxalic acid cocrystal, the exposition time was set to 3 s using 35 scans with sampling every 10 min. For malonic acid cocrystal, the transformation was faster, therefore the sampling interval was reduced to 30 s. To improve the signal to noise ratio, the exposition time was reduced to 2 s applying 13 scans (with shorter sampling time, the time available for measurement was reduced too and required settings adaptation to maximize resolution).

2.2.10. X-ray powder diffraction (XRPD)

The diffraction patterns were collected with a powder diffractometer device X'PERT PRO MPD PANalytical; X-ray beam Cu Kα ($\lambda = 1.542$ Å), measured range: $2 - 40^{\circ}$ 2θ, excitation voltage: 45 kV, anodic current: 40 mA, step size: 0.01° 2θ, remaining at a step for 0.05 s. The measurement was performed on a flat sample with an area/thickness ratio equal to 10/0.5 mm. The 0.02 rad Soller slits, 10 mm mask, and $1/4^{\circ}$ fixed antiscattering slits were used to correct the primary beam. The irradiated area of the sample was 10 mm; programmable divergent slits were used. The 0.02 rad Soller slits and 5.0 mm antiscattering slits were used to correct the secondary beam. HighScore Plus software was used to process the diffraction patterns.

2.2.11. Raman spectroscopy

Samples were measured in HPLC glass vials in a spectrometer device FTRaman RFS100/S, with germanium detector (Bruker Optics, Germany). The wavelength of the Nd:YAG laser was 1064 nm. The measuring range was from 4000 to 200 cm^{-1} with the spectral resolution of 4.0 cm^{-1}. 64 scans were accumulated for a single measurement. The software OMNIC and OPUS were used to process the obtained Raman spectra.

2.2.12. Solution NMR

Solution NMR was used to confirm the absence of oxalic acid in the hydrate sample. The sample was dissolved in d6-DMSO, and 13C NMR spectra were measured by Bruker Avance III 500 MHz NMR spectrometer equipped with Prodigy probe and with repetition delay of 10 s. The sample was proven to contain no oxalic acid.

2.2.13. Thermogravimetric analysis (TGA)

Samples were weighed in an aluminum pan (10 mg). All the measurements were performed on the TGA 6 (PerkinElmer, USA). The range of investigated temperatures was from 15 to 300 °C with the heating rate 10 °C/min.

2.2.14. Differential scanning calorimetry (DSC)

Samples were weighed in an aluminum pan (10 mg). The pan was covered, and the measurement was carried out under a nitrogen gas flow of 50 ml/min. All the measurements were performed on the TA Instruments Discovery DSC. The range of investigated temperatures was from 0 to 300 °C with the heating rate 5 °C/min.

2.3. In vivo study

2.3.1. Materials

Isoflurane (IsoFlo 250 ml, Zoetis, Czech Republic), xylazine (Rometar 20 mg/ml inj sol, Bioveta, Czech Republic) and ketamine (Narkamon 100 mg/ml inj sol, Bioveta, Czech Republic) were used for anesthesia, ketoprofen (Ketodolor 100 ml inj, LeVet Beheer B. V., Netherlands) was used for perioperative analgesia, and heparin (Heparin Léčiva 1x10 ml/50KU inj, Zentiva, k. s., Czech Republic) was used for catheter patency maintenance.

2.3.2. Animals

Male Wistar Rats were provided by Velaz (Prague, Czech Republic). Before and during the study, they were kept under standard conditions with 12-h light-dark cycle, temperature 22 ± 2 °C, and relative humidity $50 \pm 10\%$. They were fed by standard granulated diet and water *ad libitum*. The experiment was executed in conformity with the Guiding Principles for the Use of Animals in Charles University, First Faculty of Medicine. Every possible effort to minimize suffering of animals was made. The experimental animal project was approved by the Ministry of Education, Youth and Sports, Czech Republic (MSMT-11957/2021-4).

2.3.3. Preparation of tested formulation for in vivo dosing

The original drug product (Xarelto, Bayer, Germany) was crushed into powder and put into the 9el capsules (Reference formulation). For the Test formulation, the 9el capsules were filled with the powder with containing rivaroxaban as a cocrystal with oxalic acid. In both formulations, 4 mg of rivaroxaban were administered, representing 4 mg of the form I or 4,83 mg of the cocrystal.

2.3.4. Experimental design and procedure

A randomized, single dose, laboratory blinded, 2-period, 2-sequence, cross-over study was conducted in rats to compare bioavailability of a new formulation containing rivaroxaban (cocrystal with oxalic acid) with a reference product (Xarelto) in a fasted state.

Totally, 12 rats were enrolled into the study. Three days before the first dosing (period 1), right *v. jugularis* of each rat was cannulated. Anesthesia for cannulation was induced by 2.5–5% isoflurane (by inhalation) and maintained by a combination of xylazine (5 mg/kg, intramuscularly) and ketamine (100 mg/kg, intramuscularly). Ketoprofen (5 mg/kg, subcutaneously) was administered to the rats at the end of the surgery to relieve pain from the intervention. Catheters were flushed with physiological saline (200 μl), heparin (50 μl) and finally a mixture of heparin with glycerol (to seal the catheters). The rats were then randomly assigned into two groups.

After three days (period 1), one capsule of rivaroxaban formulation was administered orally to each rat, using X-9el dosing syringe (from Torpac Inc., Farfield, USA). Immediately after drug dosing, each rat was given 1 ml of water by oral gavage. Food was removed 4 h before the dosing and the rats did not have access to it for another 4 h to achieve fasted state.

Blood samples were collected via catheters before dosing and at following time points: 0.5, 1, 1.5, 2, 2.5, 3, 4, 6 and 8 h after drug administration. Totally 100 μl of blood was taken at each time point, followed by intravenous administration of physiological saline (100 μl) and a mixture of saline with heparin (1250 IU/ml, 50 μl) to replace the blood volume and prevent blood clotting in the catheter. The samples were centrifuged (4500*g*, 4 °C, 10 min), serum was separated and stored until further analysis (−80 °C).

After a 48-hour washout period, the procedures (period 2) were identical, but each study animal was administered a different formulation than in the first period according to the randomization list.

Table 1
Screening results.

Coformer	Fumaric acid	Oxalic acid	Malonic acid	Succinic acid	Tartaric acid	Glutaric acid	Malic acid
Solution	×	✓	✓	×	×	×	×
Ball-milling	×	×	✓	×	×	×	×

2.3.5. Bioanalytical methods

Concentrations of rivaroxaban were determined in serum. Before the analysis, 20 μl of serum samples were deproteinized by adding 60 μl of 100% acetonitrile (containing rivaroxaban-d4 as internal standard (IS) at a concentration of 50 ng/ml). Deproteinization was performed in an Eppendorf tube by vortexing for 15 s. Then, samples were centrifuged at 12,500*g* for 8 min, and 40 μl of supernatant was transferred into LC vials and injected into a UHPLC-MS/MS system. Measurements were performed using a Nexera X3 UHPLC coupled with Triple Quad 8045 MS (Shimadzu, Kyoto, Japan). Chromatographic analysis was performed on a Poroshell 120 SB-AQ column (100 × 2.1 mm; 2.7 μm; Agilent Technologies, Inc., Santa Clara, CA, USA). Mobile phase consisted of 0.1% formic acid in deionized water (Solvent A) and acetonitrile with 0.1 % formic acid (Solvent B). The flow rate of the mobile phase was maintained at 0.4 ml/min, and the injection volume was 1 μl. The temperature of the column was kept at 40 °C and samples were thermostated at 10 °C. Optimized gradient elution was carried out as follows (min/% B): 0/30, 3.0/70, 4.0/70, 4.5/30, and 7.0/30. Effluent from the column was directed to the MS ion source between 1.2 and 3.0 min only. For the rest of the time, the effluent was directed to the waste. The MS/MS spectrometer was operated in a positive mode. The applied conditions of the electrospray ion source were: nebulizing gas flow: 3 l/min, heating gas flow: 10 l/min, interface temperature: 300 °C, desolvation line temperature: 250 °C, heat block temperature: 400 °C, and drying gas flow: 10 l/min. The MS/MS measurement was performed in multiple reaction-monitoring mode (MRM). MRM transitions of 436.1 > 145.0 (Q1 pre-bias −12 V, Q3 pre-bias −27 V and collision energy −30 V) and 440.1 > 145.0 (Q1 pre-bias –22 V, Q3 pre-bias −25 V and collision energy −25 V) were monitored for rivaroxaban and rivaroxaban-d4, respectively.

Calibration samples were prepared in blank matrix (serum) at eight concentration levels. The ratio of the peak area of the analyte and the peak area of deuterium-labeled IS was plotted against analyte concentration. Calibration curve parameters were obtained using $1/x^2$-weighted least-squares linear regression analysis. The method was linear (coefficients of determination (R^2) higher than 0.9998) in the concentration range of 1–1000 ng/ml. The method was validated according to the requirements of the European Medicines Agency (EMA) Guideline on bioanalytical method validation (Guideline, 2021). All validation parameters fulfilled the guideline acceptance criteria for bioanalytical methods and thus proved the reliability of this method for the determination of rivaroxaban concentration in serum samples.

2.3.6. Data analysis and statistics

Measured serum concentration values were normalized to the weight of each rat before further calculations. Exact actual sampling times were used for all pharmacokinetic calculations, while scheduled sampling times were used for plotting of mean pharmacokinetic profiles in the graphs.

Phoenix WinNonlin® 8.3 (Certara, Princeton, USA) was used for pharmacokinetic and equivalence analysis. Pharmacokinetic parameters – maximum serum concentration (C_{max}), time to maximum serum concentration (t_{max}) and area under the concentration-time curve (AUC) were evaluated. The natural logarithmic transformation of C_{max} and AUC_{0-t} was used for all statistical inference. AUC_{0-t} was calculated using the trapezoidal rule, while C_{max} and t_{max} were taken directly from the observed data. The pharmacokinetic parameters were analyzed using an ANOVA model. The fixed factors included in this model were the effects

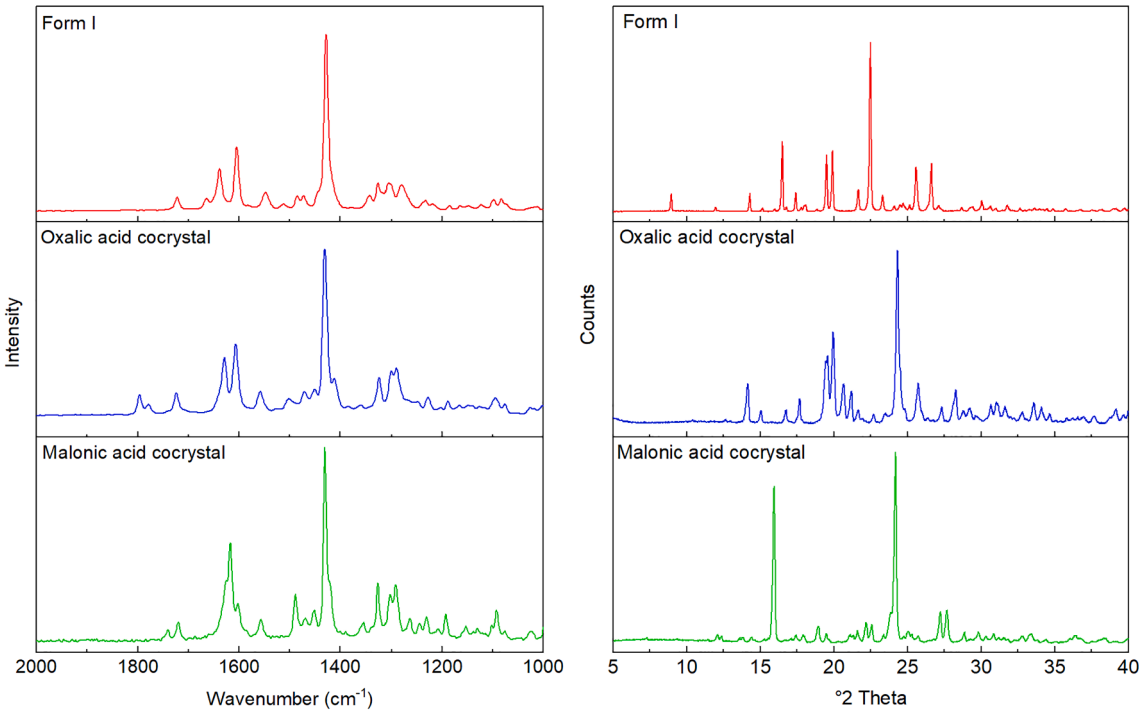

Fig. 1. Raman spectra (left) and XRPD spectra (right) of new forms prepared during screening, spectra of samples from co-crystallization screening significantly differ from the initial form I.

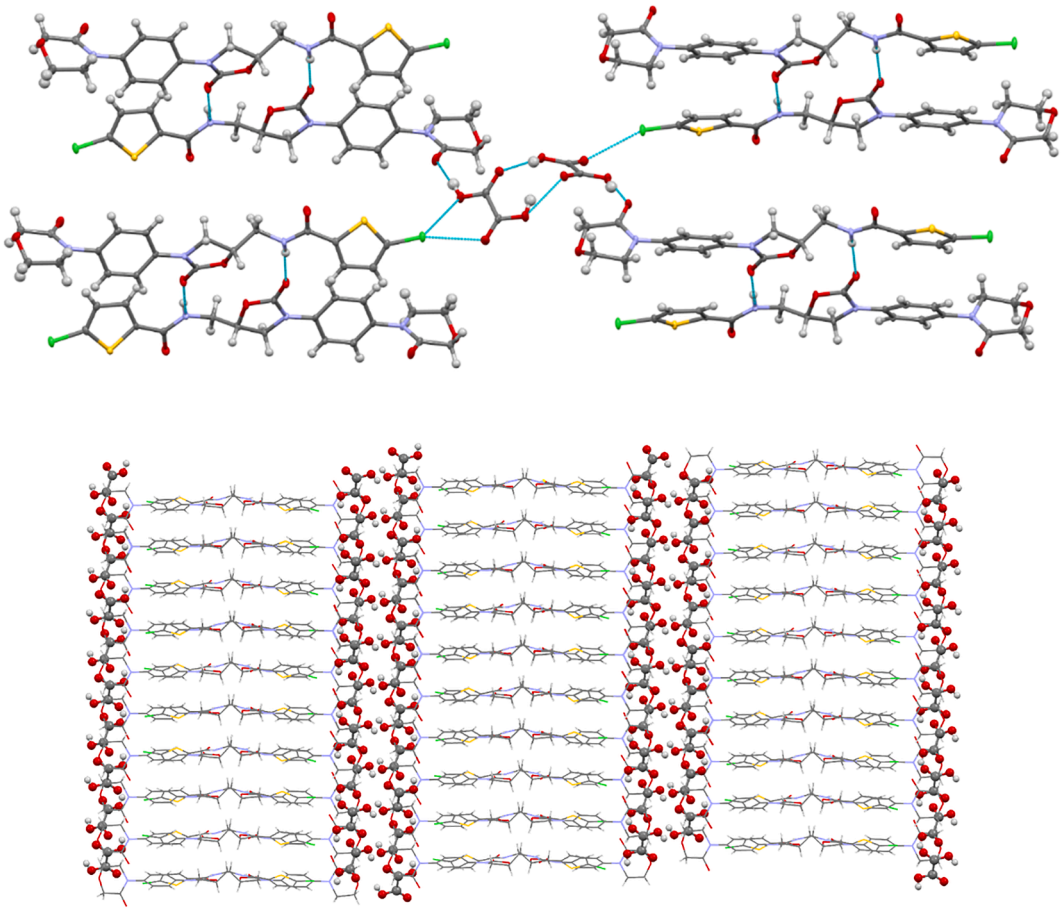

Fig. 2. Intermolecular interactions in the structure of rivaroxaban cocrystal with oxalic acid.

of subject, treatment, period, and sequence. The 90% confidence interval for the ratio of geometric least-squares means between the test and reference products was calculated.

Comparison of mean pharmacokinetic parameters and mean concentration in each sampling time was performed using paired *t*-test in GraphPad Prism version 9.1.0. (GraphPad Software, San Diego, CA, USA). Statistical significance was considered at $P \leq 0.05$.

3. Results and discussion

3.1. Screening

Based on the previously reported cocrystal of rivaroxaban with malonic acid (Kale et al., 2019), dicarboxylic acids were selected as suitable coformers for the screening. With the goal of solubility enhancement in mind, only water-soluble acids were selected, namely fumaric acid, oxalic acid, malonic acid, succinic acid, tartaric acid, glutaric acid and malic acid. The excess of the coformer was used to achieve higher coformer activity (Zhang et al., 2007) for cooling crystallization experiments. Only two strongest acids with the shortest chain length were successful in cocrystal creation, namely oxalic acid and malonic acid. In the case of other coformers only crystals of individual components were recovered after the experiment.

The same coformer set was used for the mechanochemical screening based on the ball milling experiments. Milling can be used to obtain different metastable multicomponent forms by introducing the energy into the mixture of conformer and API. Wet milling was selected because of its higher rate of success in preparation of new forms (Chatziadi et al., 2020). However, this type of screening was less successful because only the cocrystal with malonic acid was prepared (see Table 1). It can be assumed that lower success of milling can be caused by destruction of emerging cocrystal during milling. This was indicated by lower amount of malonic acid cocrystal in samples milled for longer time. Moreover, form I present during experiment can induce recrystallization back to form I instead of cocrystal formation. Theoretically, use of metastable form as an input material could result in more successful screening (Chatziadi et al., 2020).

In Fig. 1 is shown the comparison of Raman spectra and XRD difractogram of rivaroxaban Form I together with both prepared cocrystals. As can be seen, patterns for both new solid forms are significantly different compared to pure rivaroxaban, suggesting formation of a different solid form, later on found to be rivaroxaban cocrystals.

3.2. Cocrystal characterization

Both cocrystals were further characterized to select the best candidate for consequent development. The single-crystal of the rivaroxaban – oxalic acid cocrystal was successfully prepared and the structure was solved. This allowed us to compare the structure with previously reported crystal structure of the cocrystal with malonic acid (see Figs. 2 and 3).

Both cocrystals crystallize in the triclinic crystal system with non-centrosymetric *P*1 space group with four rivaroxaban molecules and four oxalic acid molecules or two malonic acid molecules in the unit cell. This finding corresponds to the molar ratio 1:1 for oxalic acid and 1:2 for malonic acid between API and coformer. In both structures, API molecules interact between each other by hydrogen bonds formed between the carbonyl group on the oxazolidine of one API molecule and the amide group of the second API molecule. These API molecules further interact with the coformer. Carboxylic functional group of the acid

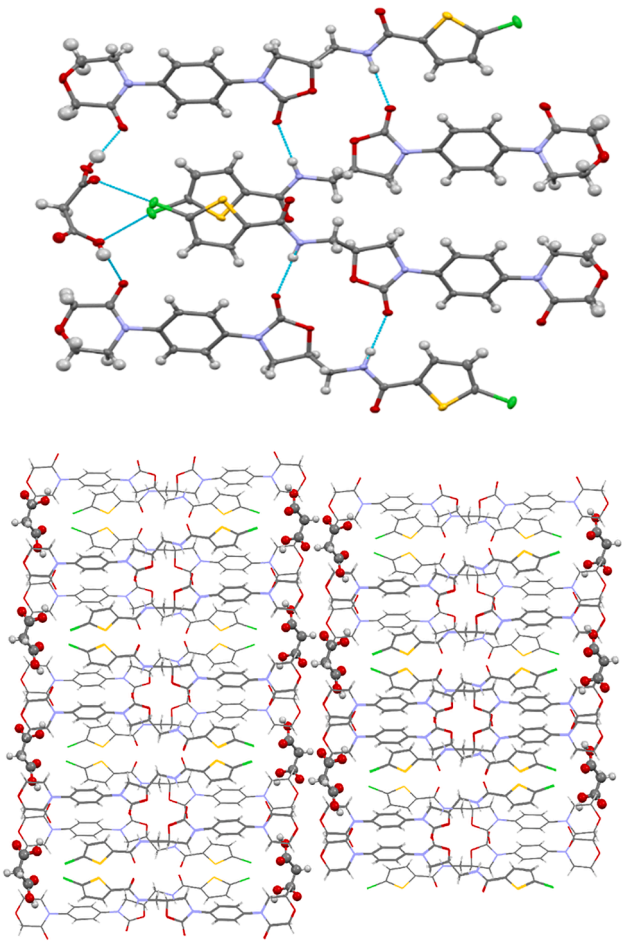

Fig. 3. Intermolecular interactions in the structure of rivaroxaban cocrystal with malonic acid. Crystal structure obtained according to Kale et al. (Kale et al., 2019).

forms hydrogen bonds oxygen atom from the oxomorpholine part and halogen bonds with chlorine. The main difference is in the number of hydrogen bonds between API and coformer molecule. Oxalic acid binds only to one chlorine atom and one oxygen atom with two more possible hydrogen bonds free for interacting between two molecules of oxalic acid. This type of the hydrogen bonds is creating structure with channels formed by the oxalic acid between parts formed by the rivaroxaban. On the other hand, one malonic acid molecule interacts with four API molecules by four hydrogen bonds.

The thermal behavior of the cocrystals was studied to see the possible temperature-dependent transformations. Both cocrystals exhibit lower melting point (see Fig. 4A) than the API. Interestingly, in the DSC curve of the cocrystal with malonic acid, there exist an endothermic event at 115 °C. This event was previously reported at the same temperature as a solid state (most probably polymorphic) transformation and was observed during hot stage microscopy (Kale et al., 2019). The difference in the melting temperatures of both cocrystals is quite low (166 °C for malonic acid vs 170 °C for oxalic acid) even though hydrogen bonding between API and coformer molecules inside crystal structures is significantly different. Both cocrystals exhibit melting and eventual transformation (in the case of malonic acid cocrystal) at sufficiently high temperature to be avoided during standard storage conditions. Both cocrystals recrystallize after their melting into form I with melting temperature 230 °C.

Further characterization of prepared solid forms was done by measuring dissolution properties. As can be seen in Fig. 4B, both cocrystals exhibit significantly higher dissolution rate in comparison with pure rivaroxaban form I. When taking into account the error bars of measurements caused by disks variation during preparation, it can be concluded that the IDR values for both cocrystals are similar. Apart from the dissolution rate measurement, we further characterized the achieved supersaturation and its evolution during biorelevant time using powder dissolution measurement (see Fig. 4C). This measurement was used to characterize kinetic solubility of the cocrystal considering cocrystal slurry in the water. Please note, that if the precipitation of the more stable form would occur within this time period, it would be noted by decrease of the achieved concentration. Therefore, it is crucial to characterize both dissolved amount and precipitation together because crystallization of the more stable form can be a reason why sufficient supersaturation is not achieved during cocrystal dissolution. The maximum achieved dissolved amount of the rivaroxaban from cocrystal with oxalic acid was higher (14.7 μg/ml ± 0.16) than the dissolved amount of rivaroxaban from the cocrystal with malonic acid (12.7 μg/ml ± 0.3). No significant decrease during the whole experiment was observed. Small fluctuations and decrease of the dissolution curve at the end of the measurement for the malonic acid cocrystal (see Fig. 4C), is caused by signal interference with the small crystals sticking to the probe, not by API precipitation. However, while the cocrystal with malonic acid achieved the maximum dissolved amount of rivaroxaban fast and remained the same for the rest of the experiment, the initially fast dissolution of the cocrystal with oxalic acid was followed by a slow increase of the curve within approximately 500 min (8 h). This behavior can indicate transformation of the solid form from cocrystal to a more soluble, metastable form.

3.3. Achievement of supersaturation with respect to form I

Presented results indicate two times higher solubility of the rivaroxaban when cocrystals are used instead of form I. Supersaturating systems usually tend to stabilize by precipitation of the stable API form. Transformation of the solid form present in the dissolution medium was previously reported in the literature (Babu and Nangia, 2011). In our dissolution measurements, the decrease of the curve related to the amount of dissolved API in the solution was not observed, even during the period of 12 h. However, slow increase of the dissolved API amount in time for the cocrystal with oxalic acid does not correspond to the high intrinsic dissolution rate that was measured previously. In situ measurement of solid form during slurrying in water was performed to confirm the presence of cocrystal during the whole experiment and to observe possible transformations that led to the growth of the dissolution curve for the cocrystal with oxalic acid.

Results in Fig. 5 show that both cocrystals transform into the same new form, but within different time intervals. Interestingly, the new form does not correspond to any known polymorphic forms of rivaroxaban. Moreover, the absence of decline of the dissolution curve indicates high solubility of the new form prepared during slurrying. Cocrystal with malonic acid has typical peaks at 1617 and 1488 cm^{-1} (see Fig. 5A). During the transformation, new form was observed by appearance of peaks at 1629 and 1611 cm^{-1}. With the proceeding transformation, typical peaks of the cocrystal are lowering until they fully disappear within 22 min. Cocrystal with oxalic acid (see Fig. 5B) has typical peaks at 1796, 1779, 1628 and 1608 cm^{-1}, with the first two most probably corresponding to the oxalic acid in the cocrystal. During the time, the peaks at 1796 and 1779 cm^{-1} are disappearing while peaks at 1628 and 1608 cm^{-1} are slowly moving to the positions towards right for the new form together with appearance of the small peak at 1644 cm^{-1}. In this case, the transformation was significantly slower taking approximately 8 h to complete.

Based on above mentioned spectral analysis we propose that the different transformation time is connected to the difference in the inner crystal structures as well as different molar ratio in the cocrystal between coformer and API. Higher amount of well soluble coformer in the cocrystal with malonic acid (1:2 M ratio) is most probably responsible

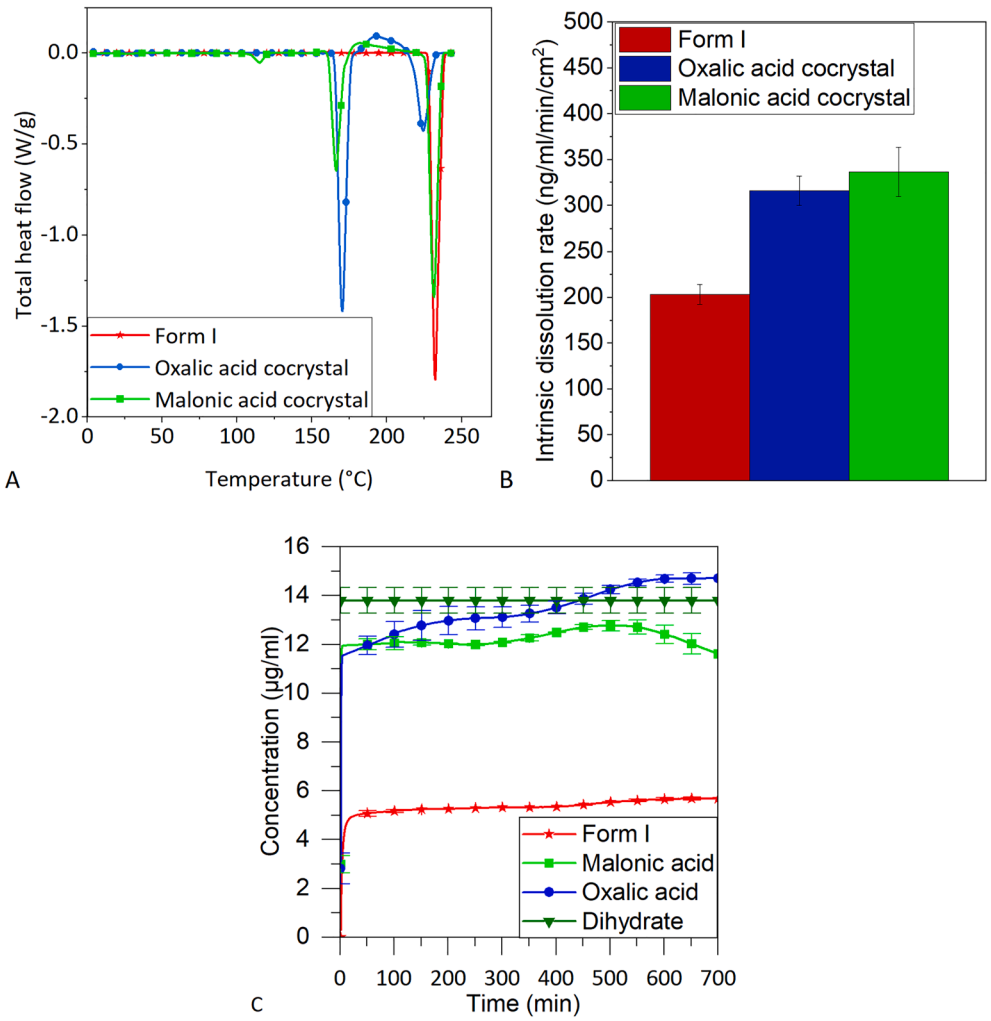

Fig. 4. A) DSC curves of both cocrystals and form I of pure API. B) Intrinsic dissolution rate values for both cocrystals compared to form I of pure API. C) 12 h long dissolution tests.

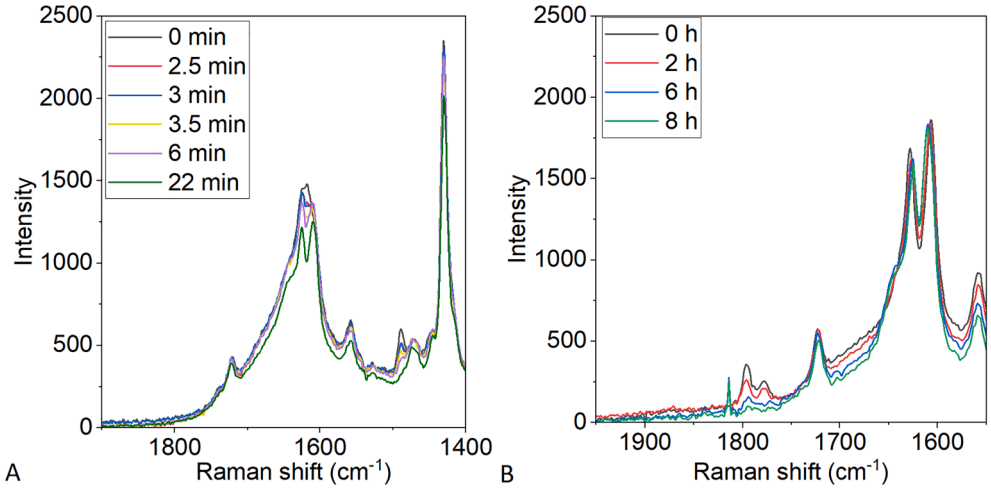

Fig. 5. A) Phase transformation of cocrystal with malonic acid in water measured by Raman probe B) Phase transformation of cocrystal with oxalic acid in water measured by Raman probe.

for its faster transformation. We believe that the mechanism of cocrystals transformation can be explained by the formation of supersaturated solution of rivaroxaban due to high dissolution rate of both cocrystals. Since highly soluble coformers are not capable to stabilize the supersaturated solution of rivaroxaban, this is precipitating into metastable form. Once precipitated, new equilibrium between new solid form and liquid phase is established on the level as presented in Fig. 4C. This was further tested by precipitation experiment of rivaroxaban from its

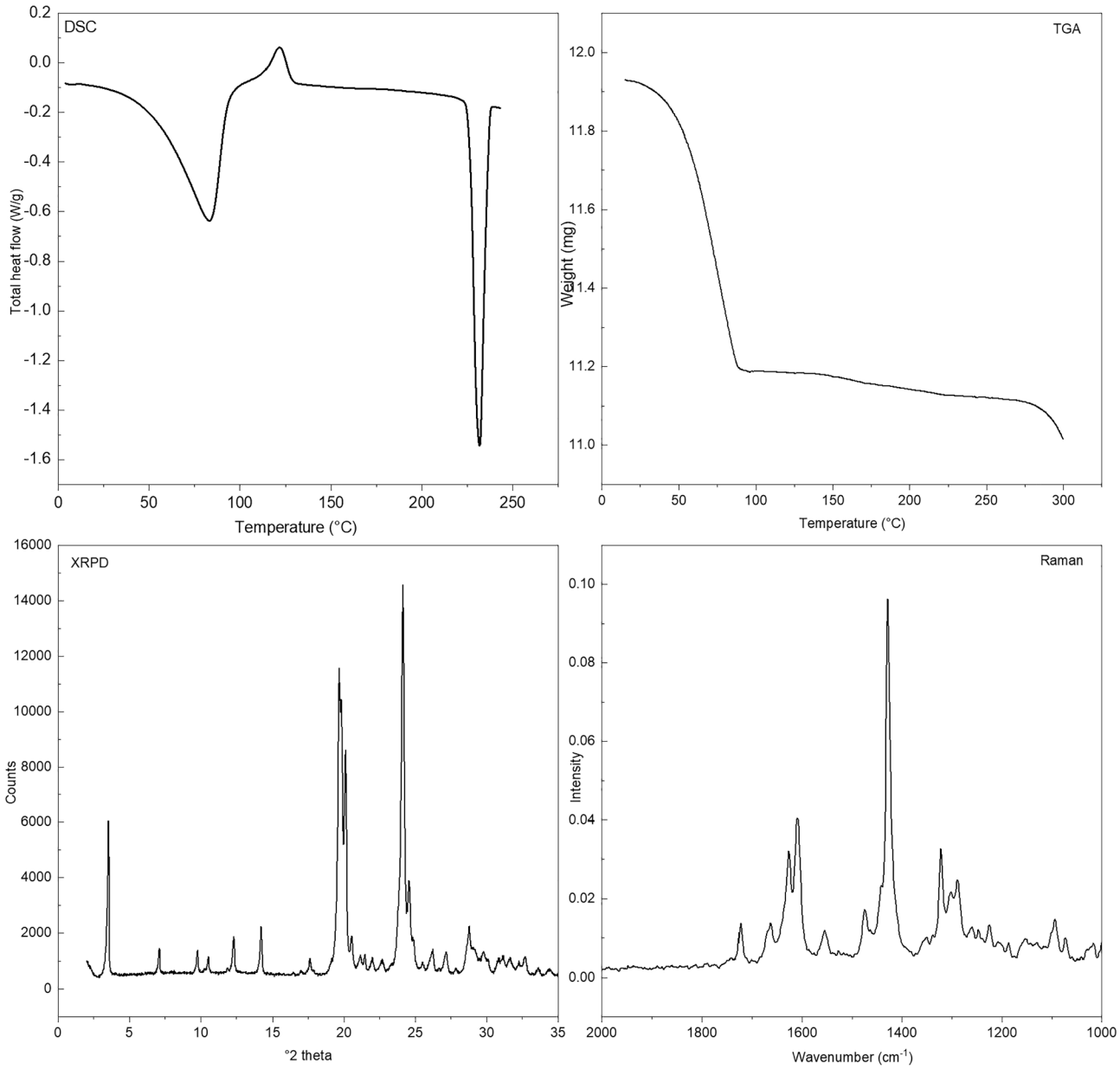

Fig. 6. Characterization of new form named as rivaroxaban dihydrate by DSC, TGA, XRPD and Raman spectroscopy.

supersaturated solution formed by solvent shift method using DMSO. Also in this case, new form of rivaroxaban was precipitating from supersaturated solution.

The characterization of the new form prepared during dissolution experiments was done to identify its chemical composition and properties. XRPD and Raman spectra of the new form (see Fig. 6) are similar to that of oxalic acid cocrystal (see Fig. 1) indicating a possible similarity between the crystal structures. Melting point of the new form is 80 °C, which is lower than both cocrystals. TGA in Fig. 6 indicated the presence of approximately 2 equivalents of the water and solution carbon NMR confirmed the absence of oxalic acid in the sample. Based on the combination of these results we can conclude that the new form is rivaroxaban dihydrate. IDR of rivaroxaban dihydrate was measured to be 457.2 ng/ml/min/cm^2, which is 1.4-times higher than for both cocrystals. This result together with the low melting temperature strongly supports its metastable nature. The solubility of the dihydrate after 12 h of slurrying was measured to be 13.8 μg/ml and is 2.3-times higher than the solubility of API form I (6 μg/ml). This trend is in contrast to previously published studies where hydrates exhibit lower solubility that anhydrous forms in water (Franklin et al., 2016; Tieger et al., 2016; Sládková et al., 2015).

Even though both cocrystals transform into the same form, the final solubility obtained from dissolution experiments is slightly different. To obtain information about the effect of coformer on the API dissolution, physical mixtures of rivaroxaban form I and coformer were prepared and their dissolution behavior was measured. As can be seen in Fig. 8, the coformer does not have statistically significant influence on the API dissolution. Moreover, the pH change during cocrystal dissolution was in the range from?? to?? in both cases. Together with neutral nature of rivaroxaban, we consider pH change during cocrystals dissolution unlikely to cause the difference between cocrystals solubility. Based on these findings, we propose that the change in dissolved amount of rivaroxaban is caused by longer transformation time in term of cocrystal with oxalic acid.

3.4. *In vivo study*

Rivaroxaban exhibits a food effect due to its poor water-solubility

Table 2
Pharmacokinetic parameters and results of bioequivalence comparison of rivaroxaban. Values are given as geometric mean with 90% confidence interval).

Formulation	C_{max} (ng/ml.g)	Test/Reference C_{max} (%)	AUC_{0-t} (ng/ml.min.g)	Test/Reference AUC_{0-t} (%)	t_{max} (min)
Reference	0.821 (0.721–0.963)	N/A	248.21 (218.6–289.9)	N/A	172 (115–292)
Test	1.626 (1.389–1.996)	198.2 (157.1–250.0)	528.2 (453.6–644.5)	212.8 (168.1–269.4)	186 (138–259)

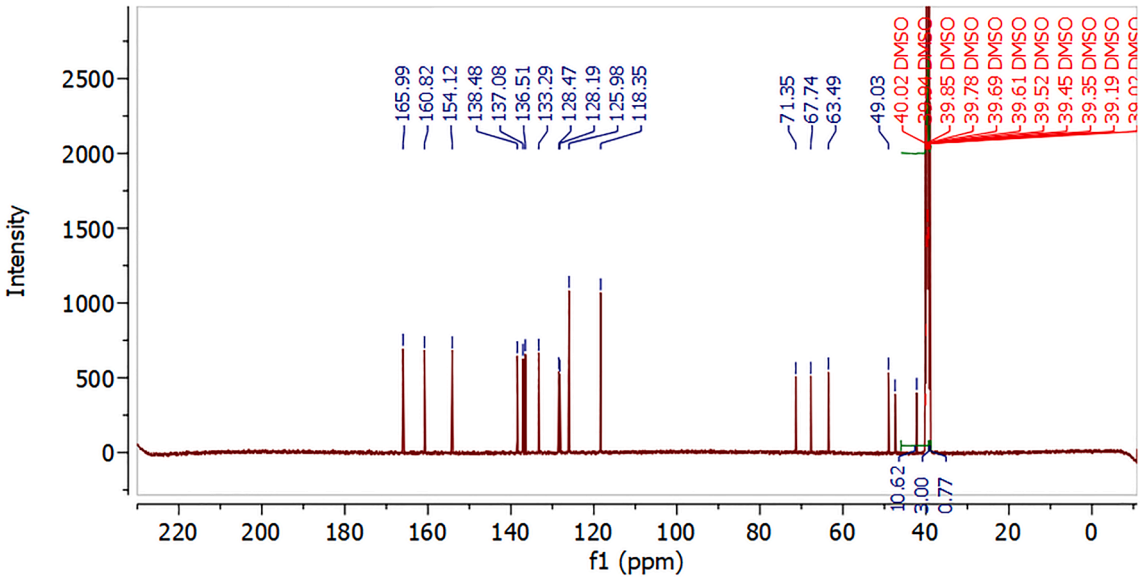

Fig. 7. Carbon liquid NMR spectrum of the rivaroxaban dihydrate.

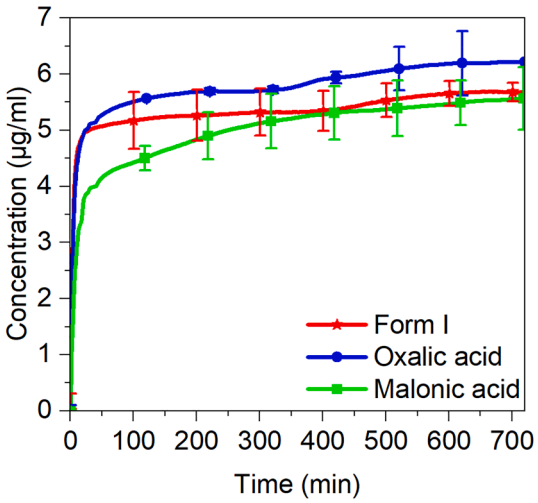

Fig. 8. Dissolution of physical mixtures of API and coformers.

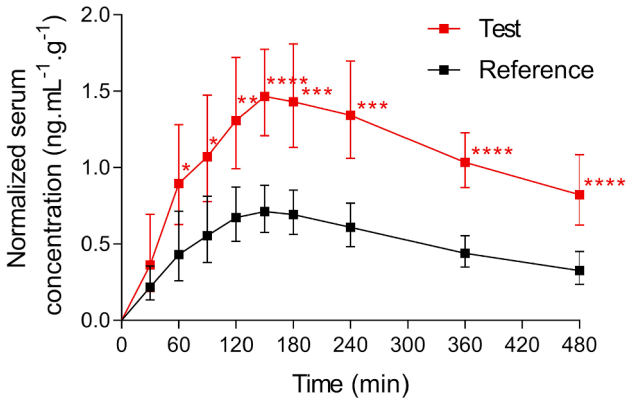

Fig. 9. Pharmacokinetic profiles of the Test and Reference formulation (expressed as geometric mean with 95% confidence interval). * P.0.05, ** P.0.01, *** P.0.001, **** P.0.0001.

(Takács-Novák et al., 2013). The low solubility is causing lower bioavailability in the fasted state. The increase of the solubility can thus have positive effect on the absorbed amount in the fasted state and diminish differences between fasted and fed state (Kushwah et al., 2021). Improved solubilization together with longer transformation kinetics creates the advantage in the solubility for cocrystal with oxalic acid when compared to the cocrystal with malonic acid. As a result, the cocrystal with the oxalic acid was selected for further study.

Pharmacokinetic profiles from 12 rats were obtained (6 rats per group). The weight of the rats varied from 344 g to 624 g. Rivaroxaban pharmacokinetic parameters are summarized in the Table 2, while pharmacokinetic profiles of the test and reference formulation are presented in the Fig. 7. Approximately twice as high C_{max} and AUC_{0-t} values occurred after administration of the cocrystal with the oxalic acid than after the reference product. Moreover, the 90% CI excluded the null difference as well as standard equivalence margins 80–125%. Both differences reached statistical significance at $P < 0.0001$. There was no significant difference in the t_{max} values ($P = 0.6625$), which means that the test formulation has similar rate of absorption as original drug product, while bioavailability is increased (see Fig. 9).

Serum concentrations before dosing were all below limit of quantification (1 ng/ml), excluding carry-over effect and proving that the wash-out period between both periods was sufficient.

4. Conclusion

In this work we studied the mechanism of maintaining supersaturation for two cocrystals of rivaroxaban. We analyzed properties of two rivaroxaban cocrystals with highly soluble coformers. Together with solid state properties, we studied dissolution behavior of both cocrystals in terms of solid and liquid phase. We proved that both cocrystals transform into new, metastable form that we characterized as rivaroxaban dihydrate. The transformation times of used cocrystals were significantly different (22 min for malonic acid versus 8 h for oxalic acid). The longer transformation time together was observed for the cocrystal with higher solubility creating more beneficial conditions for the dissolution. The formation of the dihydrate form has significant effect for the improvement of the solubility of both cocrystals. In vivo study was performed to verify positive effect of developed form. Bioavailability in fasted state was increased when rivaroxaban was administered in the form of cocrystal. This increment indicates the ability of the cocrystal to remove the food effect of rivaroxaban by improving its physical properties, especially water solubility.

CRediT authorship contribution statement

Erika Hriňová: Conceptualization, Methodology, Investigation, Writing – original draft. **Eliška Skořepová:** Conceptualization, Methodology, Investigation, Writing – review & editing. **Igor Černa:** Conceptualization, Methodology, Supervision, Funding acquisition. **Jana Královičová:** Methodology, Investigation, Writing – original draft. **Petr Kozlík:** Methodology, Investigation, Writing – original draft. **Tomáš Křížek:** Conceptualization, Methodology, Supervision, Writing – review & editing. **Jaroslava Roušarová:** Methodology, Investigation. **Pavel Ryšánek:** Methodology, Investigation. **Martin Šíma:** Conceptualization, Methodology, Investigation, Supervision, Writing – review & editing, Funding acquisition. **Ondřej Slanař:** Conceptualization, Methodology, Supervision, Writing – review & editing, Funding acquisition. **Miroslav Šoóš:** Conceptualization, Methodology, Supervision, Writing – review & editing, Funding acquisition.

Declaration of Competing Interest

The authors declare that they have no known competing financial interests or personal relationships that could have appeared to influence the work reported in this paper.

Acknowledgement

We would like to acknowledge the Research and Development department of Zentiva, k.s. for the materials and all the help provided. Our great thanks go namely to Ing. Tomáš Pekárek Ph.D., Ing. Marcela Tkadlecová CSc, RNDr. Ondřej Dammer Ph.D. and Ing. Lukáš Krejčík. This work was supported by the specific university research – grant No A1_FCHI_2022_006 and Pharmaceutical Applied Research Center (PARC). In vivo study was supported by the Cooperatio Program, research area PHAR.

References

Al-Kassas, R., Bansal, M., Shaw, J., 2017. Nanosizing techniques for improving bioavailability of drugs. J. Control Release 260, 202–212.
Anwer, M.K., Mohammad, M., Iqbal, M., Ansari, M.N., Ezzeldin, E., Fatima, F., Alshahrani, S.M., Aldawsari, M.F., Alalaiwe, A., Alzahrani, A.A., Aldayel, A.M., 2020. Sustained release and enhanced oral bioavailability of rivaroxaban by PLGA nanoparticles with no food effect. J. Thromb Thrombol. 49 (3), 404–412.
Babu, N.J., Nangia, A., 2011. Solubility Advantage of Amorphous Drugs and Pharmaceutical Cocrystals. Cryst. Growth Des. 11 (7), 2662–2679.
Betteridge, W. CRYSTALS; 2003.
Bhardwaj, S., Lipert, M., Bak, A., 2017. Mitigating Cocrystal Physical Stability Liabilities in Preclinical Formulations. J. Pharm. Sci. 106 (1), 31–38.
Cao, F., Amidon, G.L., Rodriguez-Hornedo, N., Amidon, G.E., 2016. Mechanistic Analysis of Cocrystal Dissolution as a Function of pH and Micellar Solubilization. Mol. Pharmaceutics 13 (3), 1030–1046.
Chatziadi, A., Skořepová, E., Rohlíček, J., Dušek, M., Ridvan, L., Šoóš, M., 2020. Mechanochemically Induced Polymorphic Transformations of Sofosbuvir. Cryst. Growth Des. 20 (1), 139–147.
CrysAlisPro; Oxford Diffraction, 2002.
Demir, H., Gulsun, T., Ozkan, M.H., Nemutlu, E., Sahin, S., Öner, L., 2020. Assessment of Dose Proportionality of Rivaroxaban Nanocrystals. Pharm. Sci. Tech. 21, 228.
Desiraju, G.R., 2003. Crystal and co-crystal. CrystEngComm 5 (82), 466. https://doi.org/10.1039/b313552g.
Elder, D.P., Holm, R., Diego, H.L.d., 2013. Use of pharmaceutical salts and cocrystals to address the issue of poor solubility. Int. J. Phar. 453 (1), 88–100.
Franklin, S.J., Younis, U.S., Myrdal, P.B., 2016. Estimating the Aqueous Solubility of Pharmaceutical Hydrates. J. Pharm. Sci. 105 (6), 1914–1919.
Ganesh, M., Shekar, B.C., Madhusudan, Y., 2016. Design and Optimization of Rivaroxaban Lipid Solid Dispersion for Dissolution Enhancement using Statistical Experimental Design. Asian J. Pharm. 10, 59–64.
Good, D.J., Rodríguez-Hornedo, N., 2009. Solubility advantage of pharmaceutical cocrystals. Cryst. Growth Des. 9 (5), 2252–2264.
EMA Guideline on bioanalytical method validation online available 28th September, 2021 (https://www.ema.europa.eu/en/ich-m10-bioanalytical-method-validation).
Jirát, J., Zvoníček, V., Babor, M., Ridvan, L., Skořepová, E., Dušek, M., Šoóš, M., 2020. Formation of the first non-isostructural cocrystal of apremilast explained. Cryst. Growth Des. 20 (9), 5785–5795.
Kale, D.P., Ugale, B., Nagaraja, C.M., Dubey, G., Bharatam, P.V., Bansal, A.K., 2019. Molecular Basis of Water Sorption Behavior of Rivaroxaban-Malonic Acid Cocrystal. Mol. Pharmaceutics 16 (7), 2980–2991.
Kapourani, A., Vardaka, E., Katopodis, K., Kachrimanis, K., Barmpalexis, P., 2019. Rivaroxaban polymeric amorphous solid dispersions: moisture-induced thermodynamic phase behavior and intermolecular interactions. Eur. J. Pharm. Biopharm 145, 98–112.
Khandavilli, U.B.R., Skořepová, E., Sinha, A.S., Bhogala, B.R., Maguire, N.M., Maguire, A. R., Lawrence, S.E., 2018. Cocrystals and a salt of the bioactive flavonoid: naringenin. Cryst. Growth Des. 18 (8), 4571–4577.
Kushwah, V., Arora, S., Tamás Katona, M., Modhave, D., Fröhlich, E., Paudel, A., 2021. On Absorption Modeling and Food Effect Prediction of Rivaroxaban, a BCS II Drug Orally Administered as an Immediate-Release Tablet. Pharmaceutics 13 (2), 283. https://doi.org/10.3390/pharmaceutics13020283.
Lee, J.-H., Jeong, H.S., Jeong, J.-W., Koo, T.-S., Kim, D.-K., Cho, Y.H., Lee, G.W., 2021. The Development and Optimization of Hot-Melt Extruded Amorphous Solid Dispersions Containing Rivaroxaban in Combination with Polymers. Pharmaceutics 13 (3), 344. https://doi.org/10.3390/pharmaceutics13030344.
Machado, T.C., Kuminek, G., Cardoso, S.G., Rodríguez-Hornedo, N., 2020. The role of pH and dose/solubility ratio on cocrystal dissolution, drug supersaturation and precipitation. Eur. Pharm. Sci. 152, 105422. https://doi.org/10.1016/j.ejps.2020.105422.
Mercury; CCDC, 2007.
Metre, S., Mukesh, S., Samal, S.K., Chand, M., Sangamwar, A.T., 2018. Enhanced Biopharmaceutical Performance of Rivaroxaban through Polymeric Amorphous Solid Dispersion. Mol. Pharma. 15 (2), 652–668.
Ober, C.A., Montgomery, S.E., Gupta, R.B., 2013. Formation of itraconazole/L-malic acid cocrystals by gas antisolvent cocrystallization. Powder Technol. 236, 122–131.
Omori, M., Uekusa, T., Oki, J., Inoue, D., Sugano, K., 2020. Solution-mediated phase transformation at particle surface during cocrystal dissolution. J. Drug Del. Sci. Technol. 56, 101566. https://doi.org/10.1016/j.jddst.2020.101566.
Palatinus, L., Chapuis, G., 2007. J. Appl. Crystallogr. 40 (4), 786–790.
Petricek; Palatinus. Jana, 2006. Institute of Physics: Prague, The Czech Republic.
Sherje, A.P., Jadhav, M., 2018. β-Cyclodextrin-based inclusion complexes and nanocomposites of rivaroxaban for solubility enhancement. J. Mater. Sci.: Mater. Med. 29, 186.
Shiraki, K., Takata, N., Takano, R., Hayashi, Y., Terada, K., 2008. Dissolution Improvement and the Mechanism of the Improvement from Cocrystallization of Poorly Water-soluble Compounds. Pharm. Res. 25 (11), 2581–2592.
Skořepová, E., Hušák, M., Čejka, J., Zámostný, P., Kratochvíl, B., 2014. Increasing dissolution of trospium chloride by co-crystallization with urea. J. Cryst. Growth 399, 19–26.
Sládková, V., Skalická, T., Skořepová, E., Čejka, J., Eigner, V., Kratochvíl, B., 2015. Systematic solvate screening of trospium chloride: discovering hydrates of a long-established pharmaceutical. CrystEngComm 17 (25), 4712–4721.
Sládková, V., Dammer, O., Sedmak, G., Skořepová, E., Kratochvíl, B., 2017. Ivabradine Hydrochloride (S)-Mandelic Acid Co-Crystal: In Situ Preparation during Formulation. Crystals 7 (1), 13. https://doi.org/10.3390/cryst7010013.
Takács-Novák, K., Szőke, V., Völgyi, G., Horváth, P., Ambrus, R., Szabó-Révész, P., 2013. Biorelevant solubility of poorly soluble drugs: Rivaroxaban, furosemide, papaverine and niflumic acid. J. Pharm. Biomed. Anal. 83, 279–285.
Tieger, E., Kiss, V., Pokol, G., Finta, Z., Dušek, M., Rohlíček, J., Skořepová, E., Brázda, P., 2016. Studies on the crystal structure and arrangement of water in sitagliptin L-tartrate hydrates. CrystEngComm 18, 3819–3831.
Xue, X.u., Cao, M., Ren, L., Qian, Y., Chen, G., 2018. Preparation and Optimization of Rivaroxaban by Self-Nanoemulsifying Drug Delivery System (SNEDDS) for Enhanced Oral Bioavailability and No Food Effect. Pharm. Sci. Tech. 19 (4), 1847–1859.
Zhang, G.G.Z., Henry, R.F., Borchardt, T.B., Lou, X., 2007. Efficient Co-crystal Screening Using Solution-Mediated Phase Transformation. J. Pharm. Sci. 96 (5), 990–995.

Příloha 3

BOLESLAVSKA, T., RYCHECKY, O., KROV, M., ZVATORA, P., DAMMER, O., BERANEK, J., KOZLIK, P., KRIZEK, T., HORINKOVA, J., RYSANEK, P., ROUSAROVA, J., CANOVA, N. K., SIMA, M., SLANAR, O. & STEPANEK, F. 2020. Bioavailability Enhancement and Food Effect Elimination of Abiraterone Acetate by Encapsulation in Surfactant-Enriched Oil Marbles. *AAPS J,* 22**,** 122.

The AAPS Journal (2020) 22: 122
DOI: 10.1208/s12248-020-00505-5

Research Article

Bioavailability Enhancement and Food Effect Elimination of Abiraterone Acetate by Encapsulation in Surfactant-Enriched Oil Marbles

Tereza Boleslavská,[1,2] Ondřej Rychecký,[1,2] Martin Krov,[2] Pavel Žvátora,[1] Ondřej Dammer,[1] Josef Beránek,[1] Petr Kozlík,[3] Tomáš Křížek,[3] Jana Hořínková,[4] Pavel Ryšánek,[4] Jaroslava Roušarová,[4] Nikolina Kutinová Canová,[4] Martin Šíma,[4] Ondřej Slanař,[4] and František Štěpánek[2,5]

Received 29 June 2020; accepted 27 August 2020; published online 25 September 2020

Abstract. Abiraterone acetate has limited bioavailability in the fasted state and exhibits a strong positive food effect. We present a novel formulation concept based on the so-called oil marbles (OMs) and show by *in vitro* and *in vivo* experiments that the food effect can be suppressed. OMs are spherical particles with a core-shell structure, formed by coating oil-based droplets that contain the dissolved drug by a layer of powder that prevents the cores from sticking and coalescence. OMs prepared in this work contained abiraterone acetate in the amorphous form and showed enhanced dissolution properties during *in vitro* experiments when compared with originally marketed formulation of abiraterone acetate (Zytiga®). Based on *in vitro* comparison of OMs containing different oil/surfactant combinations, the most promising formulation was chosen for *in vivo* studies. To ensure relevance, it was verified that the food effect previously reported for Zytiga® in humans was translated into the rat animal model. The bioavailability of abiraterone acetate formulated in OMs in the fasted state was then found to be enhanced by a factor of 2.7 in terms of AUC and by a factor of 4.0 in terms of C_{max}. Crucially, the food effect reported in the literature for other abiraterone acetate formulations was successfully eliminated and OMs showed comparable extent of bioavailability in a fed-fasted study. Oil marbles therefore seem to be a promising formulation concept not only for abiraterone acetate but potentially also for other poorly soluble drugs that reveal a positive food effect.

KEY WORDS: bioavailability; bioequivalence; food effect; formulation; liquid marble.

INTRODUCTION

Poorly soluble drugs (i.e., drugs belonging to BCS groups II and IV) and their limited oral bioavailability currently present a major challenge to pharmaceutical scientists (1). An example of such a hard-to-formulate drug is abiraterone acetate, a prodrug of androgen biosynthesis inhibitor abiraterone, marketed under the original brand name Zytiga® and used as a medication for the treatment of metastatic castration–resistant prostate cancer (2). Abiraterone acetate has an extremely low bioavailability in the fasted state (estimated to be less than 10%) and exhibits a highly variable increase in bioavailability in the fed state (3–5). It has been reported that intake with high-fat meal leads to increase in overall exposures by approximately 17- and 10-fold, in terms C_{max} and AUC, respectively. The original formulation must therefore be taken on a fasting stomach in high doses, 1000 mg daily (2). This not only is inconvenient for the patients, but also presents a risk of accidental overdose. Attempts have been made to establish safe dosing regimen for lower doses of Zytiga® administered with food—these attempts have however been unsuccessful so far

Tereza Boleslavská and Ondřej Rychecký contributed equally to this work.

Electronic supplementary material The online version of this article (https://doi.org/10.1208/s12248-020-00505-5) contains supplementary material, which is available to authorized users.

[1] Zentiva, k.s., U Kabelovny 130, 102 37, Prague, Czech Republic.
[2] Department of Chemical Engineering, University of Chemistry and Technology, Prague, Technická 5, 166 28, Prague, Czech Republic.
[3] Department of Analytical Chemistry, Faculty of Science, Charles University, Prague, Czech Republic.
[4] Institute of Pharmacology, First Faculty of Medicine, Charles University and General University Hospital in Prague, Prague, Czech Republic.
[5] To whom correspondence should be addressed. (e–mail: Frantisek.Stepanek@vscht.cz)

Abbreviations: *API,* active pharmaceutical ingredient; *ASD*, amorphous solid dispersions; *AUC*, area under the curve; *ODP*, original drug product; *OM*, oil marble; *SEDDS*, self-emulsifying drug delivery system; *SMEEDS*, self-microemulsifying drug delivery system;

(3). This implies a need for the development of novel formulation strategies that would allow food effect elimination and thus safe dosing regimen for abiraterone acetate.

Therefore, it can be hypothesized that by using advanced formulation approaches to increase the bioavailability of abiraterone acetate on a fasting stomach, the dangerous food effect can be suppressed (6). Administration of the crystalline drug in the form of nanoparticles allowed dose reduction to 500 mg (7,8). Solymosi *et al.* reported a negligible food effect for a novel formulation based on continuous flow precipitation with Soluplus (9,10). Finally, we have shown in a recent study that amorphous solid dispersion (ASD) formulation based on precipitation inhibitor allowed 2.5-fold bioavailability enhancement in fasted rats (11).

Alternatively, lipid-based formulations of abiraterone acetate have been investigated recently (12). Complex lipid-based formulations can contain various oils, surfactants, and co-solvents. These systems can be categorized based on the Lipid Formulation Classification System (LFCS) into several groups among which the self-emulsifying drug delivery systems (SEDDS) and the self-microemulsifying drug delivery systems (SMEDDS) are of particular significance (13–15). These liquid formulations are usually filled into soft gelatin capsules. Even though these systems can be highly effective in bioavailability enhancement, they also have some drawbacks when compared with solid dosage forms.

As SEDDS and SMEDDS are essentially liquid formulations, it is not easily possible to alter their dissolution kinetics as such (16). Once the soft gelatin capsule is opened, it releases the whole content at once, forming a fine emulsion. The lipids are then available for enzymatic digestion (lipolysis), which is believed to be the critical step for drug absorption (15,17). Moreover, there are several challenges associated with soft gelatin capsules—e.g., cross-linking to the gelatin (which can result in poor dissolution) or the necessity to employ a special production line (18). Due to these aspects of liquid oil–based drug delivery systems, there have been efforts towards the solidification of these types of formulations (15). SEDDS solidification techniques have been reviewed recently by Joyce *et al.* (19) In the present work, we are introducing a novel approach towards the preparation of solidified oil-based formulations of abiraterone acetate based on the so-called oil marbles.

The general term "liquid marble" refers to a droplet covered by a layer of non-wetting solid particles that stabilize the interface and cause the droplet to behave and roll as if it were a rigid sphere. (20,21) Most of the existing literature on pharmaceutical applications of liquid marbles is concerned with water-based systems covered by hydrophobic powders (22). Such marbles typically contain about 90% w/w of the liquid core, depending on the interfacial tension, the droplet diameter, and the particle size. Solid particles on the surface prevent the encapsulated liquid from evaporation or leakage and protect the marbles from agglomeration, thus improving their handling properties (20,21). Although oil-based liquid marbles can be prepared as well, they are not so well documented in the literature and their practical application has so far been hindered by a limited choice of sufficiently oleophobic powders for coating (23). A fully liquid oil core combined with an insufficiently oleophobic powder leads to an unfavorable ratio between the oily core and the shell material, which ultimately limits the achievable drug load in the formulation.

Therefore, the aim of the present work was to overcome this limitation by formulating the oil-based core in such way that it can be combined even with wettable powders without their excessive absorption into the core. The resulting oil marbles (OMs) combine the advantages of oil-based formulations in terms of bioavailability enhancement and those of solid dosage forms in terms of handling the product. It will be shown that OMs can be filled into hard gelatin capsules and handled similarly as a solid material once they are prepared. We will demonstrate that unlike fully liquid formulations, OMs can provide a range of dissolution profiles depending on the matrix composition and OM size. Crucially, it will be shown that OM formulation of abiraterone acetate leads not only to improved dissolution *in vitro* but also to significant bioavailability enhancement *in vivo* and ultimately successful elimination of the food effect.

MATERIALS AND METHODS

Materials

Abiraterone acetate was provided by Zentiva, k.s. (Prague, Czech Republic). Capmul oil MCM NF was purchased from Abitec (Columbus, USA); Capryol PGMC was kindly donated by Gattefossé (Saint-Priest, France). Surfactants (summarized in Supplementary Material, Table S1) were purchased from Sigma-Aldrich. Natural oils (olive oil, rapeseed oil, and castor oil) were purchased from Merck (Germany). Hydroxypropyl methylcellulose (HPMCAS-LF) was bought from Shin-Etsu Chemical. Powders for biorelevant media were purchased from Biorelevant.com Ltd. (London, UK). The biorelevant dissolution media were prepared according to the manufacturer's protocol. All solvents used were at least of HPLC grade.

Solubility Measurements

In order to select the most appropriate oil for the OMs, the solubility of abiraterone acetate in several candidate oils was determined using the shake flask method. Briefly, an excess of abiraterone acetate was added to an Eppendorf vial containing 1 mL of the oil and the resulting suspension was shaken at 37°C for 24 h. At the end of the experiment, the vials were centrifuged at 10,000 RPM for 10 min, the supernatant was diluted ten times into isopropyl alcohol, and the concentration of abiraterone acetate in the resulting solution was determined by HPLC (method adapted from our previous study) (11).

As an additional component of the OM formulation, surfactants were screened for their ability to enhance the solubility of abiraterone acetate in aqueous media. The solubility was determined using the shake flask method described above. Surfactants with relatively higher melting point (around 50°C) were selected along with several commonly used non-ionic surfactants such as Tween. The full list of surfactants is provided in Supplementary Material, Table S1. Phosphate buffer pH 6.8 supplemented with these surfactants at different concentrations (namely 1.0, 0.5, 0.25,

and 0.125 mg/L) was used as the dissolution media in the shake flask method.

Preparation of Oil Marbles

All components of the oil core (abiraterone acetate, oil, surfactant) were weighted and placed into a flask. The mixture was heated in a bath at 56°C and stirred for 20 min at 250 RPM to allow complete dissolution and homogenization of the mixture. Oil Marbles were created by dripping the liquid at a rate of 2 Hz using a 30G needle connected to a precise syringe pump, into a powder bed placed in Petri dish that moved underneath the needle tip at a velocity or approximately 10 mm/s in order to allow sufficient distance between the individual OMs. The powder bed was maintained at room temperature (approximately 20°C); HPMCAS-LF was used as the covering powder material. After 3 min (time necessary for the droplets to cool down and partially solidify), the Petri dish was shaken to fully cover the droplets by the powder. Thanks to the surface cooling of the droplets, the HPMCAS powder remained just on the surface even though it is not fully oleophobic. The final product—the oil marble—therefore behaves as a non-sticking solid sphere regardless of the physical consistency of the oily core.

Physicochemical Characterization

Sieve Analysis

After preparation, the OMs were separated by sieving to obtain size classes with a defined diameter. To assess the effect of OM size on *in vitro* dissolution properties of the formulation, the following size fractions were collected: 1.4–2 mm, 2–3 mm, 3–4 mm, 4–5 mm, 5–6 mm, and > 6 mm. Since the rat capsules intended for an *in vivo* study have an inner diameter of 2 mm, only the smallest fraction (1.4 to 2 mm) of OMs was used for the *in vivo* study.

X-ray Powder Diffraction Analysis

X-ray powder diffraction (XRPD) patterns were obtained with the laboratory X-ray diffractometer X'PERT PRO MPD PANalytical with copper radiation CuKα (λ = 1.542 Å, 45 kV/40 mA), 2-theta range 2–40°, with step size 0.02° 2θ and time per step 300 s. Primary optics setting is as follows: Soller slits 0.02 rad, automatic PDS, 10 mm mask, 1/4° anti-scatter slit, irradiated sample area 10 mm. Secondary optics setting is as follows: 5.0 mm anti-scatter slit, Soller slits 0.02 rad, detector X'Celerator with maximal active length. Silicon zero background holders were used for measurement. A few OMs were placed on the holder and gently pressed by a Petri dish to obtain a flat surface. All samples of OM were measured on XRPD to confirm if abiraterone acetate inside the marbles was present in the crystalline or amorphous form.

Drug Load Analysis

The actual drug load in the oil marbles was determined by extraction into methanol. Approximately 80 mg of OMs was weighted into a 20-mL volumetric flask and extracted into methanol. The resulting solution was diluted 10 times, and the concentration of abiraterone acetate was determined on HPLC using a method adapted from our previous study (11).

In Vitro Dissolution Testing

Dissolution experiments were conducted using standard USP 2 dissolution bath equipped with a mini-paddle apparatus (Sotax, Switzerland). The dissolution media were preheated to 37°C and the stirrer speed was set to 125 RPM; these conditions were kept constant throughout the experiment. OMs were placed into a weighing boat and administered directly into the dissolution vessel. The weight of abiraterone acetate corresponded to 20 mg in all dissolution experiments. Liquid samples (500 μL) were collected in predefined time points, filtered through a 0.45-μm filter, immediately diluted with 500 μL of MeOH, and analyzed on HPLC. Unlike the dissolution medium, the filtrate was clear, suggesting the absence of any particles or droplets that would scatter light.

As dissolution media simulating fasted and fed conditions, biorelevant buffers were used—FeSSIF v2 pH 5.8, FaSSIF pH 6.5, and FaSSIF pH 6.5 supplemented with pancreatin (10 mg/mL) (24). Furthermore, pH shift experiment was designed. Briefly, 130 mL of 10 mM HCl pH 2 was used to simulate gastric conditions. After 30 min, concentrated FaSSIF buffer was added to the dissolution vessel to obtain 195 mL of FaSSIF buffer pH 6.5.

In Vivo Bioequivalence Study

Chemicals

Ketamine (Narkamon 100 mg/mL inj. sol.; Bioveta, Ivanovice na Hané, Czech Republic), xylazine (Rometar 20 mg/mL inj. sol.; Bioveta, Ivanovice na Hané, Czech Republic), and isoflurane (IsoFlo 250 mL; Zoetis/Pfizer, Czech Republic) were used for anesthetization. Enoxaparin (Clexane inj. 4000 IU/0.4 mL; Sanofi-Aventis, Czech Republic), heparin (Heparin Léčiva inj. 1 × 10 mL/50KU; Zentiva, Czech Republic), amoxicillin with clavulanic acid (Synulox RTU inj. 100 mL; Zoetis/Pfizer, Czech Republic), and ketoprofen (Ketodolor inj. 100 mL; LeVet Pharma b.v., Netherlands) were used for peri-operative anti-coagulant, antibiotic, and analgesic treatments, respectively. Surgical Skin Glue was purchased from Henry Schein (Brno, Czech Republic). For dosing, mini gelatin drug delivery capsules, size 9el (Harvard Apparatus, USA), were used.

Animals

Male Wistar rats purchased from Velaz (Prague, Czech Republic) were housed under standard conditions (12-h light-dark cycle, 22 ± 2°C temperature and 50 ± 10% relative humidity) and fed on water and standard granulated diet *ad libitum*. All experiments were performed in accordance with the Guiding Principles for the Use of Animals in Charles University, First Faculty of Medicine, and every effort was made to minimize animal suffering. The experimental animal project was approved by the Ministry of

Education, Youth and Sports, Czech Republic (MSMT-9445/2018-8).

Preparation of Capsules for In Vivo Dosing

The mini capsules containing reference formulation were filled with the crushed original drug product Zytiga® to contain approximately 4.2 mg of abiraterone acetate. For the test formulation, two capsules were filled with OM formulation pre-selected on the basis of previous *in vitro* studies. Each capsule contained approximately 2.1 mg of abiraterone acetate—two capsules containing the test formulation were given to each animal by oral gavage.

Experimental Design and Procedure

A randomized, single-dose, laboratory-blinded, 2-period, 2-sequence, crossover bioequivalence study was conducted under fasting conditions in rats to compare the bioavailability of abiraterone after oral administration of test and reference (Zytiga®, Janssen-Cilag SpA, Latina, Italy) formulations (Table I part A). Another randomized, single-dose, laboratory-blinded, 2-period, 4-sequence, crossover comparative bioavailability study was conducted in rats to compare the effect of food on bioavailability of abiraterone after oral administration of test and reference formulations (Table I part B).

All rats underwent cannulation of *a. carotis* with catheters made from medical-grade polyurethane (1.9-3Fr, Instech Laboratories, Plymouth Meeting, USA). Prior to the surgery, 2.5–5% isoflurane was used to anesthetize the rats, continued with ketamine (100 mg/kg, i.m.) and xylazine (5 mg/kg, i.m.). Prophylactic amoxicillin with clavulanic acid (1 mL/kg, s.c.) was administered prior to the surgery to minimize the risk of an infection. After the cannulation, ketoprofen (5 mg/kg, s.c.) was applied. Catheters were flushed with 200 μL of physiological saline and 50 μL of heparin and sealed by 20 μL of glycerol with heparin every day. Peri-procedural thromboembolism prophylaxis with enoxaparin (10 mg/kg, s.c. q.d.) was applied from 12 h prior to surgery until the end of study. The third day after the cannulation, rats were randomly assigned into study groups and dosing of abiraterone acetate containing formulation was performed.

For dosing under fasted state, the access of the animals to food was restricted between 4 h prior to dosing and 4 h after that, and capsule was administered by X-9el dosing syringe (Torpac Inc., Fairfield, USA) followed by 1 mL of water via oral gavage. For dosing under fed state, administered capsule was immediately followed by 1 mL of homogenized mixture (1:1) of olive oil with Nutridrink (Nutricia, Danone, Amsterdam, Netherlands) via oral gavage and the access of the animals to food was not restricted. Total dose of abiraterone acetate was measured in each capsule and ranged between 4.18–4.53 mg and 4.00–4.27 mg for reference and test formulations, respectively. Therefore, all concentration data has been normalized to body weight of each animal. Blood samples (100 μL) were then collected for 7 h (0, 0.5, 1, 1.5, 2, 2.5, 3, 4, 5, and 7 h) after the dosing. Volume replacement with 100 μL of saline was provided after each sampling and 50 μL of heparinized saline flush (1250 IU/mL) of the catheter together with sealing by heparinized glycerol used to secure the catheter patency. Blood samples were centrifuged for 10 min (4500×*g*, 4°C) and serum aliquots were stored at −80°C until analyses. A wash-out period of 48 h between consecutive doses was applied.

Table I. Experimental Design of *In Vivo* Studies

A	**Group no.**	**Formulation sequence**
	1	R–T
	2	T–R
B	**Group no.**	**Formulation/condition sequence**
	1	R (fasted)–R (fed)
	2	T (fasted)–T (fed)
	3	R (fed)–R (fasted)
	4	T (fed)–T (fasted)

R reference, *T* tested formulation

Analytical Methods

Determination of abiraterone in plasma samples was carried out on the Shimadzu UHPLC Nexera X3 coupled with a Triple Quad 8045 tandem mass spectrometer (Shimadzu, Kyoto, Japan). Kinetex EVO C18 column (100 mm × 2.1 mm, 1.7 μm particle size) from Phenomenex (Torrance, USA), thermostatted at 40°C, was used for the analysis. The mobile phase consisted of 0.1% formic acid in deionized water (solvent A) and acetonitrile (solvent B). The flow rate of the mobile phase was maintained at 0.35 mL/min. The optimized gradient program (min/% B) was 0/30, 1.5/90, 3.0/90, 3.5/30, and 6.0/30. The injection volume was 2 μL, and samples were kept at 10°C. To reduce the cleaning time of the ion source, we switched the MS six-port valve to waste for the first 2.6 min and for the last 2.2 min of analysis. The tandem mass spectrometry measurement was performed in multiple reaction monitoring (MRM) mode using positive electrospray ionization. MRM transitions of 350.3 > 156.1 (Q1 pre-bias −17 V, Q3 pre-bias −27 V, and collision energy −57 V) and 354.3 > 160.1 (Q1 pre-bias −17 V, Q3 pre-bias −30 V, and collision energy −57 V) were monitored for abiraterone and abiraterone-d4 (internal standard), respectively. The ion source was set as follows: nebulizing gas flow: 3 L/min, heating gas flow: 10 L/min, interface temperature: 300°C, desolvation line temperature: 250°C, heat block temperature: 400°C, and drying gas flow: 10 L/min. A total of 100 μL of 100% acetonitrile (containing abiraterone-d4; $c = 32$ ng/mL) was added to 25 μL of plasma, shaken (vortex), and centrifuged (10 min/9800×*g*). A total of 70 μL of supernatant was transferred into a chromatographic vial.

The method was validated in terms of linearity, LOD, accuracy, precision, selectivity, recovery, and matrix effects. The calibration curve was constructed in the blank plasma with seven concentrations by plotting the ratio of the peak area of the analyte to that of deuterium-labeled IS against analyte concentration. The calibration curve was statistically analyzed by $1/x^2$ weighted linear regression analysis using the least squares regression method, which improved the accuracy in low concentrations. The developed method was linear (coefficients of determination (R^2) higher than 0.9996) in the concentration range of 0.5–600 ng/mL with the

accuracy (relative error %) within ± 7.1%, and the interday and intraday precisions (RSD %) ranged from 2.4 to 5.2%. LOD value was determined as $3.3 \times \sigma/S$ ratio, where σ is the baseline noise obtained from the blank matrix and S is the slope of the regression line (based on peak heights) obtained from the linearity data. The mean of LOD value was 0.03 ng/mL, which showed satisfactory sensitivity for abiraterone determination in plasma samples. Recovery was evaluated by comparing concentration of abiraterone found in the pre-protein-precipitation spiked plasma sample with the concentration found in the corresponding post-protein-precipitation spiked sample at three concentrations (1, 50, and 250 ng/mL). Method selectivity was monitored by injecting six plasma samples (mass spectrometer was set in scan mode). These chromatograms showed no interfering compound within the retention time window of abiraterone. Moreover, the developed method uses a tandem mass spectrometer in specific SRM mode, which ensures high selectivity. Matrix effect was evaluated at two concentration levels (1 and 100 ng/mL) of six plasma samples. It was determined by comparing the concentration of abiraterone found in the post-protein-precipitation spiked plasma sample with that found in the 80% acetonitrile spiked with abiraterone (without matrix effect). The matrix effect ranged from 80 to 108%. To assess the validity of the analytical method, calibration was performed every day before measuring samples and quality control samples were injected after each 7th sample.

Data Analysis and Statistics

Statistical and pharmacokinetic analysis was performed using Phoenix WinNonlin® (Certara, Princeton, USA). C_{max}, T_{max}, and AUC were evaluated. The natural logarithmic transformation of C_{max} and AUC was used for all statistical inference. AUC was calculated using the trapezoidal rule, and C_{max} and T_{max} were taken directly from the observed data. The pharmacokinetic parameters were analyzed using an ANOVA model. The fixed factors included in this model were the effects of subject, treatment, period, and sequence. The 90% confidence interval for the ratio of geometric least squares means between the test and reference products was calculated. Actual sampling times were used for all pharmacokinetic calculations, while scheduled sampling times were used only for plotting of mean pharmacokinetic profiles. The maximum difference between actual and per-protocol sampling times was 5 min. GraphPad Prism version 8.00 for Windows (GraphPad Software, La Jolla, USA) was used to plot mean pharmacokinetic profiles.

RESULTS

Selection of Formulation Components Based on Solubility

Based on recently published SMEDDS formulations of abiraterone acetate that contained mixtures of castor oil and artificial oils (12), it was decided to explore the solubility of abiraterone acetate in other natural oils (rapeseed oil and olive oil) compared with castor oil, as well as in several artificial oils (Capmul MCM NF and Capryol PGMC). The results are summarized in Fig. 1a (the underlying values can be found in Supplementary Material, Table S2). From the natural oils, castor oil with solubility of abiraterone acetate 137.7 mg/L was chosen for the preparation of oil marbles due to its highest solubility. For the artificial oils (Capmul MCM NF dissolved 53.3 m/L and Capryol PGMC 735.1 mg/L), both were used in combination with different surfactants as described in "Preparation of Oil Marbles and Their Physicochemical Characterization." Surfactants for the formulation were selected based on their solubilization effect for abiraterone acetate and their physical consistency. The preparation of OMs coated by HPMCAS powder requires the usage of solid or semi-solid excipients. Thus, surfactants with a melting point around 50°C (based on manufacturer and literature data) (25–30) were included in the list of possible surfactants (Supplementary Material, Table S1). Along with these, the solubilization capacity of some commonly used non-ionic surfactants (such as Tweens) was tested. The ability of selected surfactants to enhance the solubility of abiraterone acetate was assessed in a phosphate buffer pH 6.8. The solubility of abiraterone acetate alone was under the detection limit of the UPLC method. The highest enhancements were occurred for Kolliphor RH40, Tween 80, Tween 20, and Pluronic F127 (see Fig. 1b).

Preparation of Oil Marbles and Their Physicochemical Characterization

Based on the solubility data, we prepared four types of OMs with a different composition of the inner core, as summarized in Table II. We focused mainly on the manufacturability of the marbles while using surfactants that provided the highest solubility for abiraterone acetate. Some of the surfactants that provided good solubility were found to be unsuitable for the preparation of oil marbles, namely Tween 20 and Tween 80. Both are liquid at room temperature, and we were not able to prepare a mixture that would allow the formation of stable OMs coated by a thin layer of HPMCAS powder. Butylated hydroxyanisole (BHA) was added to all formulations in order to decrease undesired oxidation processes.

For mixture A, solid surfactant Pluronic F-127 was used as the main solubilizing agent (this surfactant showed good solubility for abiraterone acetate in phosphate buffer). Tween 65 was used as a solidifying agent. The resulting mixture thus formed a rather solid core. For mixture B, both used surfactants (solid Pluronic F-127 and liquid Kolliphor RH40) showed the ability to solubilize abiraterone acetate. Their mixture also allowed formation of a solid oil core at room temperature although softer than when using mixture A. Mixture C was prepared using surfactants that have a high melting point, but they did not perform well in the solubility measurements. We therefore assumed that this mixture would not perform well in the dissolution studies although the solid core could still contain molecularly dispersed abiraterone acetate (see Fig. 3). For mixture D, both used surfactants (Pluronic F-127 and Span 40) are solid materials but only Pluronic F-127 showed solubility enhancement.

As a covering material, HPMCAS-LF, a polymeric excipient with pH-dependent solubility, was used. This covering material was chosen for two main reasons: (i) pH-dependent solubility of this polymer allows pH-controlled

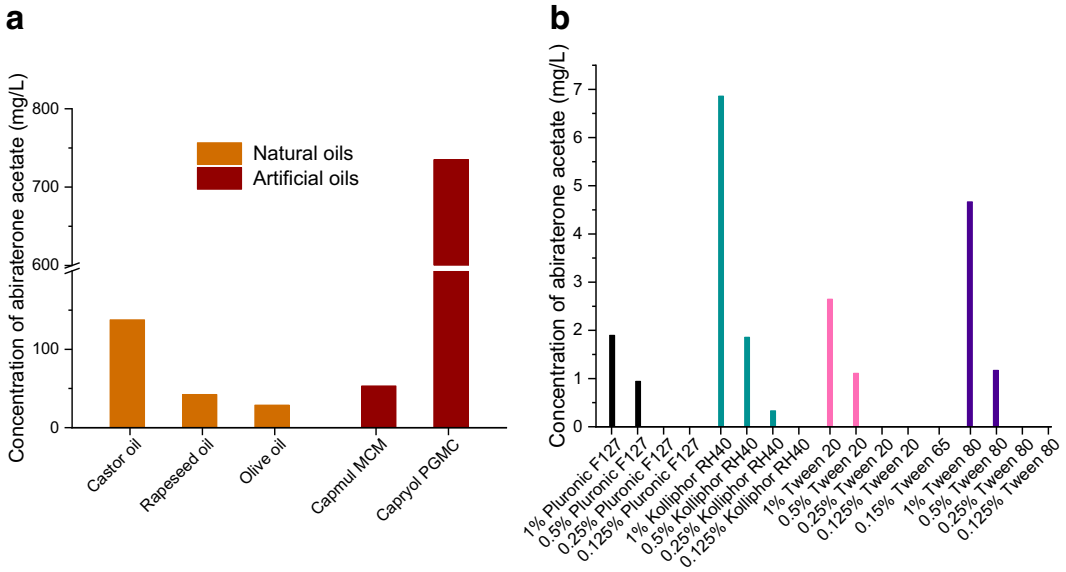

Fig. 1. **a** Solubility of abiraterone acetate in various natural and artificial oils. **b** The solubility enhancement of abiraterone acetate due to various surfactants in phosphate buffer pH 6.8

release since we believe that tuning the release of abiraterone acetate based on pH is crucial for food effect elimination; (ii) in our previous study (11), HPMCAS-LF was identified as a potent precipitation inhibitor—this might allow drug absorption even when supersaturated state is reached in a given environment (this phenomenon is usually referred to as parachute effect) (31). We were able to prepare marbles smaller than 2 mm in diameter that could be filled into capsules for rodents (capsule size 9el) as shown in Fig. 2. Larger size fractions were also prepared and used for studying the impact of OM size on the dissolution properties (see "*In Vitro* Dissolution Testing").

Figure 3 shows XRPD diffractograms of OM samples. Crystalline abiraterone acetate was not detected in any of the samples. It can be concluded that abiraterone acetate is probably molecularly dispersed in all four formulations. The detected diffraction peaks correspond to excipients, namely to triblock copolymers (Poloxamer 188, Pluronic F-127, Kolliphor) and solid co-surfactants (Span 65, Span 40). The XRPD diffractograms of these excipients are summarized in Supplementary Material, Fig. S1. The drug load as determined by methanol extraction corresponded with theoretical drug load in the melt. As anticipated, the actual drug load is decreased by addition of a thin layer of HPMCAS. The actual drug content determined for OM sample B (intended for the *in vivo* study) was found to be 6.2%.

In Vitro Dissolution Testing

As bioavailability of abiraterone acetate is reported to be limited in fasting conditions, special attention should be paid to dissolution in media closely mimicking these conditions. For this purpose, a pH shift experiment that represents a transfer of API from a fasting stomach to a fasting intestine was designed. The results for OM formulation B are shown in Fig. 4a. Less than 10% of abiraterone acetate was released under acidic condition—this is due to poor solubility of the coating material (HPMCAS-LF) in acidic pH. Coverage of the oil marbles by this polymeric excipient therefore seems to be very efficient. Interestingly, when OMs were administered to the dissolution test in the rodent capsules, there was a slight increase in the release rate in acidic pH (and a subsequent shift of dissolution curve in the FaSSIF stage). This is most probably due to mechanical damage of the covering powder layer of the marbles when they are placed into the capsules. Although the damage of the powder layer apparently translates into dissolution behavior, the overall effect on dissolution properties was considered negligible and hence all subsequent studies were performed without the capsules.

Having established that the HPMCAS-LF coating on the OMs effectively prevents dissolution under acidic conditions, all four OM formulations were then compared in a dissolu-

Table II. Oil Marbles—Different Samples and Their Composition (Weight Percent)

Sample	Abiraterone acetate (%)	Capmul oil MCM NF (%)	Capryol PGMC (%)	Castor oil (%)	Pluronics F-127 (%)	Kolliphor RH40 (%)	Tween 65 (%)	Span 40 (%)	Span 65 (%)	Poloxamer 188 (%)	BHA (%)
OM A	6.9	23.1	-	23.1	23.2	-	23.6	-	-	-	0.1
OM B	7.0	23.1	-	23.3	23.5	23.0	-	-	-	-	0.1
OM C	8.1	-	23.0	22.8	-	-	-	-	22.9	23.1	0.1
OM D	7.8	-	22.6	22.1	24.5	-	-	22.8	-	-	0.1

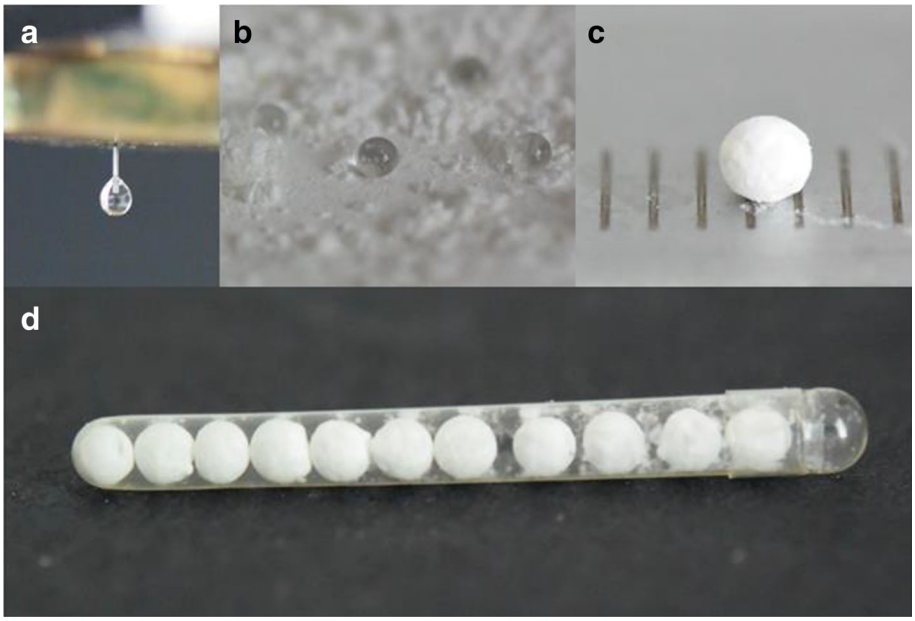

Fig. 2. Formation of oil marbles. **a** Initial droplet of the core material. **b** Droplets after deposition on a powder bed. **c** Finished oil marble coated by HPMCAS-LF. **d** Sub-2-mm OMs filled into rodent capsules size 9el

tion experiment in FaSSIF media (Fig. 4b). As a reference, the dissolution of a crushed Zytiga® tablet (original drug product containing abiraterone acetate) (2) under the same conditions is shown as reported in our previous study (11). The fraction dissolved for most OM formulations except formulation C is considerably higher. Also, no precipitation was observed throughout the experiment suggesting maintained supersaturation of abiraterone acetate when compared with crystalline API present in the original drug product.

OM formulation C contained only surfactants that did not show significant solubility enhancing properties (Span 65 and Poloxamer 188). On the other hand, significant improvement in dissolution rate was seen for both OM formulations A and D. Both of these formulations contained one surfactant that showed solubility enhancing properties (Pluronic F-127) and one that either showed only minor or no effect (Span 40 or Tween 65). Finally, the fastest dissolution rate was observed for OM formulation B; both surfactants used in this formulation increase the solubility of abiraterone acetate. As the release rate in FaSSIF buffer was the highest for OM formulation B and no precipitation was observed, this formulation was retained for further studies.

The effect of OM size on the release kinetics was assessed next. Although the size needed for *in vivo* study in the rat animal model was determined by the inner diameter of the rodent capsules, understanding the effect of OM is useful for further formulation development. The results of dissolution experiment plotted in Fig. 4c clearly show that marble size has a direct effect on the release rate from the oil marble. It is therefore possible to control the release rate from OMs just by changing their diameter. This might be especially useful when targeting certain dissolution profile. It is also a major distinguishing feature of OMs compared with liquid SMEDDS formulations.

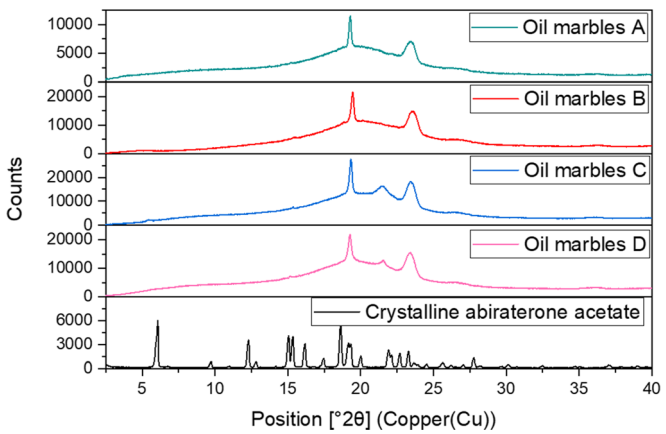

Fig. 3. XRPD diffractograms of OM formulations A–D compared with crystalline abiraterone acetate—the XRPD diffractograms of individual formulation components can be found in Supplementary Material, Fig. S1

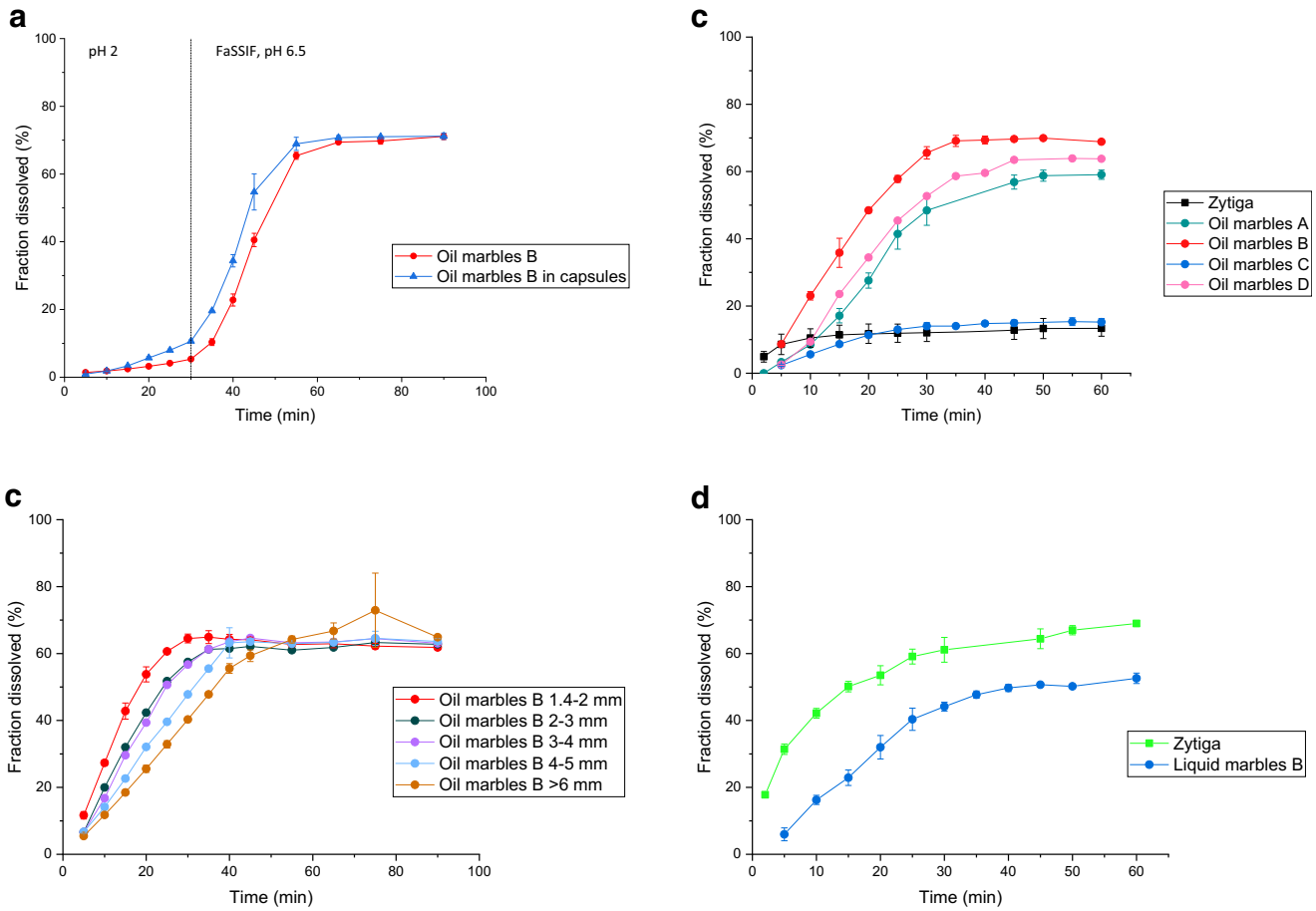

Fig. 4. Mean (± SD, $n = 3$) *in vitro* dissolution profiles of **a** OM formulation B in pH shift dissolution experiment. 0–30 min 10 mM HCl pH 2, 130 mL; 30–90 min FaSSIF pH 6.5, 195 mL; mini-paddles at 125RPM; **b** oil marbles A–D compared with Zytiga® in FaSSIF media, pH 6.5, 200 mL, mini-paddles at 125RPM; **c** different marble sizes of OM formulation B in FaSSIF media, pH 6.5, 200 mL, mini-paddles at 125RPM; **d** OM formulation B compared with Zytiga® in FeSSIF v2 media, pH 5.8, 200 mL, mini-paddles at 125RPM. Fraction dissolved corresponds to abiraterone acetate—abiraterone (product of hydrolysis of abiraterone acetate) was not detected in neither of the experiments. Fraction dissolved corresponds to abiraterone acetate—abiraterone (product of hydrolysis of abiraterone acetate) was not detected in neither of the experiments

As abiraterone acetate is prone to enzymatic hydrolysis upon oral administration (24,32), a dissolution experiment in biorelevant media supplemented with pancreatic enzymes was designed. Also, the effect of lipolysis is assessed when pancreatic enzymes are present in the dissolution media (17). The digestion of lipidic excipients present in the OM formulation might play an important role in the absorption of the drug even though the mixtures prepared in this study fall into group III according to LFCS—drugs can be reportedly absorbed from type III formulations even without digestion (13,14). Three different formulations were tested in the presence of pancreatic enzymes: (i) original drug product Zytiga®; (ii) amorphous solid dispersion with HPMCAS-LF as a carrier (11); (iii) formulation in oil marbles (OM B). The concentration of abiraterone acetate, its hydrolysis product abiraterone, and the total concentration of both compounds are plotted over time in Fig. 5. The area under the curve was calculated for total concentration as a measure of the overall quantity of the API theoretically available for absorption.

It is believed that both abiraterone acetate and abiraterone can permeate through the intestinal wall (32). These results therefore imply that highest bioavailability should be reached for the OM formulation. Moreover, the dissolution curves in pancreatin-enriched media provide an insight into the lipolysis of lipids. The release rate of the drug (when plotted as the combined concentration of abiraterone and abiraterone acetate) is slightly higher when compared with dissolution experiment in FaSSIF (see Fig. 4). This might be caused by the degradation of lipids thus releasing the drug. Also, last time point (90 min) indicates some precipitation of the drug. However, the time window in which the drug is solubilized should be wide enough to allow drug absorption before the precipitation starts.

Finally, since our goal is to suppress food effect reported for abiraterone acetate, also *in vitro* experiments simulating fed conditions were evaluated. For this purpose, dissolution in FeSSIF v2 was conducted. The results are plotted in Fig. 4d.

FeSSIF v2 media have pH 5.8, which is close to the borderline where HPMCAS-LF dissolves (pH 5.5–6). That explains why less API is released from the oil marbles in the fed state simulated fluid (approximately 53% of the administered dose) than in the fasted state simulated fluid (68% of the administered dose). For Zytiga®, only 13% of the

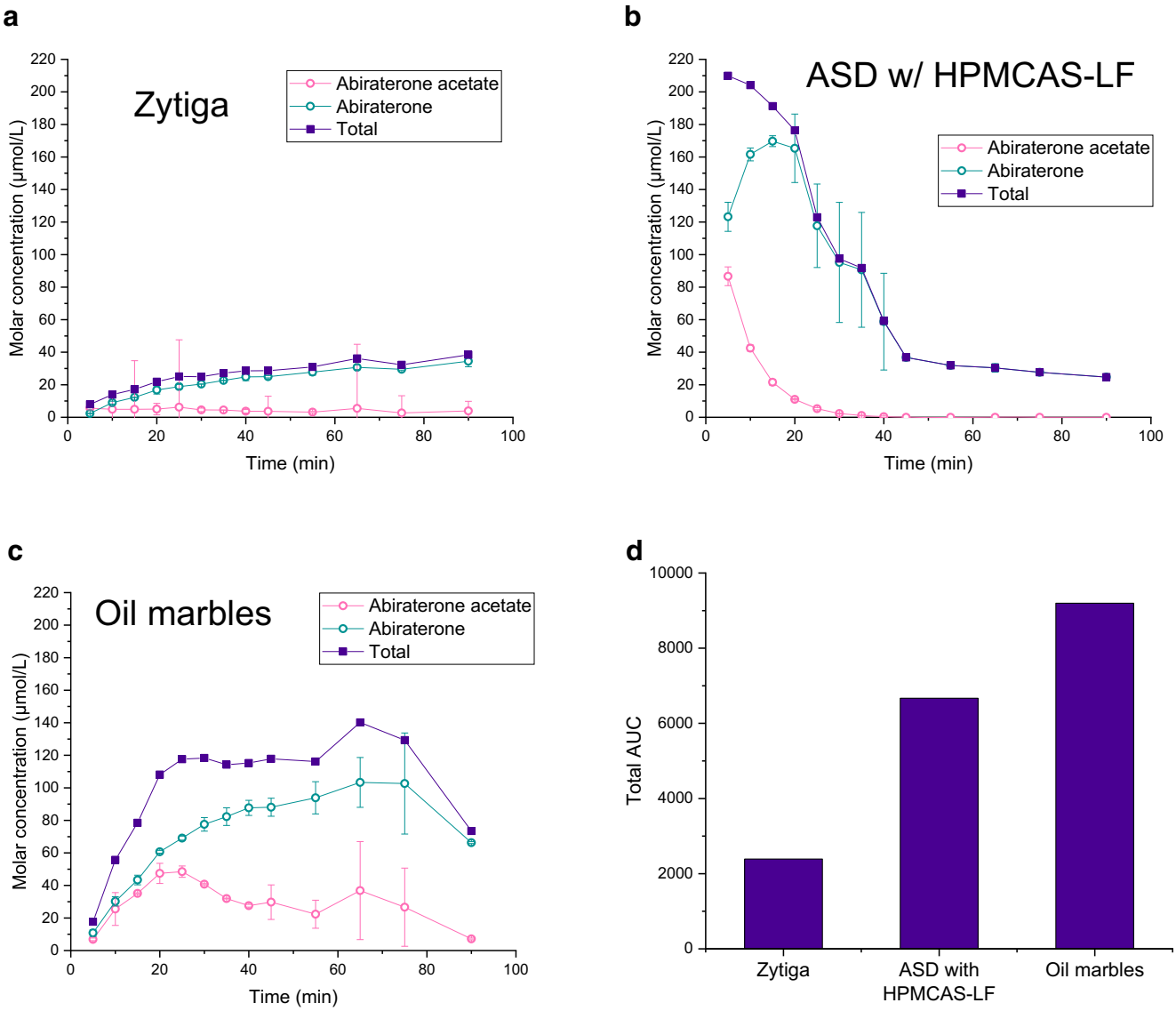

Fig. 5. *In vitro* dissolution in FaSSIF buffer supplemented with pancreatin. Abiraterone acetate (in pink), abiraterone (in green), and total concentration of both compounds (in blue) are plotted. **a** Original drug product Zytiga®. **b** Amorphous solid dispersion with HPMCAS-LF as carrier. **c** Oil marbles B. **d** Total API available for absorption plotted as area under the curve of all three formulations

administered dose is dissolved under simulated fasted conditions compared with 69% of the administered dose dissolved under simulated fed conditions. Moreover, Zytiga® apparently dissolves faster in the fed state simulated intestinal fluids than the OM formulation. If this behavior translates into *in vivo* scenario, the positive food effect reported for original drug product Zytiga® that can lead to toxic exposures of abiraterone acetate could be suppressed.

In Vivo Study

In crossover bioavailability study design, 8 rats completed both periods as planned. The weight of enrolled rats ranged between 309 and 428 g, while administered weigh-normalized doses ranged from 10.30 to 13.78 mg/kg.

Abiraterone pharmacokinetic parameters after administration of test (oil marbles B) and reference (Zytiga®) formulations to fasted rats are summarized in Table III. The rate of drug absorption was substantially higher after administration of test formulation in comparison to reference product as documented by approximately 4-fold C_{max} and shorter T_{max}, although the difference in T_{max} values between test and reference formulations did not reach statistical significance. The extent of abiraterone absorption was approximately 2.7-fold higher after the test formulation in comparison to the reference product. Figure 6a shows the mean abiraterone pharmacokinetic profiles after both products.

Concentrations of pre-dose blood samples were all below the limit of quantification (1 ng/mL) indicating that the wash-out period (48 h) was sufficient. However, the sampling interval, although derived from our previous experience (11), was rather short as the β elimination phase has not been covered in 3 and 2 pharmacokinetic profiles after administration of reference and test formulations, respectively. The AUC_{last}/AUC_{inf} ratio in the rest of animals ranged from 0.71

Table III. Abiraterone PK Parameters After Administration of Test (OM B) and Reference (Zytiga®) Formulations to Rats ($n = 8$) in the Fasted State. T_{max} Values Are Given as Median (interquartile range). C_{max}, AUC_{last}, and Test/Reference Ratios Are Given as Geometric Mean (90% Confidence Intervals)

Formulation	C_{max} (ng/mL g)	T/R C_{max} (%)	AUC_{last} (mg/mL min g)	T/R AUC_{last} (%)	T_{max} (min)
Reference	0.143 (0.073–0.281)	N/A	30.3 (14.3–64.2)	N/A	244 (228–420)
Test	0.569 (0.206–1.566)	397.8 (213.8–740.1)	81.0 (32.1–204.4)	267.4 (165.7–431.6)	168 (114–252)

to 0.99 for the reference formulation and 0.58 to 0.95 for the test formulation, which indicates that the difference in total exposure between formulations is underestimated and would be probably even higher, if the sampling interval covered the whole PK profile thoroughly.

A total of 12 rats were enrolled into the food effect study to get complete pharmacokinetic profiles from 11 subjects. One of the rats had to be excluded due to difficulties with sample collection. Thus, pharmacokinetic profiles under fasted and fed conditions were compared after administration of reference and test formulations in 5 and 6 subjects, respectively. The weight of rats ranged between 355 and 432 g. Weight-normalized doses of abiraterone ranged from 10.75 to 13.33 mg/kg. Table IV shows summarized pharmacokinetic parameters after administration of test (OM B) and reference (Zytiga®) products under fasted or fed state. The reference formulation resulted in approximately twice as high as AUC_{last} in the fed state compared with fasted rats, which corresponds to significantly increased exposure of abiraterone observed with food in humans (2).

There was, however, no food effect on abiraterone absorption from test formulation evidenced by similar C_{max} and AUC_{last} values under the fasted and fed states. For both formulations, absorption was prolonged in the fed state. The test formulation required less time to reach the maximum plasma concentration than the reference. Mean (SD) abiraterone pharmacokinetic profiles are showed in Fig. 6b and c.

Concentrations of pre-dose blood samples were all below the limit of quantification (1 ng/mL), suggesting that the wash-out period between dosing (48 h) was sufficient. Although this food effect study was not powered to compare differences between formulations in fasting conditions, the results correspond with observations from the first part of the study. Zytiga® is standardly administrated in the fasted state. When comparing abiraterone exposure of both formulations, administration of oil marbles led to twice as high AUC_{last} as Zytiga® in the same dose. If we consider the advantage of eliminated food effect, oil marbles seem to be a promising drug formulation for abiraterone acetate.

DISCUSSION

The main goal of this work was to prepare and test a new formulation concept for abiraterone acetate based on the so-called oil marbles (OMs). We have successfully prepared OMs from different mixtures of oils and surfactants that showed an ability to solubilize abiraterone acetate. Although the design space for the preparation of oil marbles was not covered exhaustively, we have shown several manufacturable OM formulations using surfactants of different chemical structures and physical properties.

All prepared samples of OMs exhibited an amorphous character which shows that abiraterone acetate remains molecularly dispersed in the oil-based matrix even after it cools down to room temperature. This implies that the dissolution rate from the OM formulation will depend only on the rate at which the matrix components are being dispersed in the dissolution media. The marble size hence turned out to be the crucial parameter for the *in vitro* performance of the oil marbles. While keeping in mind that the performance of lipid-based formulations does not rely solely on the dissolution profiles, the results showed that

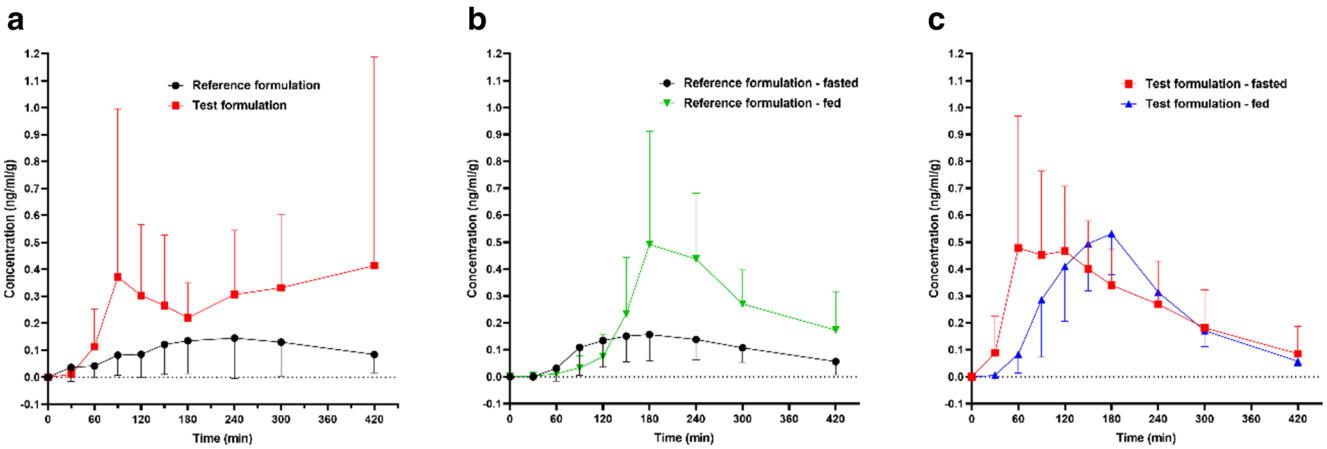

Fig. 6. Mean (± SD) abiraterone pharmacokinetic profiles in rats: **a** after administration of reference and test formulations in fasted condition; **b** after administration of reference formulation in fasted and fed conditions; **c** after administration of test formulation in fasted and fed conditions

Table IV. Abiraterone PK Parameters After Administration of Test and Reference Formulations to Rats ($n = 11$) in Fasted and Fed Conditions. T_{max} Values Are Given as Median (Interquartile Range). C_{max}, AUC_{last}, and Fed/Fasted Ratios Are Given as Geometric Mean (90% Confidence Intervals)

Formulation	C_{max} (ng/mL g)	Fed/fasted C_{max} (%)	AUC_{last} (mg/mL min g)	Fed/fasted AUC_{last} (%)	T_{max} (min)
Reference fasted	0.231 (0.176–0.302)	N/A	40.0 (31.3–51.1)	N/A	179 (157–226)
Reference fed	0.550 (0.318–0.950)	238.5 (131.1–433.9)	80.7 (40.6–160.4)	201.8 (86.7–469.4)	218 (185–288)
Test fasted	0.546 (0.199–1.480)	N/A	94.7 (43.2–207.4)	N/A	125 (68–178)
Test fed	0.530 (0.351–0.801)	103.8 (58.3–184.9)	93.6 (62.6–140.1)	105.1 (76.4–144.5)	152 (148–178)

release profiles can be controlled simply by adjusting the size of OMs. This can be crucial when targeting certain dissolution/absorption profile.

To further understand the behavior of OM formulation, *in vitro* experiment with pancreatic enzymes was designed. Overall, all conducted *in vitro* tests showed a tendency towards higher fraction dissolved under fasting conditions for OM formulation when compared with the original drug formulation Zytiga®. These results provided a solid base for subsequent *in vivo* testing, where a significantly higher relative bioavailability of OMs was indeed observed.

In order to address the effect of food on the bioavailability of different abiraterone acetate formulations, a fasted-fed *in vivo* study was designed and conducted. It had been shown before that a high fat content in meal has a significant impact on the bioavailability of abiraterone acetate (5). Limited bioavailability of the original drug product Zytiga® under fasting conditions resulted in a significant positive food effect in the rat animal model, which is consistent with previously conducted human studies.

A 1:1 mixture of olive oil and Nutridrink was dosed to rats to create the fed state. The use of this mixture was based not only on previous experience but also on conditions described in the literature. The administration of 1–2 mL of oil is a standard approach to introduce fed conditions in rat PK studies (33,34). However, since the formulation was dosed in hard gelatin capsules, we had to ensure that the rat stomach also contains some aqueous phase in which the capsules could dissolve.

The fasted state comparative bioavailability study has shown a rather unexpected double C_{max} pattern for abiraterone after OM (Fig. 6a). This finding was mainly driven by a single animal outlying with exceptionally high abiraterone serum concentrations at the sampling points between 240 and 420 min. In the food effect study, the C_{max} and AUC values demonstrated limited effect of food for OM formulation, but the T_{max} was substantially prolonged at the fed state, which could be a result of a non-formulation-dependent effect of the presence of food in the gastrointestinal tract that increased secretion, delayed gastric emptying, influenced intestinal peristaltic movement, or competed with drugs on absorption transporters (35). Furthermore, a large variability in the serum drug concentrations has been observed in the OM group at the fasted state. This observation was caused by the fact that always one of the animals achieved C_{max} was at 60, 90, and 120 min, while in the rest of the group, a "plateau" was seen between 90 and 300 min with no clear T_{max}. These findings point out to the main limitation of our studies, which is limited study population. Another limitation is that the pharmacokinetic performance of OM has been studied *in vivo* in a rat model, which is known to have different gastrointestinal physiologies and conditions that may make direct extrapolation of the findings to man difficult. However, the food effect, which is known from human studies, has been well captured in our food effect study, which suggests sufficient study sensitivity. Furthermore, we applied a crossover comparative study design, which allows to limit the study population as it is the most robust study design to limit intersubject variability for the comparison of performance of two (or more) formulations. The limitation of the small study sample is that we could not reliably describe the T_{max} and some other pharmacokinetic variables but the between-formulation comparison, which was the aim of the study, has been well demonstrated. The relatively higher bioavailability of oil marbles under fasting conditions resulted in a significantly suppressed food effect in rats.

CONCLUSION

Overall, it can be concluded that oil marbles represent a promising formulation approach that combines the advantages of liquid-state lipidic formulations such as SEDDS/SMEDDS, namely rapid dissolution, with advantages of solid dosage form such as handling, ability to be filled into hard gelatin capsules, and the possibility to adjust release rate by size. In the specific case of abiraterone acetate, the oil marble formulation made it possible to suppress differences in the oral bioavailability under fed and fasted conditions in rats, and therefore help to eliminate the strong positive food effect for which this molecule has been known. Due to natural differences in rat and human gastrointestinal physiology, these results should be confirmed in human studies as the next step.

AUTHOR CONTRIBUTIONS

The manuscript was written through contributions of all authors. All authors have given approval to the final version of the manuscript.

FUNDING

T.B. received support from the Specific University Research (project MŠMT no. 21-SVV/2019). F.Š. received support from the Czech Science Foundation (project GAČR no. 19-26127X). O.R. received support from the Technology Agency of the Czech Republic (project no. TJ02000143). T.K.

received support from Charles University Research Centre program no. UNCE/SCI/014. O.S. received support from the Charles University project PROGRES Q25/LF1. This work received support from Zentiva, k.s.

COMPLIANCE WITH ETHICAL STANDARDS

All experiments were performed in accordance with the Guiding Principles for the Use of Animals in Charles University, First Faculty of Medicine, and every effort was made to minimize animal suffering. The experimental animal project was approved by the Ministry of Education, Youth and Sports, Czech Republic (MSMT-9445/2018-8).

Conflict of Interest The authors declare that they have no competing interests.

REFERENCES

1. Boyd BJ, Bergstrom CAS, Vinarov Z, Kuentz M, Brouwers J, Augustijns P, et al. Successful oral delivery of poorly water-soluble drugs both depends on the intraluminal behavior of drugs and of appropriate advanced drug delivery systems. Eur J Pharm Sci. 2019;137:104967.
2. Zytiga, EMA/CHMP/542871 – Assessment report for Zytiga, EMA (European Medicines Agency). 2011.
3. Lubberman FJE, Benoist GE, Gerritsen W, Burger DM, Mehra N, Hamberg P, et al. A prospective phase I multicentre randomized cross-over pharmacokinetic study to determine the effect of food on abiraterone pharmacokinetics. Cancer Chemother Pharmacol. 2019;84(6):1179–85.
4. Chi KN, Spratlin J, Kollmannsberger C, North S, Pankras C, Gonzalez M, et al. Food effects on abiraterone pharmacokinetics in healthy subjects and patients with metastatic castration-resistant prostate cancer. J Clin Pharmacol. 2015;55(12):1406–14.
5. Chien C, Smith M, Porre P. Effect of food on abiraterone pharmacokinetics: a review. Int J Pharm. 2017;2.
6. Schultz HB, Meola TR, Thomas N, Prestidge CA. Oral formulation strategies to improve the bioavailability and mitigate the food effect of abiraterone acetate. Int J Pharm. 2020;577:119069.
7. Yonsa, Drug Approval Package: YONSA (abiraterone acetate), FDA (U.S. Food and Drug Administration). Food and Drug Admistration (FDA). 2018.
8. Goldwater R, Hussaini A, Bosch B, Nemeth P. Comparison of a novel formulation of abiraterone acetate vs. the originator formulation in healthy male subjects: two randomized, open-label, crossover studies. Clin Pharmacokinet. 2017;56(7):803–13.
9. Solymosi T, Ötvös Z, Angi R, Ordasi B, Jordán T, Molnár L, et al. Novel formulation of abiraterone acetate might allow significant dose reduction and eliminates substantial positive food effect. Cancer Chemother Pharmacol. 2017;80(4):723–8.
10. Solymosi T, Ötvös Z, Angi R, Ordasi B, Jordán T, Semsey S, et al. Development of an abiraterone acetate formulation with improved oral bioavailability guided by absorption modeling based on in vitro dissolution and permeability measurements. Int J Pharm. 2017;532(1):427–34.
11. Boleslavská T, Světlík S, Žvátora P, Bosák J, Dammer O, Beránek J, et al. Preclinical evaluation of new formulation concepts for abiraterone acetate bioavailability enhancement based on the inhibition of pH-induced precipitation. Eur J Pharm Biopharm. 2020;151:81–90.
12. Legen I, Peternel L, Novak Stagoj M, Homar M, Rozman Peterka T, Klancar U. Self-microemulsifying drug delivery system of abiraterone or abiraterone acetate, WO 2014/009434 A1 2014.
13. Pouton CW, Porter CJ. Formulation of lipid-based delivery systems for oral administration: materials, methods and strategies. Adv Drug Deliv Rev. 2008;60(6):625–37.
14. Mullertz A, Ogbonna A, Ren S, Rades T. New perspectives on lipid and surfactant based drug delivery systems for oral delivery of poorly soluble drugs. J Pharm Pharmacol. 2010;62(11):1622–36.
15. Mu H, Holm R, Müllertz A. Lipid-based formulations for oral administration of poorly water-soluble drugs. Int J Pharm. 2013;453(1):215–24.
16. Bernkop-Schnurch A, Jalil A. Do drug release studies from SEDDS make any sense? J Control Release. 2018;271:55–9.
17. Carriere F. Impact of gastrointestinal lipolysis on oral lipid-based formulations and bioavailability of lipophilic drugs. Biochimie. 2016;125:297–305.
18. Sonali BH, Sushmita SC, Sonali SK, Suchita LS, Sugave RV. A review on: soft gelatine capsule. Int J Innov Pharm Sci Res. 2018;6(6):59–71.
19. Joyce P, Dening TJ, Meola TR, Schultz HB, Holm R, Thomas N, et al. Solidification to improve the biopharmaceutical performance of SEDDS: opportunities and challenges. Adv Drug Deliv Rev. 2019;142:102–17.
20. Aussillous P, Quéré D. Liquid marbles. Nature. 2001;411(6840):924–7.
21. McHale G, Newton MI. Liquid marbles: principles and applications. Soft Matter. 2011;7(12):5473.
22. Hapgood KP, Khanmohammadi B. Granulation of hydrophobic powders. Powder Technol. 2009;189(2):253–62.
23. Janská P, Rychecký O, Zadražil A, Štěpánek F, Čejková J. Liquid oil marbles: increasing the bioavailability of poorly water-soluble drugs. J Pharm Sci. 2019;108(6):2136–42.
24. Geboers S, Stappaerts J, Mols R, Snoeys J, Tack J, Annaert P, et al. The effect of food on the intraluminal behavior of abiraterone acetate in man. J Pharm Sci. 2016;105(9):2974–81.
25. Rowe RC, Sheskey PJ, Quinn ME. Handbook of pharmaceutical excipients. 6th ed. USA: Pharmaceutical Press and American Pharmacists Association; 2009.
26. Kabanov AV, Batrakova EV, Alakhov VY. Pluronic® block copolymers as novel polymer therapeutics for drug and gene delivery. J Control Release. 2002;82(2):189–212.
27. Kolliphor RH40, BASF Technical information no. 03_111141e-01.
28. Tween 20, Sigma Alrdich Product information no. 1379.
29. Tween 80, Sigma Aldrich Product information no. 1754.
30. Kolliphor EL, BASF Technical information no. 03_111139e-02.
31. Brouwers J, Brewster ME, Augustijns P. Supersaturating drug delivery systems: the answer to solubility-limited oral bioavailability? J Pharm Sci. 2009;98(8):2549–72.
32. Stappaerts J, Geboers S, Snoeys J, Brouwers J, Tack J, Annaert P, et al. Rapid conversion of the ester prodrug abiraterone acetate results in intestinal supersaturation and enhanced absorption of abiraterone: in vitro, rat in situ and human in vivo studies. Eur J Pharm Biopharm. 2015;90:1–7.
33. Brocks DR, Wasan KM. The influence of lipids on stereoselective pharmacokinetics of halofantrine: important implications in food-effect studies involving drugs that bind to lipoproteins. J Pharm Sci. 2002;91(8):1817–26.
34. Shayeganpour A, Jun AS, Brocks DR. Pharmacokinetics of Amiodarone in hyperlipidemic and simulated high fat-meal rat models. Biopharm Drug Dispos. 2005;26(6):249–57.
35. Welling PG. Effects of food on drug absorption. Annu Rev Nutr. 1996;16:383–415.

Příloha 4

JELINEK, P. [#], ROUSAROVA, J. [#], RYSANEK, P., JEZKOVA, M., HAVLUJOVA, T., POZNIAK, J., KOZLIK, P., KRIZEK, T., KUCERA, T., SIMA, M., SLANAR, O. & SOOS, M. 2022. Application of Oil-in-Water Cannabidiol Emulsion for the Treatment of Rheumatoid Arthritis. Cannabis Cannabinoid Res.

Cannabis and Cannabinoid Research
Volume X, Number X, 2022

DOI: 10.1089/can.2022.0176

Application of Oil-in-Water Cannabidiol Emulsion for the Treatment of Rheumatoid Arthritis

Petr Jelínek,[1,†] Jaroslava Roušarová,[2,†] Pavel Ryšánek,[2] Martina Ježková,[1] Tereza Havlůjová,[1] Jiří Pozniak,[3] Petr Kozlík,[4] Tomáš Křížek,[4] Tomáš Kučera,[5] Martin Šíma,[2] Ondřej Slanař,[2] and Miroslav Šoóš[1,*]

Abstract

Introduction: Rheumatoid arthritis (RA) is a chronic autoimmune disease with unknown cause. It mainly affects joints and, without proper treatment, negatively impacts their movement, causes painful deformities, and reduces the patients' quality of life. Current treatment options consist of various types of disease-modifying antirheumatic drugs (DMARDs), however 20–30% of patients are partially resistant to them. Therefore, development of new drugs is necessary. Possible option are compounds exhibiting their action via endocannabinoid system, which plays an important role in pain and inflammation modulation. One such compound – cannabidiol (CBD) has already been shown to attenuate synovitis in animal model of RA in in vivo studies. However, it has low bioavailability due to its low water solubility and lipophilicity. This issue can be addressed by preparation of a lipid containing formulation targeting lymphatic system, another route of absorption in the body.

Materials and Methods: CBD-containing emulsion was prepared by high-shear homogenization and its droplet size distribution was analysed by optical microscopy. The relative oral bioavailability compared to oil solution as well as total availability of CBD were assessed in a cross-over study in rats and absorption of CBD via lymphatic system was observed. The effect of CBD on the animal model of RA was determined.

Results: Compared to oil solution, the emulsion exhibited higher absolute oral bioavailability. Significant lymphatic transport of CBD was observed in all formulations and the concentrations in lymph were calculated. The therapeutic effect of CBD on RA was confirmed as an improvement in clinical symptoms as well as morphological signs of disease activity were observed during the study.

Conclusion: In this work, we prepared a simple stable emulsion formulation, determined the pharmacokinetic parameters of CBD and calculated its absolute bioavailability in rats. Moreover, we successfully tested the pharmaceutical application of such a formulation and demonstrated the positive effect of CBD in an animal model of RA.

Keywords: rheumatoid arthritis; cannabidiol; emulsion; *in vivo* study; bioavailability; lymphatic absorption

Introduction

Rheumatoid arthritis (RA) is a chronic autoimmune inflammatory disease affecting mainly small joints, but it can also spread to other tissues and organs; for example, skin, lungs, or heart. RA can progress into periarticular bone and cartilage damage resulting in debilitating deformities, significantly reducing quality of life. As RA is a chronic disease with an unknown cause, the main therapeutic objective is to stop the progression of the disease and achieve sustained remission; that is, to reduce the pain and inflammation of affected joints, maximize their function, and prevent irreversible periarticular damage.[1]

Current treatment options consist of synthetic, targeted synthetic, and biologic disease-modifying

[1]Department of Chemical Engineering, Faculty of Chemical Engineering, University of Chemistry and Technology, Prague, Czech Republic.
[2]Institute of Pharmacology, First Faculty of Medicine, Charles University and General University Hospital in Prague, Prague, Czech Republic.
[3]Third Department of Surgery, First Faculty of Medicine, Charles University in Prague and Motol University Hospital, Prague, Czech Republic.
[4]Department of Analytical Chemistry, Faculty of Science, Charles University, Prague, Czech Republic.
[5]Institute of Histology and Embryology, First Faculty of Medicine, Charles University, Prague, Czech Republic.
[†]Equally contributing authors.

*Address correspondence to: Prof. MUDr. Ondřej Slanař, PhD, Institute of Pharmacology, First Faculty of Medicine, Charles University and General University Hospital in Prague, Kateřinská 32, Prague 121 08, Czech Republic, E-mail: ondrej.slanar@lf1.cuni.cz; Prof. Ing. Miroslav Šoóš, PhD, Department of Chemical Engineering, Faculty of Chemical Engineering, University of Chemistry and Technology, Technická 1905/5, Prague 16628, Czech Republic, E-mail: miroslav.soos@vscht.cz

antirheumatic drugs (DMARDs), supplemented by glucocorticoids, nonsteroidal antirheumatic drugs, and analgesics for symptomatic treatment of pain and inflammation. However, the disease is rather heterogenic, and a combination of DMARDs is often necessary for inducing remission and maintaining low disease activity. Although the introduction of biologics dramatically improved the prognosis of patients as well as therapeutic outcomes, there are still ~20–30% of patients partially resistant to current treatment options. Other downsides are high cost of biologic DMARDs and the need for parenteral administration. For this reason, new therapies are urgently needed.[2]

One group of candidate drugs with therapeutic potential for RA treatment are natural compounds exhibiting their action through the endocannabinoid system, which plays an important role in pain and inflammation modulation. There are two types of cannabinoid (CB) receptors. CB1 receptors, expressed mainly in the central nervous system, are responsible for neurobehavioral effects and nociceptive transmission in the brain.

The other type, CB2 receptors, found in immune cells, lymph nodes, and nodular corona of Peyers patches, plays an important role in immunomodulation and inflammatory pain response. The activation of CB2 receptors mediates immune cell suppression. It inhibits the production of proinflammatory cytokines, autoantibodies, and matrix metalloproteinases (MMPs). Furthermore, it suppresses the proliferation of fibroblast-like synoviocytes, NFκB-dependent apoptotic responses, and T-helper–mediated functions.[3]

Cannabidiol (CBD), obtained from *Cannabis sativa*, is a promising nonpsychoactive compound affecting endocannabinoid system. CB oils are widely commercially available as food supplements, not only for humans but also for animals. CBD itself has been shown to attenuate synovitis and joint destruction in collagen-induced arthritis (CIA), an animal model of RA in *in vivo* studies.[4,5]

Despite this, Epidiolex/Epidyolex, a solution of CBD and flavorings in sesame oil used to treat seizures in rare forms of epilepsy, and Sativex, oromucosal spray for spastic symptoms of multiple sclerosis, remain the only Food and Drug Administration- and European Medicines Agency (EMA)-approved oral drugs that contain CBD.[6] This is because although CBD has high solubility in lipids and organic solvents, it is almost insoluble in water. Low water solubility leads to low bioavailability and subsequently noneffective plasma concentrations after oral administration. Nevertheless, there is a promising way to increase the absorption from the gastrointestinal tract by targeting another specific means of drug transport in the body; the lymphatic system.

Lymphatic transport is an important pharmacokinetic characteristic of numerous highly lipophilic compounds.[7] Robust evidence suggests that only compounds with log $p > 5$ have an inherent affinity toward intestinal lymph.[8,9] The presence of drug in the lymph can have major pharmacokinetic and pharmacodynamic implications, as oral bioavailability increases due to higher absorption and circumvention of liver first-pass effect.

Furthermore, the lymphatic system plays an important role in immunomodulation due to presence of leukocytes in lymph and associated lymph nodes. Therefore, it is an important potential target for immunomodulatory drugs, and better treatment efficacy is expected. CBD with its high lipophilicity (log p 6.3), significant first-pass metabolism, and immunomodulatory effect is a suitable candidate to exploit all these advantages.[10]

Therefore, assessment of CBD lymphatic transport is of great importance for the pharmaceutical science. Zgair et al. have already reported a significant CBD concentration in mesenteric lymph (250 times higher compared with plasma) after the administration of the sesame oil formulation.[11] However, a precise and comprehensive quantification of CBD lymphatic transport assessing its absolute and relative contribution to overall systemic bioavailability is still lacking.

To enable lymphatic absorption, the presence of a lipidic excipient is necessary, as it helps solubilize the drug and mediates its association with chylomicrons.[11,12] Therefore, most CBD-containing formulations used in *in vivo* studies are oil based.[4,13,14] Emulsions, formulations consisting of both oil and aqueous phase, are tolerable, and another advantage is their enhanced surface area for absorption due to increase in droplet area, which can enhance bioavailability, as demonstrated by Francke et al[15] for CBD-containing nanoemulsion. Despite this success, careful selection of excipients is crucial because different oil vehicles and surfactants can affect the bioavailability of CBs, and thus, the efficiency of RA treatment.[16] Consequently, an appropriate combination of *in vitro* and *in vivo* investigations is essential for formulation optimization.

Based on the information discussed above, we prepared CBD microemulsion composed of surfactant-stabilized oil droplets dispersed in water. We determined its droplet size and tested coalescence stability. The main focus of this study was characterization of CBD pharmacokinetic parameters and therapeutic effect in the treatment of RA.

Materials and Methods

Chemicals

The following chemicals were used for the preparation of CBD formulations. CBD (98.9 wt %) was purchased from PharmaHemp® (Slovenia). Sunflower oil (standardized product of pharmaceutical quality) was purchased from Fagron a.s. (Czech Republic). L-α-Lecithin (soybean, >94% phosphatidylcholine) manufactured by Calbiochem® was purchased from Sigma-Aldrich (Germany). Capryol® PGMC and Transcutol® P were kindly donated by Gattefossé (France). Kolliphor® EL was purchased from BASF (Germany). Aqual® Ultrapur demineralized water was used for the preparation of the formulations.

Preparation of formulations containing CBD

The emulsion formulation for oral delivery composed of sunflower oil and water (1:4 wt ratio) was prepared by high-shear homogenization. First, CBD (112.5 mg) was dissolved in sunflower oil (3 g) in a glass vial using mild magnetic stirring. Then, lecithin (1.5 g) was added to the oil phase. Ultra-Turrax® T 25 (IKA; Germany) disperser with S25N-10G-ST dispersing tool was immersed in the vial with the CBD oil phase and lecithin. Approximately half of the aqueous phase fraction (12 g) was added to the mixture to reach the necessary immersion level of the dispersing tool.

The stirring speed was set to 15,000 rpm for 5 min, during which the rest of the aqueous phase was manually dripped into the vial using a syringe with long needle. After the high-shear homogenization, the emulsion was shaken for 1 min using a vortex mixer (Vortex mixer VV3, VWR) to eliminate the surface foam. The final concentration of CBD in the emulsion was 7.5 mg/mL. The oil solution, which was used as a reference with the same CBD concentration, was prepared by dissolution of CBD (24.4 mg) in sunflower oil (3 g) applying mild magnetic stirring.

The formulation for intravenous delivery was composed of CBD (60 mg), Capryol PGMC (0.4 g), Cremophor EL (1 g), Transcutol P (0.6 g), and distilled water up to the total volume of 6 mL. First, CBD was dissolved in the mixture of nonaqueous components. Then, water was added, and the concoction was stirred magnetically (900 rpm). The final concentration of CBD in the emulsion was 1 mg/100 μL.

Optical microscopy and image analysis of the emulsion containing CBD

Optical microscopy was performed using a system composed of Resolv4K lenses (Navitar, the United States) and Olympus (the United States) objective lenses connected to the high-speed camera PL-D725MU-T (PixeLINK; Navitar). Emulsion droplet was placed between the support and cover glass slide. Image analysis was performed using software ImageJ (NIH, the United States). Maximum Feret diameters were calculated considering 500–600 oil droplets.

Animals

Wistar rats (300–450 g) were purchased from Velaz (Prague, Czech Republic). The rats were housed under standard conditions (temperature of 22 ± 2°C, relative humidity of 50 ± 10%, 12-h light–dark cycle). The animals had access to water and standard granulated diet *ad libitum*. All parts of experiment were carried out with respect to Guiding Principles for the Use of Animals at Charles University, First Faculty of Medicine. The permission for the experimental animal project was conferred by the Ministry of Education, Youth and Sports, Czech Republic (MSMT-26838/2021–4).

General anesthesia was induced using isoflurane (IsoFlo, 250 mL; Zoetis/Pfizer, Czech Republic), ketamine (Narkamon, 100 mg/mL, inj. Sol.; Bioveta, Ivanovice na Hané, Czech Republic), and xylazine (Rometar, 20 mg/mL, inj. Sol.; Bioveta). Heparin (Heparin Léčiva, inj. Sol., 1 × 10 mL/50 KU; Zentiva, Czech Republic), ketoprofen (Ketodolor, inj. Sol., 100 mL; LeVet Pharma b.v., Netherlands), and Carbethopendecinium bromide (Ophthalmo-Septonex, eye ointment, 1 × 5 g; Zentiva) were used in pursuance of the perioperative anticoagulant, analgesic, and antiseptic treatment, respectively.

Bovine type II collagen and incomplete Freund's adjuvant for arthritis induction were purchased from Chondrex. The combination of mebezonium iodide, embutramide, and tetracaine hydrochloride (T 61, inj. Sol.; Intervet International, B.V., Netherlands) was used for the euthanasia at the end of the experiment.

CBD bioavailability

To allow repeated blood sampling, a polyurethane catheter (3Fr; Intech Laboratories, Plymouth Meeting, the United States) was inserted into the external jugular vein 3 days before first dosing. The procedure was performed under general anesthesia using 2.5–5% isoflurane followed by 100 mg/kg of intramuscular ketamine and 5 mg/kg of intramuscular xylazine. At the end of the surgical procedure, 5 mg/kg ketoprofen was administered subcutaneously as an analgesic. The catheter was flushed with 200 μL saline and 50 μL heparin, and sealed with a combination of 20 μL glycerol and heparin.

The relative oral bioavailability of CBD emulsion compared with simple oil solution was assessed in a randomized, single-dose, two-sequence, and two-period, laboratory-blinded, crossover bioequivalence study. Adult male rats were fasted with unrestricted access to water for 4 h before and after dosing. The administration of 1 mL (equivalent to 7.5 mg of CBD) of both the oil and emulsion formulation was conducted using oral gavage. Systemic blood samples (120 μL) were collected predose (second period) and at 1, 2, 3, 4, 5, 6, 8, 10, and 24 h postdose (both periods) from the jugular vein catheter. Each blood sample was substituted with an equal volume of saline. The washout period between the first and the second dosing took 72 h.

In addition, another group of animals was dosed intravenously for the purpose of absolute bioavailability calculation of both formulations used in the bioequivalence study. For this experiment, both jugular veins were cannulated. CBD formulation (1 mg, 100 μL) was administered into the left jugular vein. Blood samples were then drawn from the right jugular vein catheter at 5, 15, and 30 min and at 1, 2, 4, 6, and 10 h.

Blood samples were centrifuged for 10 min (2000 *g*, 4°C), and serum was extracted. Serum samples were stored at −80°C until analysis.

CBD lymphatic absorption

Anesthetized mesenteric lymph duct cannulated rat model was used as previously described with slight modifications.[17] Adult male rats were left on a normal diet and given 1 mL olive oil 1 h before surgery to visualize the mesenteric lymph duct. They were anesthetized using isoflurane, ketamine, and xylazine as described above. Transverse laparotomy was performed. The mesenteric duct was identified cranially to the superior mesenteric artery and cannulated using heparin prefilled 0.97 mm O.D., 0.58 mm I.D. polyethylene catheter (Instech Laboratories, Plymouth Meeting, the United States).

The catheter was fixed in place with two to three drops of tissue adhesive (Surgibond®; SMI AG, Belgium). A duodenal catheter (same parameters as for the lymphatic catheter) was also placed through a small duodenotomy and fixed with tissue adhesive. The abdominal wall was sutured with both catheters leaving the abdominal cavity through the right flank of the animal. At the end of the procedure, the right jugular vein was cannulated for blood sampling. The rats were placed on heated pads and covered with blankets to prevent heat loss.

After the surgery, 1 mL of oil solution or emulsion (both containing 7.5 mg of CBD) was dosed through duodenal catheter for >30 min. The whole lymph was collected in regularly changed Eppendorf tubes from the time drug administration started. Rats were continuously hydrated with normal saline at a rate of 3 mL/h intraduodenally using an infusion pump (Perfusor® compact plus; B. Braun, Melsungen AG, Germany). Anesthesia was maintained throughout the rest of the experiment, and additional ketamine i.m. boluses were administered whenever necessary. Eppendorf tubes were changed every 1 h, and systemic blood was drawn at the same time points.

Lymph samples were processed without further adjustments and stored at −80°C until analysis.

CBD emulsion in the treatment of CIA

Collagen emulsion for CIA induction was prepared according to the Chondrex protocol by emulsification of incomplete Freund's adjuvant with collagen dissolved in 0.05 M acetic acid. The initial 0.2 mL emulsion dose was applied subcutaneously into the bases of adult female rats' tails. The 0.1 mL booster injection was administered 7 days later. Rats in the negative control group were injected with the same volumes of saline.

The required number of rats suffering from CIA was obtained 17 days after the first immunization. On this day (Day 0), the CIA rats were symmetrically randomized into two groups. The first group (CBD group) was treated orally with 2 mL microemulsion containing 15 mg CBD once daily ($n=6$), and the second group (Placebo group) was treated with the same volume of saline ($n=6$). Rats in the negative control group were administered saline ($n=3$). Treatment lasted 24 days in all three groups.

The treatment progression was monitored throughout the experiment by visually assessing and recording the state of both hind paws of each rat every 3 days. The four-point scoring scale per leg was used with the following grading: 0 = normal joint; 1 = swelling or redness in 1 joint; 2 = swelling or redness in >1 joint; 3 = whole-paw swelling; 4 = joint deformity or ankylosis, immobility. Ankle edema was evaluated by measuring the width of both hindlimb ankles using digital calipers on the day of randomization (Day 0) and at the end of the experiment (Day 24).

Blood samples were taken on Day 0 and Day 24 to evaluate MMP-3 levels in serum. Blood was sampled from the tail on Day 0 and from the myocardium immediately before the euthanasia on Day 24. Blood was centrifuged and the obtained serum was stored at

−20°C until analysis. MMP-3 levels were determined using an enzyme-linked immunosorbent assay (Rat MMP3 ELISA kit ab270216; Abcam, Cambridge, United Kingdom).

On Day 24, immediately after the euthanasia, each rat's right hindlimb was amputated above the ankle. The samples were fixed in 4% formaldehyde in PBS, and subsequently decalcified in the 10% formic acid solution. This process lasted 2–3 months with solution replacement twice a week. After decalcification, the phalangeal part was separated, rinsed in water, and embedded in paraffin using a common procedure. Seven-micrometer-thick sections were stained with hematoxylin eosin and mounted in Canada balsam.

The imaging was performed using Leica DMLB microscope and LAS software (Leica Microsystems GmbH, Wetzlar, Germany). Sections through the phalangeal joints were scored according to the level of structural damage and disease activity. The structural damage score was based on the following characteristics: cartilage erosion, bone erosion and resorption, and synovial inflammation plus pannus invasion. The levels were 0 = healthy joint; 1 = mild changes; 2 = advanced changes; and 3 = severe damage. The disease activity score was established as follows: 0 = no osteoclasts, 1 = occasional osteoclasts present; 2 = focal presence of osteoclasts; 3 = widespread infiltration of osteoclasts.

Analytical methods

The concentration of CBD in serum and lymph was determined. For serum and lymph samples, protein precipitation was used. The samples were processed as follows: 80 μL of 100% acetonitrile (containing 30.0 ng/mL CBD-d3 as an internal standard) were added to 20 μL of the sample. The mixture was vortexed and centrifuged at 10,000 *g* for 8 min. Sixty microliters of supernatant were transferred to an chromatography vial. For the UHPLC-MS/MS analysis, the Shimadzu UHPLC Nexera X3 coupled with a Triple Quad 8045 tandem mass spectrometer (Shimadzu, Kyoto, Japan) was used. Chromatographic analysis was performed on a Poroshell 120 EC-C18 column (50 × 2.1 mm; 1.9 μm; Agilent Technologies, Inc., Santa Clara, CA, the United States).

The mobile phase consisted of 0.1% formic acid in deionized water (Solvent A) and methanol with 0.1% formic acid (Solvent B). The flow rate of the mobile phase was maintained at 0.4 mL/min, and the injection volume was 2 μL. The column temperature was kept at 40°C, and the samples were thermostated at 10°C. The optimized gradient elution was carried out as follows (min/% B): 0/50, 0.5/50, 2.5/90, 3.5/90, 4.0/50, and 5.5/50. The MS/MS spectrometer was operated in a positive mode.

The applied conditions of the electrospray ion source were as follows: nebulizing gas flow: 3 L/min, heating gas flow: 10 L/min, interface temperature: 300°C, desolvation line temperature: 250°C, heat block temperature: 400°C, and drying gas flow: 10 L/min. The MS/MS measurement was performed in multiple reaction-monitoring mode (MRM). MRM transitions of 315.2 > 193.1 (Q1 prebias −16 V, Q3 prebias −20 V, and collision energy −22 V) and 318.2 > 196.1 (Q1 prebias −16 V, Q3 prebias −22 V, and collision energy −35 V) were monitored for CBD and CBD-d3, respectively.

The calibration curves were constructed in each blank matrix (serum and lymph) with seven concentrations by plotting the ratio of the peak area of CBD to that of internal standard against CBD concentration. The weighted least-squares linear regression method was used with a weighting factor of $1/x^2$, which improved the accuracy in low concentrations. The method was linear (coefficients of determination [R^2] > 0.9997) in the concentration range of 1–1000 ng/mL. The method was validated according to the requirements of the EMA Guideline on bioanalytical method validation and the guideline acceptance criteria.[18]

Data analysis and statistics

Serum and lymph concentrations in all pharmacokinetic studies were dose-normalized to 1 mg/kg before further calculations. Exact actual sampling times were used for all pharmacokinetic calculations, while scheduled sampling times were used only for plotting of mean pharmacokinetic profiles in the graphs. Pharmacokinetic analysis was performed using Phoenix WinNonlin® (Certara, Princeton, the United States) and PK solver add-on for MS Excel. Area under the curve (AUC) was calculated using the trapezoidal rule, while C_{max} and T_{max} were directly observed.

Lymphatic transport parameters were calculated as previously described.[19] In brief, absolute bioavailability through the lymphatic system (F_{AL}) was defined as the percentage of administered drug that appeared in the intestinal lymph. It was determined directly using lymph volume and CBD concentrations in lymph duct cannulated rats. Analogically, absolute bioavailability through portal vein (F_{AP}) was defined as the

percentage of administered drug dose reaching the systemic circulation after direct absorption into the blood.

It was calculated as $F_{AP} = AUC_{ent}/AUC_{iv}$, where AUC_{ent} is the area under the dose-normalized blood concentration–time curve after enteral dosing in lymph duct cannulated (i.e., lymph-deprived) rats, and AUC_{iv} is the respective parameter in a separate intravenously dosed group. Total absolute bioavailability (F) in lymph duct cannulated rats was calculated as the sum of F_{AL} and F_{AP}. Finally, relative bioavailability through lymph (F_{RL}) was defined as the percentage of systemically available drug that was absorbed through lymph. It was calculated as $F_{RL} = F_{AL}/F$.

GraphPad Prism version 9.1.0 (GraphPad Software, San Diego, CA, the United States) was used for statistical analyses and graph plotting. Paired t-test was used to compare mean serum concentrations, whereas the Wilcoxon nonparametric test was used to compare median T_{max} values. The AUC and C_{max} values were compared by applying the standard ANOVA model for bioequivalence assessment using 90% confidence interval for the ratio of geometric least-squares means. Comparison of the results of arthritis score, MMP-3 levels, ankle widths, rat weights, and histological scores between the treatment groups was evaluated using the Mann–Whitney U-test. The level of statistical significance was set to $p < 0.05$.

Results and Discussion

Emulsion formulation

Sunflower oil droplets containing CBD were stabilized using soybean lecithin in the aqueous phase (the final CBD concentration was 7.5 mg/mL). The emulsion consisted of droplets with diameters ranging from 2 to 293 μm with the average Feret diameter equal to 42 ± 47 μm immediately after the preparation (see Day 1 in Fig. 1). As can be seen in Figure 2, on Day 1, the droplet distribution was bimodal with two characteristic peaks ~ 8 and 80 μm. After a weeklong storage at 4°C, the droplet size distribution shifted slightly in favor of larger droplets, as shown in images referring to Day 8 in Figure 1. On Day 8, the minimal and maximal Feret diameters were 3 and 374 μm, respectively, and the average Feret diameter increased by $\sim 25\%$ to 52 ± 59 μm (see Fig. 2). However, the bimodal character of the size distribution remained preserved.

Although mild droplet coalescence was observed, a few seconds of vortex mixing eliminated the presence of large droplets on Day 8 with the average Feret diameter dropping from 52 ± 59 to 38 ± 33 μm (see Fig. 2). That represents an $\sim 10\%$ decrease of the average size compared with Day 1 and a 30% narrower size distribution. The emulsion was easily mixable by vortexing even a month after the preparation. Based on this

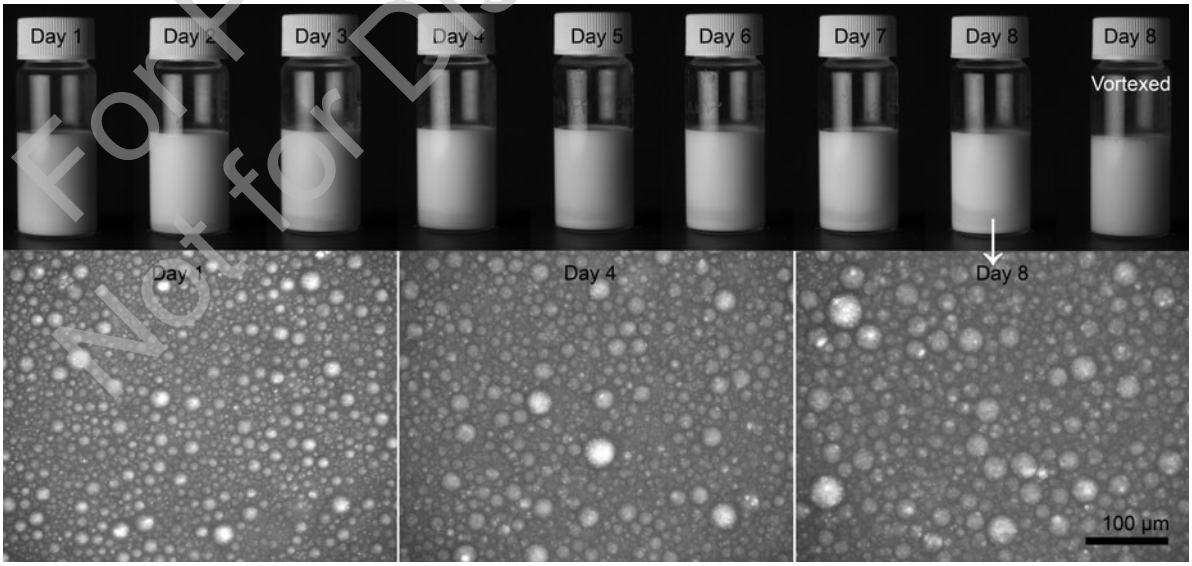

FIG. 1. An emulsion formulation captured for eight consecutive days (upper row) and analyzed by optical microscopy on Days 1, 4, and 8. After 8 days, slight phase separation was easily eliminated by brief vortex mixing (see the last vial entitled vortexed).

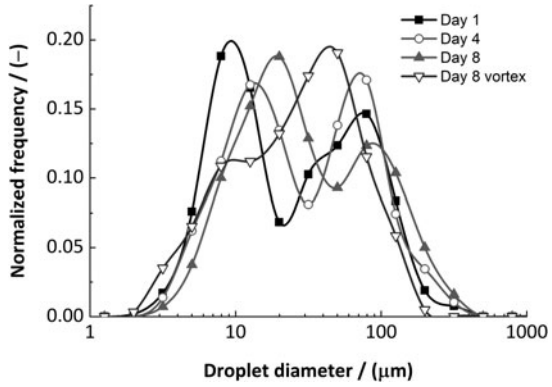

FIG. 2. Feret diameter distributions of oil droplets captured on various days. The sample after brief vortex mixing at Day 8 is also shown for comparison.

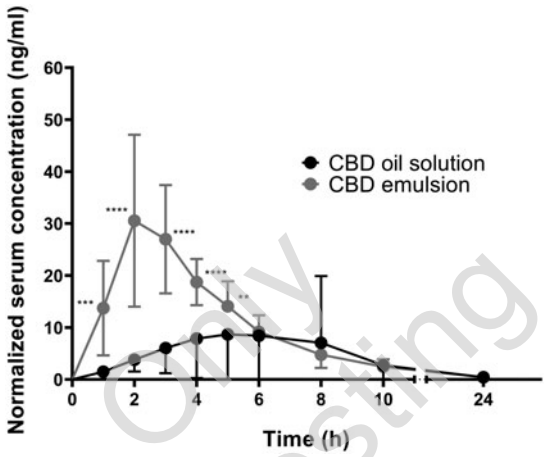

FIG. 3. Mean ± SD CBD serum pharmacokinetic profiles after oral administration of CBD 7.5 mg in the form of oil solution and emulsion to rats ($n = 14$) using a crossover study design. All concentrations are dose-normalized to 1 mg/kg. $^{**}p < 0.01$, $^{***}p < 0.001$, $^{****}p < 0.0001$. CBD, cannabidiol.

stability test, before every application, the emulsion was briefly vortexed (few seconds) to ensure the same droplet size distribution.

CBD bioavailability

Fourteen rats completed the crossover study assessing the relative performance of CBD emulsion compared with oil solution. There was a higher degree of absorption after the administration of the CBD emulsion (Table 1 and Fig. 3). There was also a trend toward higher absorption rate. Nevertheless, the difference in T_{max} did not reach statistical significance ($p = 0.06$). CBD pharmacokinetic parameters after intravenous dosing are summarized in Table 2. Using mean i.v. AUC value from this experiment, the mean ± SD absolute oral bioavailability of CBD was calculated as 24.7 ± 3.6% for emulsion and 14.4 ± 12.2% for oil solution.

Table 1. Pharmacokinetic Parameters of Cannabidiol After Administration in the Form of Oil Solution and Emulsion to Rats ($n = 14$) Using a Crossover Study Design

Formulation	CBD oil solution	CBD emulsion
C_{max} (ng/mL)	8.95 (5.6–14.2)	34.4 (29.8–39.8)
Emulsion/oil solution C_{max} (%)	–	324 (181–581)
T_{max} (h)	4.05 (2.05–7.98)	2.54 (2.02–5.00)
AUC_{inf} (ng·h/mL)	66.8 ± 20.8 (46.0–96.8)	153 ± 11 (142–163)
Emulsion/oil solution AUC_{inf} (%)	–	210 (124–355)

C_{max}, AUC_{inf} and emulsion/solution ratios are given as geometric mean (90% confidence interval). T_{max} is given as median (range). All concentrations and AUCs are dose-normalized to 1 mg/kg.

AUCs, area under the curves; CBD, cannabidiol.

The observed normalized serum C_{max} concentrations of 10–35 ng/mL after oral administration of the two CBD formulations are in line with previously reported data in rats.[16,20–23] There are only sparse reports on absolute bioavailability of CBD. The value of 25% observed after oral administration of CBD emulsion appears to slightly exceed the range of 5–20% reported in other species, including man.[19]

Studies using different formulations have already been published as CBs are an attractive group of compounds exhibiting a wide range of pharmacological effects throughout the body.[24] However, the intestinal absorption of CBD can be significantly affected by their composition. In case of emulsion formulations, which consist of two immiscible stabilized phases (oil and water), the most important excipients are as follows: solvents, cosolvents, surfactants, and cosurfactants.

Table 2. Mean ± SD Cannabidiol Pharmacokinetic Parameters After Intravenous Cannabidiol (1 mg) Administration to Rats ($n = 7$)

C_0 (ng/mL)	1178 ± 421
$T_{1/2}$ (h)	2.5 ± 0.5
V_{ss} (L/kg)	2.9 ± 1.1
Cl (L/h·kg)	1.7 ± 0.6
AUC_{inf} (ng·h/mL)	623 ± 141

Concentration and AUC values are dose-normalized to 1 mg/kg.

C_0, maximum concentration; $T_{1/2}$ - biological half-life; V_{ss}, volume of distribution; Cl, clearance.

Feng et al[21] had already demonstrated that oil selection significantly affects the absorption of CBs. Izgelov et al[16] prepared formulation based on self-nano emulsifying drug delivery systems to investigate the effect of medium- and long-chain glycerides in oil phase. The subsequent pharmacokinetic studies suggested high absorption. However, all the tested formulations contained a range of surfactants combined with significant amounts of ethyl lactate together with *n*-butanol. Our results present a rather simple formulation based on fully biologically degradable compounds, where impact of various oils[21] and droplet size on oral absorption can be easily evaluated.

Lymphatic absorption of CBD

Significant lymphatic transport after administration of both CBD emulsion and oil solution was observed (Table 3 and Fig. 4). CBD lymph concentrations were two to three orders of magnitude higher than serum concentrations. After administration of the CBD emulsion, there was a trend toward faster absorption into the lymph with lymphatic C_{max} reaching at ~4 h. On the contrary, absorption from the oil solution was more sustained, and the lymph concentrations observed at the end of the sampling period exceeded those of the CBD emulsion. Overall, the extent of lymphatic transport did not differ significantly between the two CBD formulations.

High levels of CBD in the lymph are similar to those reported by Zgair et al.[11] Relative bioavailability through lymph of ~50% is comparable with compounds with very high lymphatic transport, such as halofantrine and vitamin D.[25,26] It is evident that lymphatic transport after oral administration plays a substantial role in the CBD pharmacokinetics and contributes significantly to total bioavailability. This fact is of a great importance for further pharmaceutical applications. As mentioned above, CBD undergoes first-pass metabolism, which results in low plasma concentration. It has been estimated that as much as 70–75% of

Table 3. Mean±SD Cannabidiol Lymphatic Transport Parameters After Intraduodenal Administration of 7.5 mg of Cannabidiol in the Form of the Emulsion or Oil Solution (*n*=3 for Each Formulation) as Assessed at 8 h in Mesenteric Lymph Duct Cannulated Rats

	F (%)	F_{AL} (%)	F_{RL} (%)
CBD oil solution	4.8±1.0	2.7±0.7	55.3±8.5
CBD emulsion	12.3±12.3	3.0±1.3	39.2±27.1

F, total absolute bioavailability; F_{AL}, absolute bioavailability through lymph; F_{RL}, relative bioavailability through lymph.

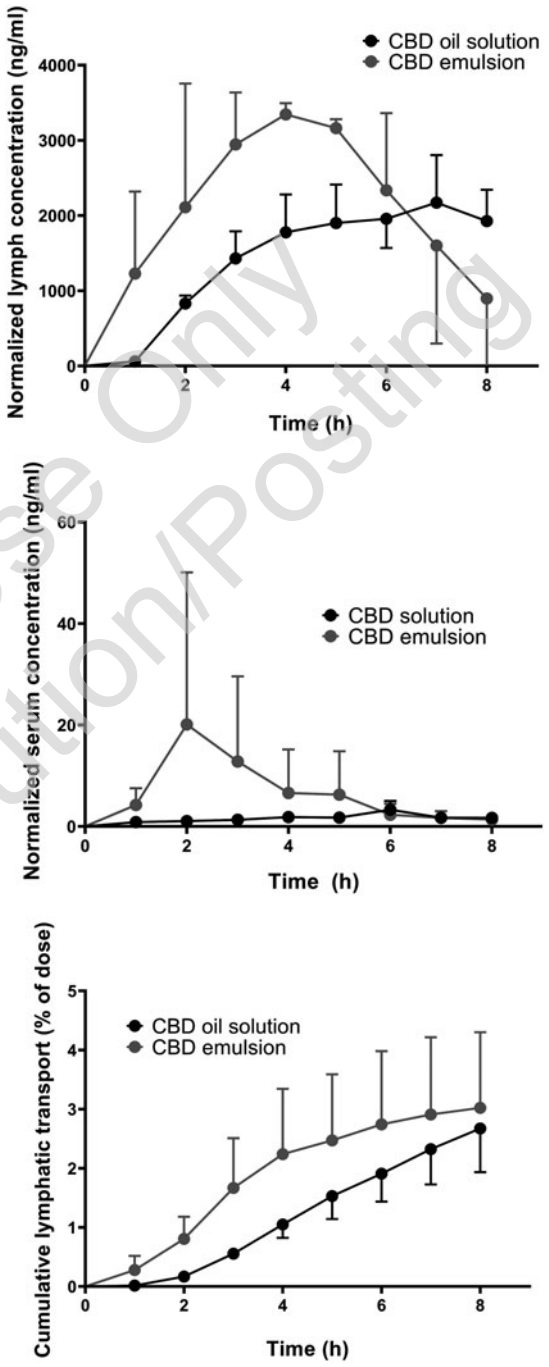

FIG. 4. Mean±SD CBD pharmacokinetic profiles in the lymph and blood and cumulative lymphatic transport after intraduodenal administration of 7.5 mg to lymph duct cannulated rats in the form of emulsion and oil solution ($n=3$ for each formulation). Lymph concentrations are dose-normalized to 1 mg/kg.

Table 4. Mean±SD Values of Ankle Width, Weight, Matrix Metaloproteinase 3 Levels in Female Wistar Rats Suffering from Collagen-Induced Arthritis ($n=6$ in Cannabidiol and Placebo Group, $n=3$ in Negative Control Group)

	Ankle width (mm)				Weight (g)		Matrix metaloproteinase 3 (% of AU)	
	Day 0		Day 24					
	Left hindlimb	Right hindlimb	Left hindlimb	Right hindlimb	Day 0	Day 24	Day 0	Day 24
Negative control	5.44±0.05	5.31±0.43	5.70±0.20	5.77±0.22	268.33±15.33	282.33±9.88	1.00±0.27	1.00±1.30
CBD group	7.77±1.40	8.60±0.60	7.88±0.93	8.27±0.22	278.67±15.83	282.17±25.53	368.22±435.36	20.23±18.69
Placebo group	7.14±1.51	7.80±1.28	8.57±0.20	8.55±0.37	264.33±23.39	271.50±19.77	154.76±220.46	27.88±12.27

absorbed dose is metabolized before reaching systemic circulation. Therefore, improving lymphatic transport, and bypassing liver, is essential for increasing bioavailability of this compound.

In sparse translational studies, it has been shown that lymphatic transport increases with increasing bodyweight of investigated species concerning both absolute and relative contributions to systemic bioavailability.[27] Based on these works, absolute bioavailability through lymph in humans is expected to be four times higher than that in rats. We observed a CBD absolute bioavailability through lymph of ~3% for both formulations in anesthetized rats. It can be expected to be two- to threefold higher in awake animals where the total bioavailability was threefold higher for oil solution and twofold higher for microemulsion. This would potentially translate to absolute bioavailability through lymph of 24–36% in humans.

Another issue is a significant food effect. Various studies have demonstrated that CBD ingestion with high-fat meal increases the C_{max} and AUC values 4 to 14 times and four to five times, respectively.[28] Using a formulation that already contains lipids not only increases the total bioavailability but it can also eliminate large differences in absorption in fasted and fed state, and sustain balanced levels of CBD throughout the treatment.

CBD emulsion in the treatment of CIA

The comparison of the results evaluating the efficacy of CBD emulsion on CIA is summarized in Table 4.

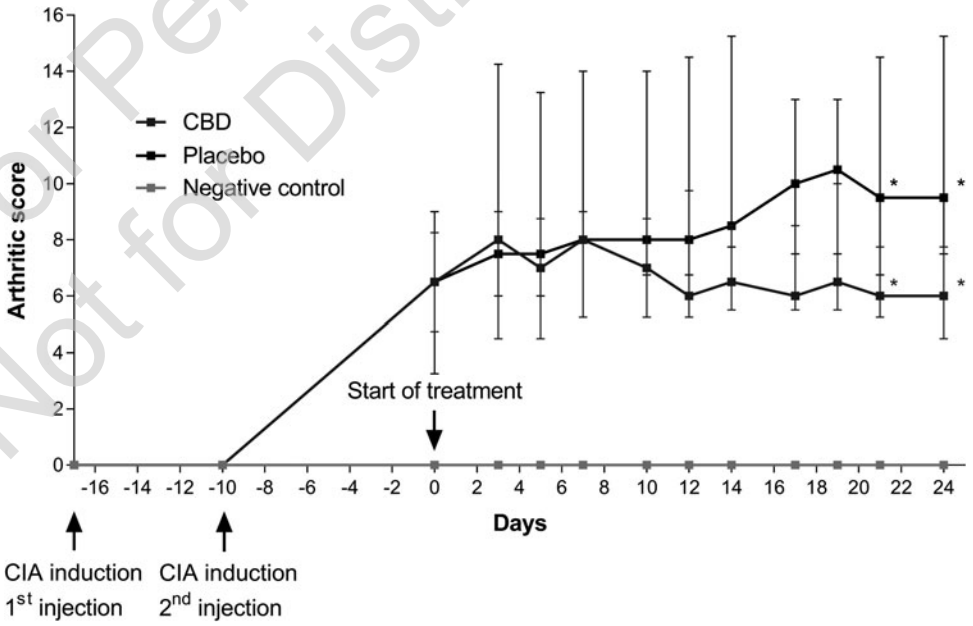

FIG. 5. Clinical progression of collagen-induced arthritis in female Wistar rats ($n=6$ in the CBD and Placebo group, $n=3$ in the Negative control group). Data are expressed as medians. *Significantly different values ($p<0.05$).

Although there is a trend toward decreased MMP-3 levels and ankle widths in the CBD group than in the Placebo group on Day 24, none of the values were significant. A significant RA clinical progression in the Placebo group in comparison with CBD group was observed since Day 21 according to the symptom scoring (Fig. 5). Representative examples of histological findings are shown in Figure 6.

Significantly lower activity of phalangeal disease in the CBD group (median score 0.5, interquartile range [IQR] 0.0–1.0) in comparison with the Placebo group (median score 2.0, IQR 1.0–3.0) was observed in histological assessment ($p = 0.04$). The difference in histologically scored structural phalangeal damage between the CBD and the Placebo group (median score 1.5 and 3.0, IQR 1.0–2.75 and 2.25–3.0, respectively) was not statistically significant ($p = 0.37$). No treatment effect in this domain was likely caused by the onset of irreversible joint damage before treatment initiation in either group of rats, as the study was designed primarily to evaluate the drug effects to diminish or stop the progression of the disease, not to describe its potential for preventing structural damage.

Clinically relevant parameters, that is, clinical symptoms scores as well as morphological signs of disease/osteoclast activity, have shown significant improvements in the treatment groups. This was accompanied by only nonsignificant, but favorable trends in the course of the serum biomarker of the disease progression MMP-3 or in the ankle diameter measurements. The lack of significance for the MMP-3 biomarker was likely caused by an imbalance at the beginning of the treatment between both the CBD and Placebo groups, corresponding to the fact that the study was not balanced for this parameter.

In summary, our results from the rat CIA model demonstrate the therapeutic effect of CBD emulsion in the treatment of RA, represented by improvement in clinical symptoms as well as lower osteoclast activity and favorable trend in MMP-3 levels and lower paw swelling. Even though CBD did not show sufficient pharmacological effect in monotherapy, positive effect on the disease is still present. The lack of sufficient response could be dose dependent as the actual therapeutic dose in this indication is still unknown. There is a possibility to use CBD as an adjuvant in combination with conventional therapy—DMARDs, as its presence might have a positive impact on the efficacy of such treatment or ameliorate its adverse effects. Similar beneficial effect has already been demonstrated by El-Sheikh et al,[29] for a combination of methotrexate or leflunomide and another natural compound affecting endocannabinoid system; that is, beta-caryophyllene.

Conclusions

Presented work was focused on evaluation of CBD absorption after oral administration with special focus

FIG. 6. Representative images of interphalangeal joints' histological scoring for tissue damage and level of disease/osteoclast activity. **(A)** Histopathological damage – Score 0. The image shows a physiological interphalangeal joint; articulating bones covered with intact cartilage and normal morphological synovial membranes with a maximum double layer of synovialocytes. **(B)** Disease/osteoclast activity – Score 0. A higher magnification of **(A)** shows an intact joint with no osteoclasts and no signs of cartilage or bone erosion. **(C)** Histopathological damage – Score 1. The inflammatory synovial pannus protrudes into the joint cavity (*). Articular cartilages are morphologically intact (*arrowheads*). **(D)** Disease/osteoclast activity – Score 1. An isolated osteoclast in Howship's lacuna next to the subchondral bone. **(E)** Histopathological damage – Score 2. Interphalangeal joint with an inflammatory synovial pannus (*), which penetrates beyond a partially eroded articular cartilage into the subchondral bone (*arrowhead*). **(F)** Disease/osteoclast activity – Score 2. Two osteoclasts (*arrowheads*) are found within the inflammatory synovial pannus. **(G)** Histopathological damage – Score 3. Joint with the highly cellular inflammatory synovial pannus completely filling the joint cavity. The pannus penetrates through heavily eroded articular cartilage across the subchondral bone deep into the bone cavity (*). **(H)** Disease/osteoclast activity – Score 3. Multiple osteoclasts (*arrowheads*) adjacent to eroding bone or within the inflammatory pannus filing the joint cavity. **(A–H)** Hematoxylin-eosin staining. Scale bars in **A**, **C**, **E**, **F**, **G**, and **H** = 100 μm, in B and D = 50 μm.

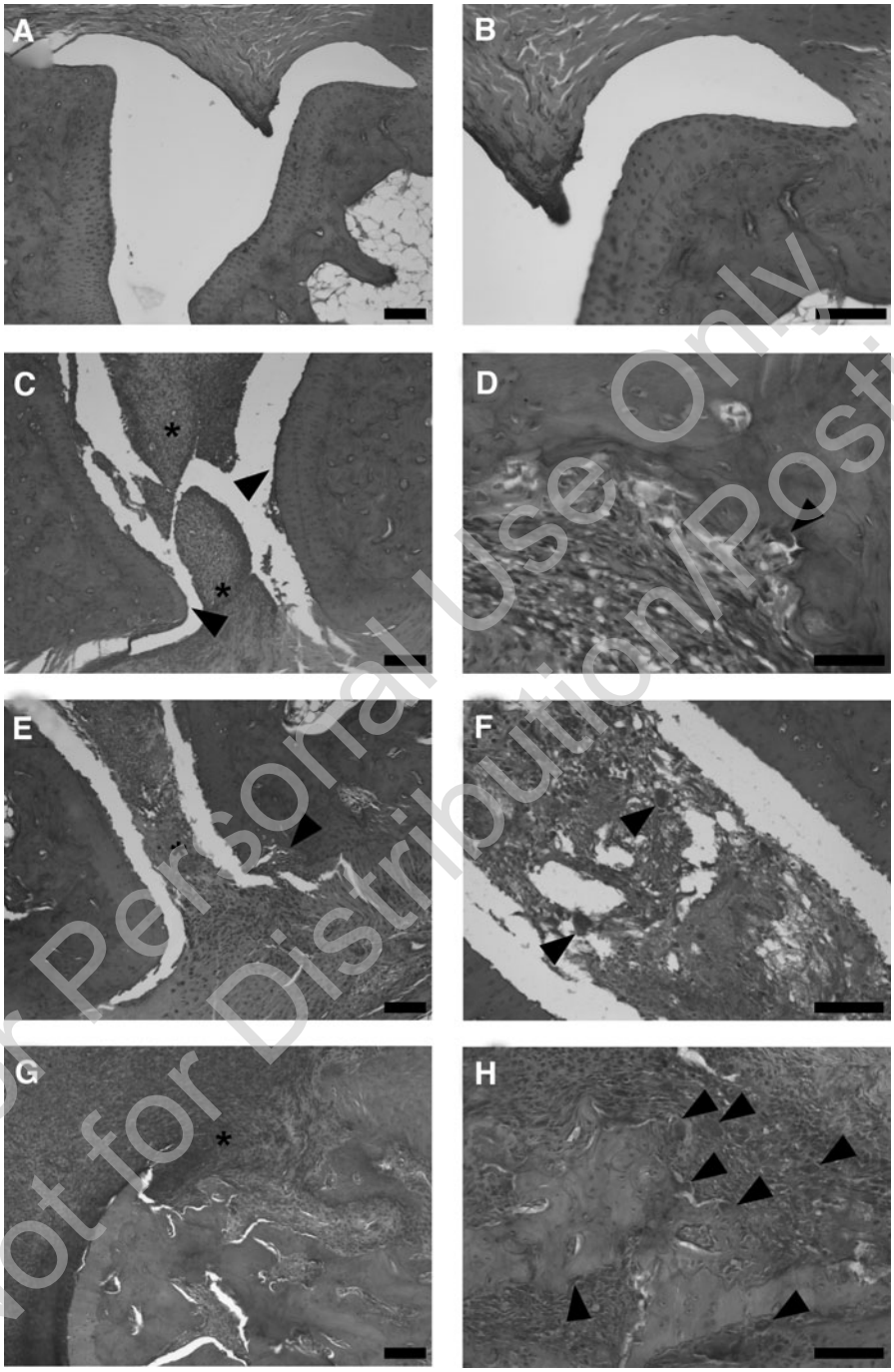

on lymphatic transport and possible therapeutic application in RA treatment. For this reason, two types of simple lipid-containing formulations, sunflower oil solution and sunflower oil microemulsion stabilized by soybean lecithin, were used. Prepared emulsion exhibited good size stability and only marginal coalescence, which was easily redispersed by shaking even after long-term storage.

In comparison with simple oil solution, our formulation exhibited improved bioavailability with 3.2 times higher C_{max} and 2.1 times higher AUC. Further pharmacokinetic experiments showed that both

formulations (oil as well as emulsion) were lymphatically absorbed to a great extent, and CBD concentrations in the lymph were two to three orders of magnitude higher than serum concentrations, thus, confirming the importance of this route of transport.

Although treatment with our formulation resulted in significant improvement in clinical symptoms and disease activity, the effect on ankle swelling, joint damage as well as the MMP-3 levels was only minor. Overall, our emulsion did not exhibit sufficient efficacy in monotherapy in the model of RA, although this may change with the dose.

We have demonstrated the beneficial effect of emulsion formulation on lymphatic absorption and subsequent increase in absolute oral bioavailability. This is important, because with further optimization even higher values could be achieved. In fact, our formulation is rather simple, and thus provides robust platform for additional testing of various components and formulation parameters; that is, oil type, droplet diameter, droplet size distribution. Furthermore, as CBD exhibits a wide range of effects on human body, its therapeutic value is not limited to RA. Understanding how to maximize its absorption is crucial, and lymphatic transport is proving to be an important pathway for highly lipophilic molecule suffering from extensive first-pass metabolism such as CBD.

Authors' Contributions

P.J., J.R., and M.J. conducted investigation; P.R. and T.K. contributed to methodology and investigation; T.H. performed writing—review and editing; J.P. provided resources; P.K. performed formal analysis and methodology; M. Šíma contributed to methodology and supervision; O.S. performed supervision and project administration; M. Šoóš contributed to supervision, writing—original draft, and project administration.

Author Disclosure Statement

All authors declare that they have no conflicts of interest.

Funding Information

This work was supported by AZV grant No. AZV NU22-08-00346, specific university research grant No. A1_FCHI_2022_006, Charles University grant GAUK No. 102322, and Charles University Program Cooperation (research area *PHAR*).

References

1. Ajeganova S, Huizinga T. Sustained remission in rheumatoid arthritis: latest evidence and clinical considerations. Ther Adv Musculoskelet Dis. 2017;9:249–262.
2. Kerschbaumer A, Sepriano A, Smolen JS, et al. Efficacy of pharmacological treatment in rheumatoid arthritis: a systematic literature research informing the 2019 update of the EULAR recommendations for management of rheumatoid arthritis. Ann Rheum Dis. 2020;79:744–759.
3. Kaur I, Behl T, Bungau S, et al. The endocannabinoid signaling pathway as an emerging target in pharmacotherapy, earmarking mitigation of destructive events in rheumatoid arthritis. Life Sci. 2020;257:118109.
4. Malfait AM, Gallily R, Sumariwalla PF, et al. The nonpsychoactive cannabis constituent cannabidiol is an oral anti-arthritic therapeutic in murine collagen-induced arthritis. Proc Natl Acad Sci U S A. 2000;97:9561–9566.
5. Trentham DE, Townes AS, Kang AH. Autoimmunity to type II collagen an experimental model of arthritis. J Exp Med. 1977;146:857–868.
6. EMA. Epidyolex; [cited 2022 May 1]. Available from: https://www.ema.europa.eu/en/medicines/human/EPAR/epidyolex
7. Porter CJ, Trevaskis NL, Charman WN. Lipids and lipid-based formulations: optimizing the oral delivery of lipophilic drugs. Nat Rev Drug Discov. 2007;6:231–248.
8. Charman WNA, Stella VJ. Estimating the maximal potential for intestinal lymphatic transport of lipophilic drug molecules. Int J Pharm. 1986;34:175–178.
9. Ryšánek P, Grus T, Šíma M, et al. Lymphatic transport of drugs after intestinal absorption: impact of drug formulation and physicochemical properties. Pharm Res. 2020;37:166.
10. Huestis MA. Human cannabinoid pharmacokinetics. Chem Biodivers. 2007;4:1770–1804.
11. Zgair A, Lee JB, Wong JCM, et al. Oral administration of cannabis with lipids leads to high levels of cannabinoids in the intestinal lymphatic system and prominent immunomodulation. Sci Rep. 2017;7:14542.
12. Franco V, Gershkovich P, Perucca E, et al. The interplay between liver first-pass effect and lymphatic absorption of cannabidiol and its implications for cannabidiol oral formulations. Clin Pharmacokinet. 2020;59:1493–1500.
13. Lowin T, Tingting R, Zurmahr J, et al. Cannabidiol (CBD): a killer for inflammatory rheumatoid arthritis synovial fibroblasts. Cell Death Dis. 2020;11:714.
14. Millar SA, Stone NL, Yates AS, et al. A systematic review on the pharmacokinetics of cannabidiol in humans. Front Pharmacol. 2018;9:1365.
15. Francke NM, Schneider F, Baumann K, et al. Formulation of cannabidiol in colloidal lipid carriers. Molecules. 2021;26:1469.
16. Izgelov D, Shmoeli E, Domb AJ, et al. The effect of medium chain and long chain triglycerides incorporated in self-nano emulsifying drug delivery systems on oral absorption of cannabinoids in rats. Int J Pharm. 2020;580:119201.
17. Trevaskis NL, Hu L, Caliph SM, et al. The mesenteric lymph duct cannulated rat model: application to the assessment of intestinal lymphatic drug transport. J Vis Exp. 2015:52389.
18. EMA. ICH guideline M10 on bioanalytical method validation and study sample analysis; [cited 2022 May 1]. Available from: https://www.ema.europa.eu/en/documents/scientific-guideline/ich-guideline-m10-bioanalytical-method-validation-step-5_en.pdf
19. Ryšánek P, Grus T, Lukáč P, et al. Validity of cycloheximide chylomicron flow blocking method for the evaluation of lymphatic transport of drugs. Br J Pharmacol. 2021;178:4663–4674.
20. Deiana S, Watanabe A, Yamasaki Y, et al. Plasma and brain pharmacokinetic profile of cannabidiol (CBD), cannabidivarine (CBDV), Δ^9-tetrahydrocannabivarin (THCV) and cannabigerol (CBG) in rats and mice following oral and intraperitoneal administration and CBD action on obsessive-compulsive behaviour. Psychopharmacology (Berl). 2012;219:859–873.
21. Feng W, Qin C, Chu Y, et al. Natural sesame oil is superior to pre-digested lipid formulations and purified triglycerides in promoting the intestinal lymphatic transport and systemic bioavailability of cannabidiol. Eur J Pharm Biopharm. 2021;162:43–49.
22. Hložek T, Uttl L, Kadeřábek L, et al. Pharmacokinetic and behavioural profile of THC, CBD, and THC+CBD combination after pulmonary, oral, and subcutaneous administration in rats and confirmation of conversion

in vivo of CBD to THC. Eur Neuropsychopharmacol. 2017;27:1223–1237.
23. Kok LY, Bannigan P, Sanaee F, et al. Development and pharmacokinetic evaluation of a self-nanoemulsifying drug delivery system for the oral delivery of cannabidiol. Eur J Pharm Sci. 2022;168:106058.
24. Stella B, Baratta F, Della Pepa C, et al. Cannabinoid formulations and delivery systems: current and future options to treat pain. Drugs. 2021;81:1513–1557.
25. Dahan A, Hoffman A. Evaluation of a chylomicron flow blocking approach to investigate the intestinal lymphatic transport of lipophilic drugs. Eur J Pharm Sci. 2005;24:381–388.
26. Karpf DM, Holm R, Kristensen HG, et al. Influence of the type of surfactant and the degree of dispersion on the lymphatic transport of halofantrine in conscious rats. Pharm Res. 2004;21:1413–1418.
27. Trevaskis NL, Lee G, Escott A, et al. Intestinal lymph flow, and lipid and drug transport scale allometrically from pre-clinical species to humans. Front Physiol. 2020;11:458.
28. Perucca E, Bialer M. Critical aspects affecting cannabidiol oral bioavailability and metabolic elimination, and related clinical implications. CNS Drugs. 2020;34:795–800.
29. El-Sheikh SMA, Abd El-Alim AEF, Galal AAA, et al. Anti-arthritic effect of β-caryophyllene and its ameliorative role on methotrexate and/or leflunomide-induced side effects in arthritic rats. Life Sci. 2019;233:116750.

Cite this article as: Jelínek P, Roušarová J, Ryšánek P, Ježková M, Havlůjová T, Pozniak J, Kozlík P, Křížek T, Kučera T, Šíma M, Slanař O, and Šoóš M (2022) Application of oil-in-water cannabidiol emulsion for the treatment of rheumatoid arthritis, *Cannabis and Cannabinoid Research* X:X, 1–13, DOI: 10.1089/can.2022.0176.

Abbreviations Used

AUC = area under the curve
CB = cannabinoid
CBD = cannabidiol
CIA = collagen-induced arthritis
DMARDs = disease-modifying antirheumatic drugs
EMA = European Medicines Agency
IQR = interquartile range
MMPs = matrix metalloproteinases
MRM = multiple reaction-monitoring mode
RA = rheumatoid arthritis